ITMO UNIVERSITY

Baranov A.V., Miropoltsev M.A., Parfenov P.S., Tikhodeeva E.O.

METHODS AND TECHNIQUES OF PHYSICAL EXPERIMENT

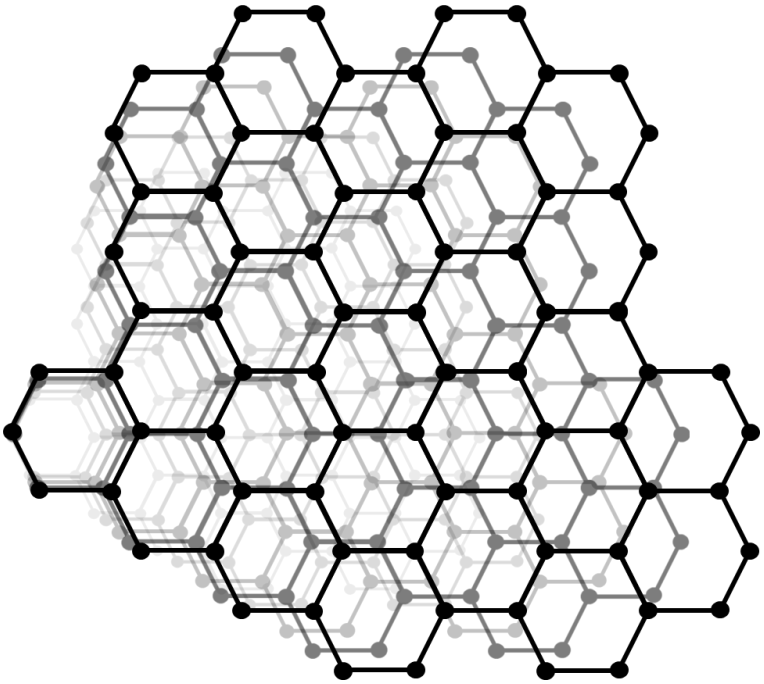

St. Petersburg
2021

МИНИСТЕРСТВО НАУКИ И ВЫСШЕГО ОБРАЗОВАНИЯ
РОССИЙСКОЙ ФЕДЕРАЦИИ

УНИВЕРСИТЕТ ИТМО

**А.В. Баранов, М.А. Миропольцев,
П.С. Парфенов, Е.О. Тиходеева**

METHODS AND TECHNIQUES OF PHYSICAL EXPERIMENT

УЧЕБНОЕ ПОСОБИЕ

РЕКОМЕНДОВАНО К ИСПОЛЬЗОВАНИЮ В УНИВЕРСИТЕТЕ ИТМО
по направлению подготовки 12.04.03 Фотоника и оптоинформатика
в качестве учебного пособия для реализации основных
профессиональных образовательных программ высшего образования
магистратуры

Санкт-Петербург
2021

Baranov A.V., Miropoltsev M.A., Parfenov P.S., Tikhodeeva E.O., Methods and Techniques of Physical Experiment. Study Guide. – St. Petersburg: ITMO University, 2021. – 95 pages.

Рецензент:
Zakharov V.V., PhD, Faculty of Photonics, ITMO University, St. Petersburg, Russia.

The present study guide is devoted to the education course "Methods and Techniques of Physical Experiment" and provides an overview of methods for fabrication and experimental analysis of nanostructures. It covers technologies for the synthesis of single nanoobjects, such as quantum dots and nanotubes, as well as the formation of hybrid nanostructures. The analytical methods discussed in the study guide include fluorescence, electron, probe microscopy, and X-ray scattering techniques, whose main task is to study geometry, internal structure, and chemical composition of nanostructures.

ITMO UNIVERSITY

ITMO University is the leading Russian university in the field of information and photonic technologies, one of the few Russian universities with the status of the national research university granted in 2009. Since 2013 ITMO University has been a participant of the Russian universities' competitiveness raising program among the world's leading academic centers known as «5 to 100». The objective of ITMO University is the establishment of a world-class research university being entrepreneurial in nature aimed at the internationalization of all fields of activity.

CONTENT

INTRODUCTION

The present book is the first part of the study guide to the course “Methods and Techniques of Physical Experiment”. The guide provides basic knowledge and ideas regarding the role of optical methods in the study of nanostructured objects, as well as the instrumental techniques and organization of a physical experiment. Particular attention is paid to the experimental approaches allowing for characterization of the nanostructure morphology, including size, shape, and mutual arrangement of single nanoparticles. In the first two chapters of the book, various types of nanostructures are introduced to the reader, together with primary examples and methods of their fabrication. In the third chapter, the main experimental methods are briefly discussed, with the emphasis on microscopic and scattering techniques. The rest of the book is devoted to the detailed description of selected techniques. The reader will learn the basics of fluorescence microscopy, electron microscopy, scanning tunneling and atomic force microscopy—powerful methods that enable comprehensive analysis of morphological and structural parameters of nanomaterials. The X-ray scattering techniques are also described, that are frequently used for deeper characterization of nanocrystalline samples. Further, dynamic light scattering is introduced, being a simple yet irreplaceable method for studying size, stability, and surface charge of colloidal nanoparticles.

The course includes lectures, discussions, and practical assignments. Lecture materials are provided to students by email or cloud sharing in advance and are available prior to each lecture. The instructor clarifies essential and complicated parts of the lecture, gives assignments, answers students’ questions, and moderates discussions throughout the lecture. As a result of the course, students will gain competences in modern experimental methods of nanostructure fabrication and research tools. They will be able to justify the choice of experimental methods for studying morphological, structural, and optical characteristics of nanomaterials (the latter is covered in the second part of the student’s guide). Students will also learn to carry out physical experiments using the described equipment, process the acquired data, and make conclusions about the research results. These practical skills are majorly developed through the realization of the students’ scientific projects and course works, as well as laboratory practices within the scope of adjacent disciplines.

This study guide is partly based on "Special Methods for Measuring Physical Quantities" by A.V. Fedorov, A.V. Baranov, A.P. Litvin, S.A. Cherevkov. St. Petersburg, ITMO University. 2014. – P.127.

CHAPTER 1. NANOSTRUCTURES & NANOTECHNOLOGIES

Modern nanoscience is one of the most promising fields of study from the practical standpoint, as it drives forward the creation of novel materials and devices with outstanding physical properties. One of the main tasks of nanoscience is to learn how various materials work on nanoscale and what possibilities they bring in terms of the real-world applications. Up to date, a wide range of nanostructures has been discovered. We can classify them based on the type of used materials, size, shape, final structural form, and possible applications.

For instance, there is a large family of carbon-based nanomaterials and nanostructures, such as famous *graphene*, *fullerenes*, and *carbon nanotubes* (*CNT*). It has been shown that different forms of carbon possess different physical properties, which is advantageous for potential applications.

Another important class is semiconductor nanocrystals, where the shape and size define the behavior of charge carriers, leading to formation of what we know as *quantum confinement effect*. The effect is observed if the size of the semiconductor in at least one dimension is comparable to its characteristic exciton Bohr radius. When it happens, the density of states in this material starts to change, leading to dramatically different optical properties. Such nanocrystals as *quantum dots* (*QD*), *quantum wells*, and *nanorods* are the representatives of different types of quantum confinement—all are extremely interesting from both fundamental and practical perspectives.

In the present chapter, we are going to discuss the effect of quantum confinement in semiconductors, as well as several prominent examples of modern nanostructures. In the next chapter, nanofabrication approaches will be thoroughly discussed.

§ 1.1 Size Effects in Semiconductors

Semiconductor nanocrystals make up one of the most promising classes of materials for photonics and biomedicine. The reason why they have gained so much interest is their exceptional optical properties as compared to traditional optical materials. Furthermore, it is possible to tailor these properties to a desired application by changing the semiconductor size and shape. The energy structure of a bulk semiconductor is determined exclusively by the material itself (i.e., the elemental composition and the crystal lattice). At the same time, when a body reaches a certain critical size, its geometry starts to play a vital role in the formation of electronic states. This is what is called the quantum confinement effect in semiconductors.

Theoretically, quantum confinement can be explained in terms of the potential barrier problem. In one-dimensional space, if a quantum particle (for example, an electron) is confined inside a potential barrier, the energies of the particle become

discrete. In this case, the transitions between the energy levels occur only with the absorption or emission of electromagnetic waves with an energy determined by the energy difference of the levels. In the three-dimensional world, it is possible to assemble a structure where the electron motion is restricted in only one, two, or all three dimensions (Figure 1.1).

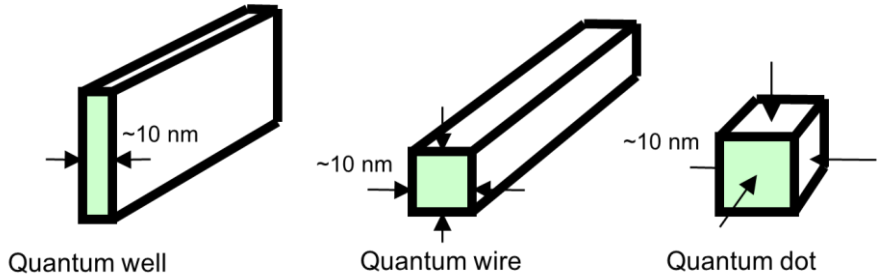

Figure 1.1. Schematic illustration of the three types of quantum confinement determined by the nanocrystal geometry.

The *strength* of confinement also matters, i.e., the size of a particle in a certain direction compared to the material's characteristic exciton Bohr radius. Together, these parameters define the electronic structure of a low-dimensional semiconductor material. For example, for a spherical quantum dot (without considering excitonic effects), the energy spectrum looks like:

$$E_{ml}^{e} = E_g + \frac{\hbar^2 \chi_{ml}^2}{2m_e^* a^2}, \tag{1.1}$$

$$E_{ml}^{h} = -\frac{\hbar^2 \chi_{ml}^2}{2m_h^* a^2}, \tag{1.2}$$

where E_{ml}^{e} and E_{ml}^{h} are the electron and hole energies, respectively, E_g is the semiconductor band gap, $\hbar$ is the reduced Planck constant, χ_{ml} are the roots of the spherical Bessel function, m_e^* and m_h^* are the effective masses of an electron and a hole, respectively, and *a* is the radius of a quantum dot. The given equations are valid for the case which is commonly called *the strong confinement regime*. It manifests itself when the size of a semiconductor is much smaller than the exciton Bohr radius, and is important primarily for the materials of II–VI and III–V elements. In this case, the quantum dot spectrum becomes linear, and the fundamental absorption edge exhibits the blue shift. As an example, absorption spectra of CdSe ranging from size 1.7 nm to 15 nm along with sharp interband transitions are shown in Figure 1.2.

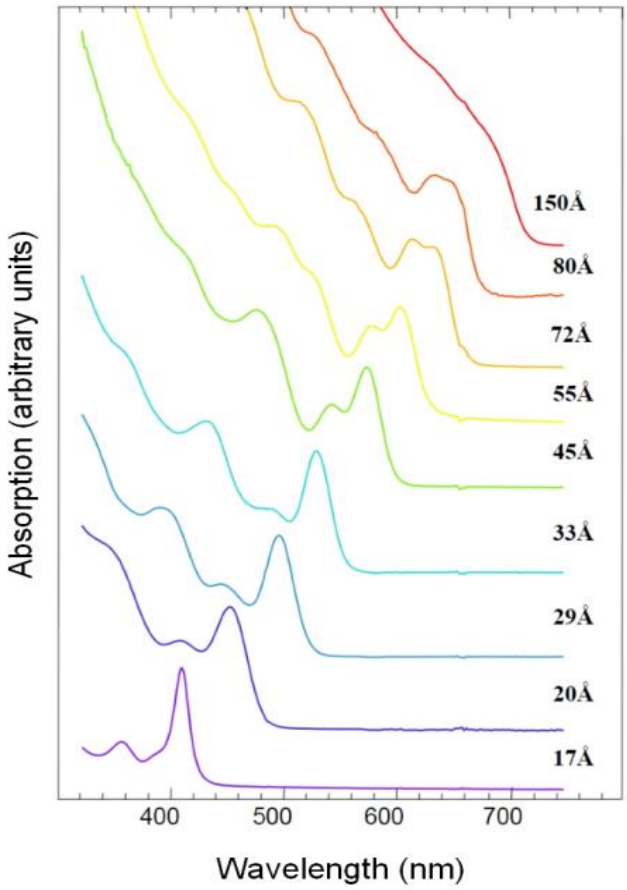

Figure 1.2. Absorption spectra of CdSe quantum dots with diameter varying from 1.7 nm to 15 nm [1.1].

Apart from zero-dimensional quantum dots, one-dimensional (e.g., quantum wires, nanorods) and two-dimensional (e.g., quantum wells, nanoplatelets) particles can be formed that enable charge carrier localization in two or only one direction, respectively. The density of states in semiconductor nanostructures with the corresponding confinement is shown in Figure 1.3.

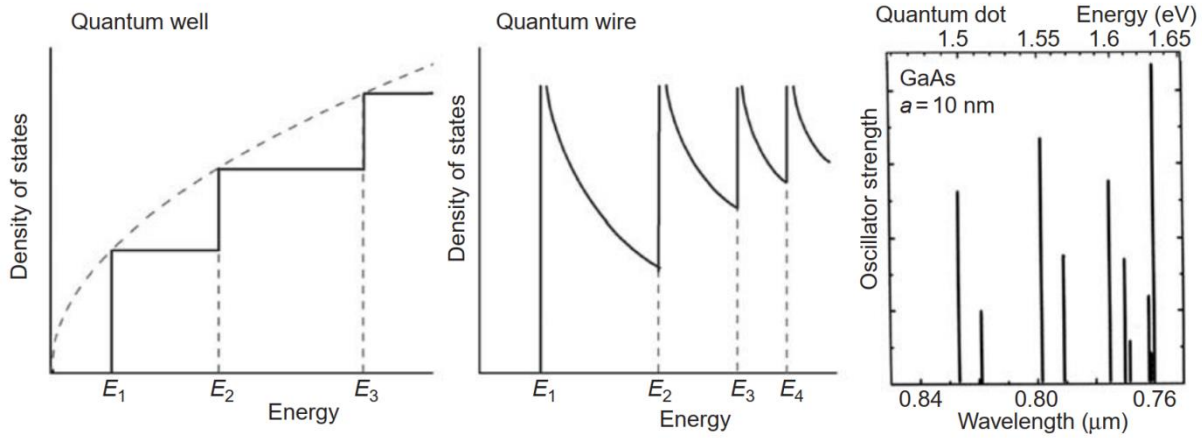

Figure 1.3. Electron density of states in a quantum well, in a quantum wire and calculated probabilities for optical transitions in a realistic GaAs quantum dot with a size of 10 nm [1.2].

The energy structure modification and the band gap broadening are valid for nanocrystals with all types of confinement, but only in the case of quantum dots the energy spectrum becomes linear. In quantum wells, where the motion of charge carriers is free in two directions, the subbands of size quantization are formed. In this case, the well thickness determines the fundamental absorption edge and the photoluminescence wavelength of two-dimensional particles.

§ 1.2 Examples of Nanostructures and Their Applications

The term *nanostructure* is generally used to describe an object with a characteristic size of 1 to 100 nm in at least one dimension. Nanostructures possess unique physicochemical parameters that differ significantly from the properties of atoms, molecules, and bulk materials. Interestingly, the properties of nanostructures are defined not only by the material itself, but also by their shape and size. This effect opens up wide possibilities for tailoring the physicochemical parameters of nanostructures by synthesizing materials with different geometry. It finally brings us to the major aim of nanotechnology: to develop and implement the methods that enable control over the physicochemical parameters of nanomaterials. Nanotechnology comprises theoretical and practical basic science as well as applied research. The former accounts for the fundamental knowledge regarding nanomaterials and their possibilities, while the latter aims to implement the existing structures into the real-world applications. Today, nanostructures are used in almost all modern electronic and photonic devices. Audio and video systems, smartphones and computers, medical systems—all include nanomaterials of different forms in their components (Figure 1.4). The ongoing research in the field of nanotechnology should lead to revolutionary changes in materials science, manufacturing processes, nanoelectronics, medicine, health care, energy, biotechnology, information technology and national security.

Figure 1.4. Examples of the existing practical applications of nanomaterials.

One should distinguish between single nanostructures (monolayer films, nanoparticles, nanoclusters) and more complex nanostructured objects, where single nanostructures are used as building blocks. Examples of such complex nanostructures are multilayer films, single and multilayer arrays of nanoparticles and nanoclusters, dendritic structures, and microscale clusters of disordered nanocrystals. The physical properties of complex nanostructures are often determined not only by the properties of individual components, but also by their interaction with each other and the environment.

Unique physicochemical parameters of nanomaterials are defined by the charge carrier confinement together with the increased role of the surface. Indeed, when the particle size decreases, the surface-to-volume ratio grows up. Therefore, the contribution of the surface effects becomes crucial. In semiconductors, further decrease in the size of nanoparticles below the exciton Bohr radius leads to spatial quantization of the translational motion of elementary excitations (excitons, electrons, holes, phonons). This, in turn, leads to the strong dependence of the material's parameters on its size and shape.

In Figure 1.5, transmission electron microscopy images of a quantum well, a quantum wire and a quantum dot are shown. These nanocrystals are made of semiconductors. They have great potential as elements for the energy conversion and as light emitters with tunable absorption and fluorescence spectra.

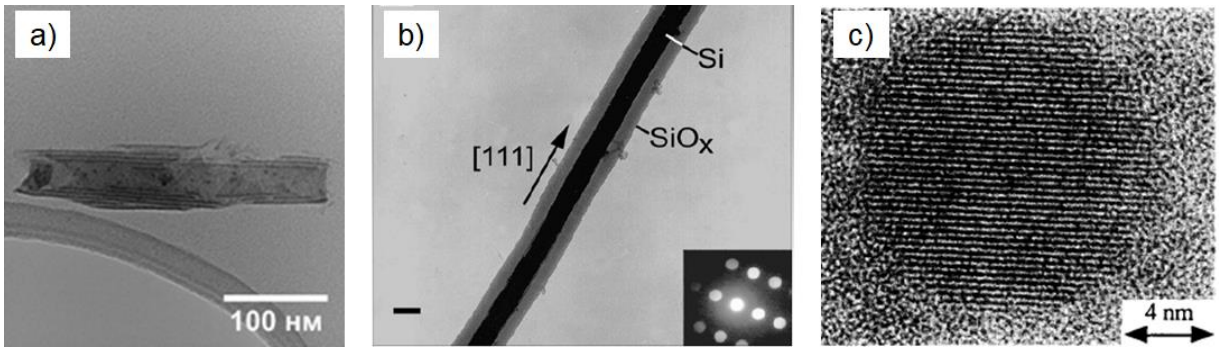

Figure 1.5. High-resolution transmission electron microscopy images of (a) rolled-up two-dimensional CdSe nanosheet, (b) silica nanowire, (c) CdSe quantum dot in a SiO_2 matrix.

They can be used separately or as a part of more complex structures (Figure 1.6). Semiconductor nanocrystals have been extensively studied since 1981 when Ekimov reported the first synthesis of the quasi-spherical quantum dots. Since then, a plethora of synthetic and modification techniques have emerged, allowing to improve the nanocrystal parameters and achieve compatibility with different environments. Quantum dots are already being used to create high-definition displays (QLED), solar cells, and luminescent biocompatible labels for multiplex diagnostics.

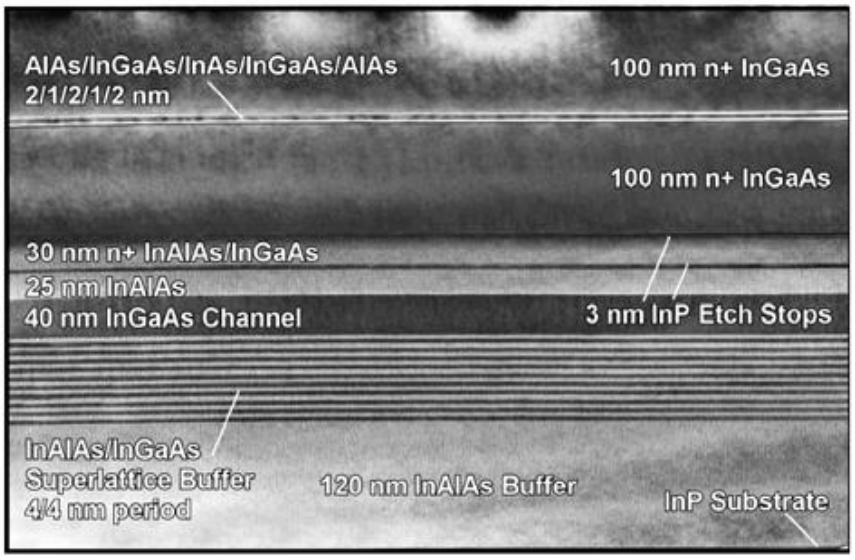

Figure 1.6. Complex multilayer nanostructure, consisting of multiple quantum wells of different compounds.

Another class of nanostructures that attracts the researchers' interest is low-dimensional carbon nanomaterials, such as fullerenes, carbon nanotubes, and graphene.

Fullerenes are one of the carbon allotropic forms. In fullerene molecules, carbon atoms are located at the nodes of regular hexagons and pentagons that form the molecule's spherical or elliptical surface. The C_{60} fullerene is the most symmetric and best-studied representative of the fullerene family. In C_{60}, carbon atoms form a truncated icosahedron that consists of 20 hexagons and 12 pentagons, so that the overall structure resembles a soccer ball (Figure 1.7).

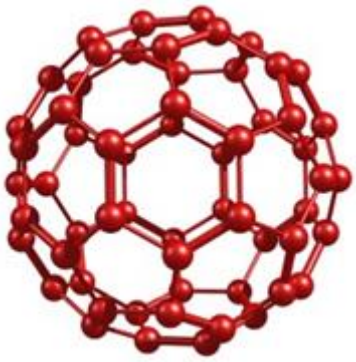

Figure 1.7. Schematic representation of the fullerene C_{60} molecule [1.3].

The C_{70} is the next most common fullerene. Its structure can be derived from the C_{60} fullerene by inserting a belt of 10 carbon atoms into the equatorial region of C_{60}. As a result, the C_{70} molecule is elongated and resembles a rugby ball.

Carbon nanotubes are cylindrical structures with a diameter of one to several tens of nanometers and a length of up to several centimeters. An ideal nanotube is a graphite plane rolled up into a cylinder, that is, a surface consisting of regular hexagons

with the carbon atoms in the nodes. The symmetry of a nanotube depends on the orientation angle of the graphite plane relative to the nanotube axis (Figure 1.8). The orientation angle determines the chirality of the nanotube, which, in turn, determines its electrical characteristics (semiconductor or metallic properties).

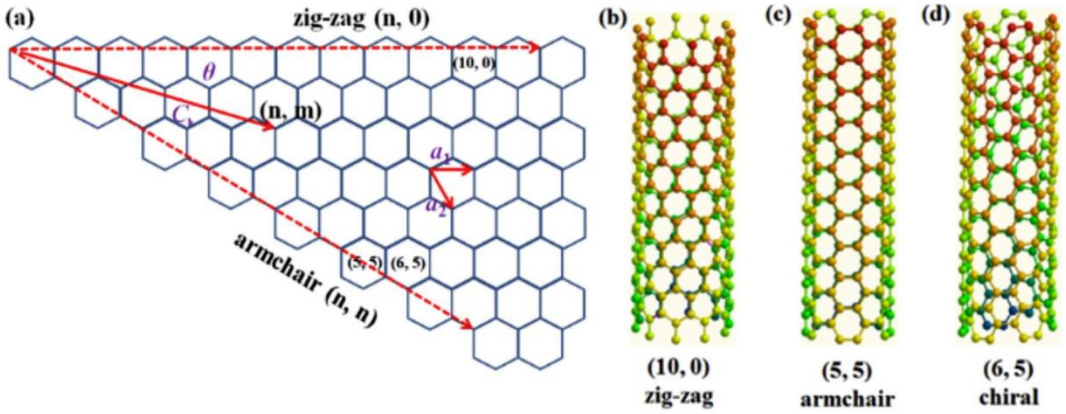

Figure 1.8. (a) Schematic representation of a single-layer graphene sheet showing the geometry of single-walled carbon nanotubes. Examples of the three nanotube morphologies: (b) sidewalls—zig-zag, (c) armchair, and (d) chiral [1.4].

Carbon nanotubes can be single-walled and multi-walled. Multi-walled nanotubes can dramatically differ from single-walled nanotubes as they possess a much wider variety of shapes and configurations. Since recently, carbon nanotubes have become interesting as drug-delivery agents in medicine and as additives to various materials for electronics and optics.

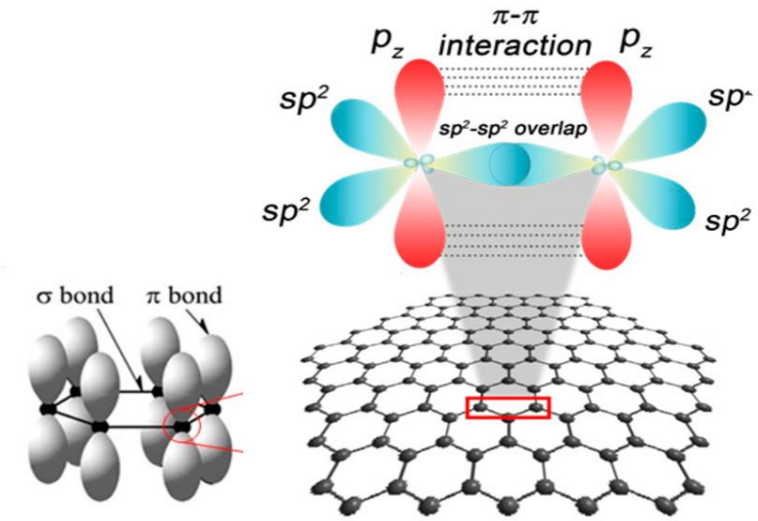

Figure 1.9. Schematic representation of graphene structure [1.5].

Graphene is a two-dimensional allotropic modification of carbon that consists of a carbon atomic monolayer. The atoms are connected by the sp^2-bonds in a honeycomb two-dimensional crystal lattice (Figure 1.9).

Graphene was first obtained only in 2004 and is still poorly understood. In principle, it can be thought of as a single graphite plane, separated from a bulk crystal. According to estimates, graphene possesses high mechanical rigidity and good thermal conductivity (~1 TPa and ~5×10^3 $Wm^{-1}K^{-1}$, respectively). The high mobility of charge carriers makes it a promising material for a wide variety of applications. In particular, graphene can be used as a basis for nanoelectronics and a possible replacement for silicon in integrated circuits.

Check Questions

1. What is a characteristic size of nanoparticles?
2. What is the size effect and the quantum confinement?
3. What is the difference between the weak and the strong confinement regimes?
4. How does the two-dimensional density of states look like?
5. What is a fullerene?

CHAPTER 2. NANOFABRICATION

There are two fundamentally different ways to create nanoscale structures. The first approach involves a sequential build-up of the material, which results in the formation of a nanostructure, this is the so-called *bottom-up approach*. According to the second way, on the contrary, "excess material" is removed from the already existing bulk structure to obtain the desired nanoscale object. This process corresponds to a *top-down approach*. Both ways and some of the corresponding nanofabrication methods will be briefly discussed below.

§ 2.1 Bottom-Up Approach

According to this approach, nanostructures are assembled from the bottom from some elementary blocks; atom-by-atom, molecule-by-molecule, or cluster-by cluster.

2.1.1 Self-Assembly

Self-assembly is a fast and cheap method in which a disordered system of pre-existing components forms an organized structure because of specific, local interactions among the components themselves (without external impact). Since the constitutive components assemble without any external influence, this technique requires neither special equipment nor a large amount of coating material. These features determine the high economic attractiveness of this method.

Various kinds of building blocks can be used for self-assembly, including not only atoms and molecules, but also a wide range of nano- and mesoscopic (100-1000 nm) objects. Chemical composition, structure, and shape of the assembling components, as well as the environmental conditions, affect the characteristics of the resulting structure. The kinds of nanomaterials prepared by the self-assembly method include single and multilayer nanofilms, nanocrystals, nanowires and nanorods, nanotubes, and nanostructures with more complex geometries. The procedure for manufacturing multilayer molecular films is shown in Figure 2.1.

A well-purified substrate is immersed into an organic solution containing the required molecules. After some time, the sample is removed and thoroughly washed with the same solvent to separate the unabsorbed molecules. The morphology and thickness of the resulting film depend on the immersion time, type of the interaction between the molecules and the substrate, concentration, and composition of the solution.

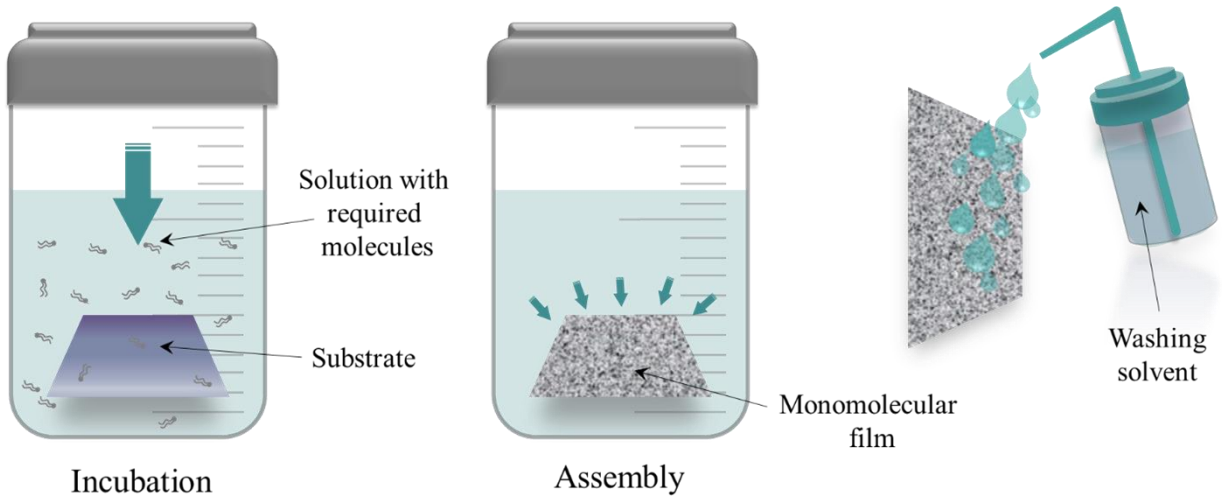

Figure 2.1. Schematic illustration of the process of creating a molecular film via self-assembly.

A stable self-assembly system is formed due to the attractive and repulsive forces caused by non-covalent or weak covalent interaction (van der Waals, electrostatic and hydrophobic interaction, hydrogen, and coordination bonds). A well-known example of self-assembly is the formation of oil droplets and films in water and on its surface, respectively. As shown in Figure 2.2, oil components, such as fatty acids, are capable of assembling micelles via hydrophobic interaction between their tails, while their hydrophilic heads are facing towards the polar environment.

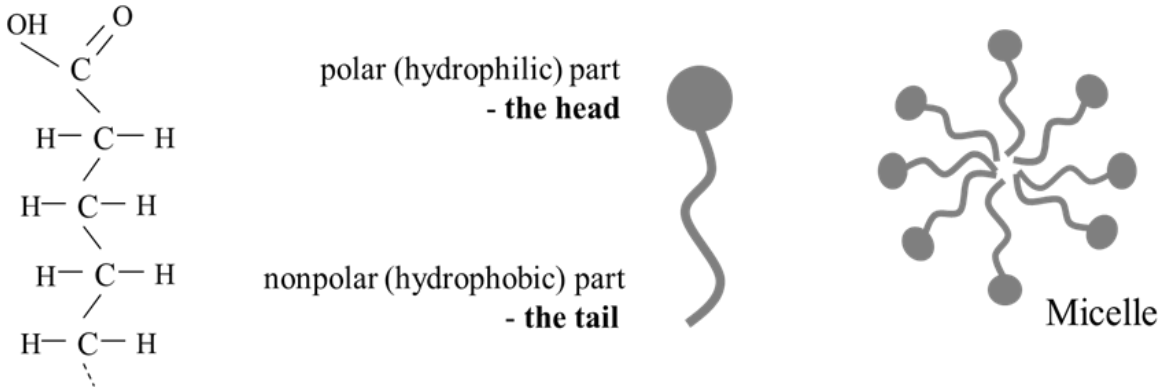

Figure 2.2. Schematic illustration of the self-assembly of fatty acid.

In the above example, we have described processes that utilize molecules as the building blocks. This is the so-called molecular self-assembly. Self-assembly of more complex components, such as quantum dots, will be described in section 2.1.6.

2.1.2 Langmuir-Blodgett Technique

The Langmuir-Blodgett technique allows applying single-molecular layers with controlled thickness and high uniformity. This method is suitable for production of the monolayers of amphiphilic molecules or inorganic nanocrystals.

A classic example of amphiphilic molecules are fatty acids that have a polar (hydrophilic) part—the head, and a nonpolar (hydrophobic) part—the tail. These molecules are dissolved in a water-immiscible volatile solvent (e.g., chloroform). The resulting solution is carefully applied to the surface of the aqueous subphase (Figure 2.3). It spreads rapidly over the surface, occupying all the free space. In this case, the hydrophilic groups are embedded in the subphase, and the hydrophobic tails remain above the surface.

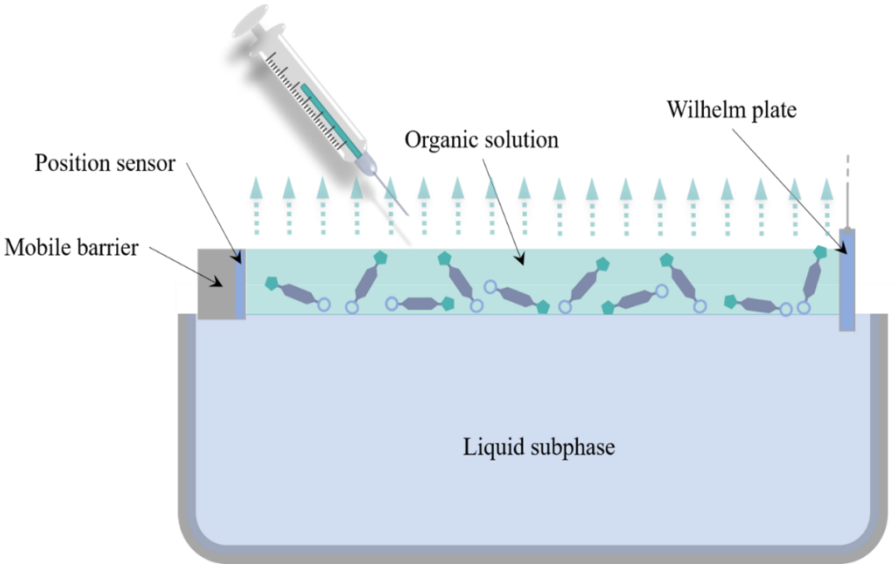

Figure 2.3. Schematic illustration of the spreading process.

At this stage, the distance between the molecules is large, they interact weakly with each other and can be represented as a gas. In this case, the presence of a monolayer has almost no effect on the surface tension of the subphase.

After complete evaporation of the solvent, the mobile barrier begins to compress the surface layer. When it moves, the area occupied by the molecules and the distance between them decreases, and, consequently, the surface pressure changes. To estimate the surface pressure the Wilhelm plate is used (Figure 2.3). It is a thin hydrophilic plate, partially immersed in a liquid, the weight of which varies under the action of the meniscus.

The main characteristic of the formed monolayer is the dependence of the surface pressure on the surface area of the subphase per molecule. This dependence is built at a constant temperature and called the *compression isotherm* (Figure 2.4).

Each state of the monolayer corresponds to a certain region of the compression isotherm. As can be seen from Figure 2.4, when the area per molecule is large, the curve describing the isotherm is almost horizontal. This state of the monolayer is called *gaseous*. With further compression of the monolayer, the distance between molecules

decreases, resulting in an increase of intermolecular interaction and conversion of the monolayer into a liquid state.

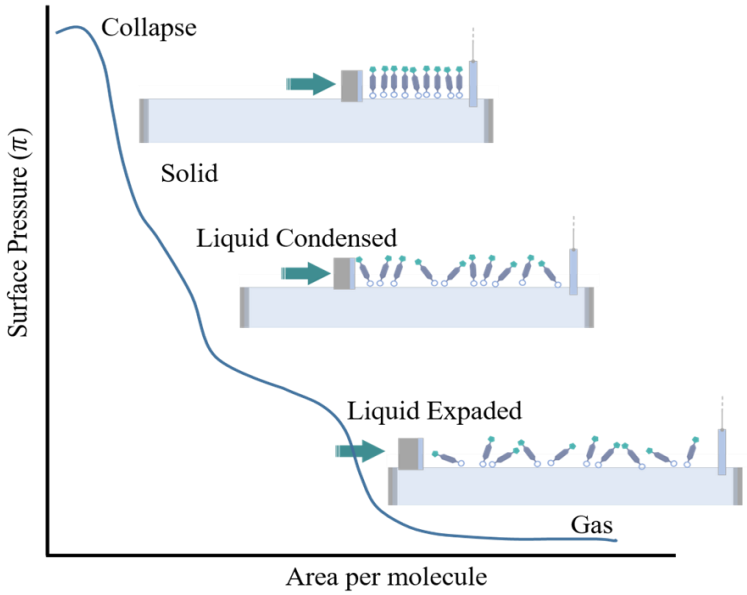

Figure 2.4. Compression isotherm with schematic illustration of monolayer states.

There are two liquid states of the monolayer. The first state is *liquid expanded*, characterized by higher compressibility compared to a conventional liquid. With further compression, the monolayer proceeds to the second state, called *liquid condensed*. At this stage, the compressibility is close to a constant (the dependence is linear), the heads are packed tightly, and the tails are partially ordered. Further compression transfers the monolayer into a *solid* state. The compressibility in this region is constant and close to the compressibility of a solid, indicating dense packing of molecules. If the compression of the monolayer is continued, it goes into a state of collapse, in which the ordering is destroyed, the molecules creep over each other and form a three-dimensional structure.

The resulting dense monolayer of molecules can be deposited in various ways. As shown in figure 2.5, depending on how the substrate contacts the subphase, layers with different molecular orientation can be formed.

This method is actively used for model studies of cell membranes and the creation of sensors because it enables the formation of layers with controlled molecular packaging. Unfortunately, the Langmuir-Blodgett technique does not provide the formation of large-area monolayer, thus its industrial use is difficult.

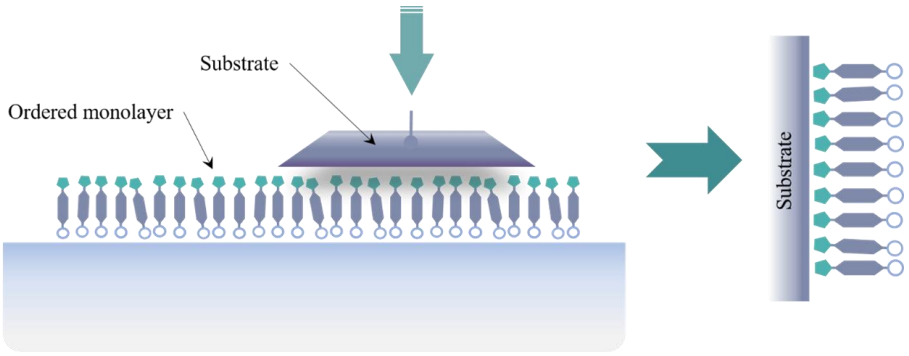

Horizontal deposition.

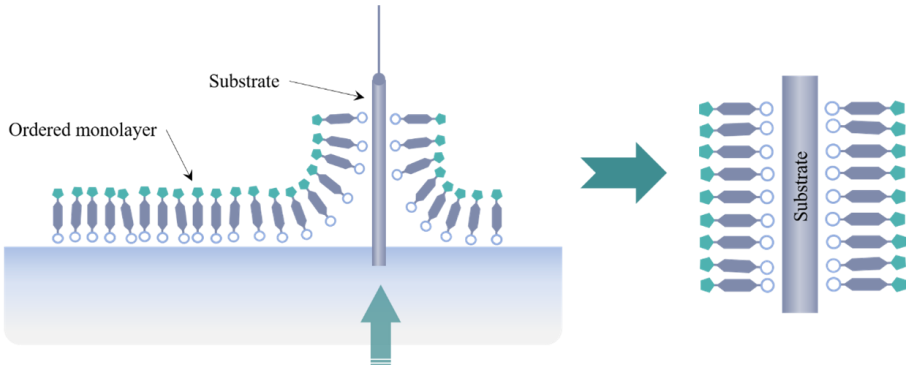

Vertical deposition (upstroke transfer).

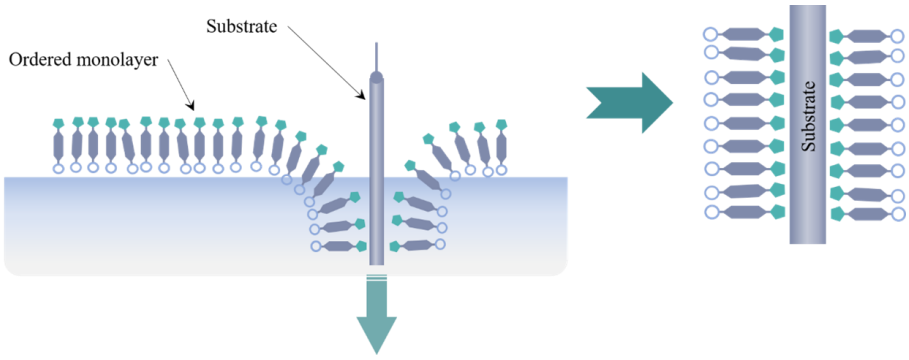

Vertical deposition (downstroke transfer).

Figure 2.5. Schematic illustration of different techniques for the deposition of Langmuir films.

2.1.3 Vapor Deposition

Vapor deposition is a coating process in which materials in vapor state condense onto a substrate to form a thin film. Since the layer is produced by vapor deposition, these processes are highly sensitive to external atmospheric conditions and should be performed in a sealed chamber.

There are two types of vapor deposition processes: *physical vapor deposition (PVD)* and *chemical vapor deposition (CVD)*. In PVD, the source is a solid or liquid material located directly inside the chamber with the substrate and converted into a gaseous phase by a physical process. In the case of CVD, the gases are pumped from an external source, rather than being produced inside the chamber by evaporation of

the material. Thus, the main difference between PVD and CVD is the means through which the vapors are generated. Consequently, there are some distinctions between the films produced by PVD and CVD methods. PVD is generally more directional, meaning there is a priority pathway for the deposition of atoms and molecules to the surface. This can lead to an inhomogeneous distribution of the material, which is especially critical in the case of geometrically complex surfaces (profiles with protrusions and trenches). In contrast, the CVD approach results in a multidirectional distribution of the material, allowing for more uniform deposition. Now that the main differences between PVD and CVD have become clear, we will discuss both methods in detail.

Chemical vapor deposition (CVD). The majority of the elements in the periodic table can be deposited by CVD techniques. The darkened boxes in Figure 2.6 indicate elements that have already been deposited using CVD.

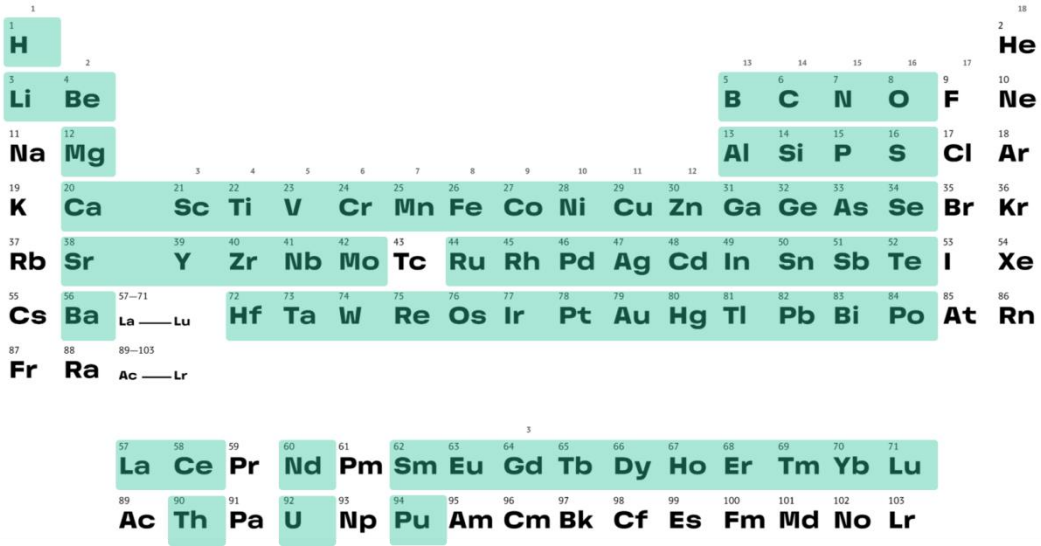

Figure 2.6. Periodic table. Darkened boxes indicate elements that can be deposited using CVD.

CVD includes a wide set of parameters that can be changed, and therefore there are many different types of CVD. For example, some processes are more sensitive and require a higher vacuum while others are not as critical. For this reason, there are different levels of CVD based on pressure. These include atmospheric pressure, low pressure, and ultrahigh vacuum chemical vapor deposition processes. Another way to differentiate CVD processes is by the energy source that initiates the chemical reactions for the formation of a thin film on the substrate. Many CVD processes use heat to help the reaction propagate. The use of high temperatures can increase the deposition rate, improve the crystallinity, and promote otherwise impossible reactions. One of the popular methods in which deposition is stimulated by temperature is metalorganic CVD.

Metalorganic chemical vapor deposition (MOCVD). In the MOCVD method, epitaxial growth of materials on the substrate is realized due to the deposition of products of *thermal decomposition of organic gases* containing the necessary chemical elements (precursors). In contrast to Molecular-Beam Epitaxy (see the subsection 2.1.4), MOCVD is conducted not in a vacuum, but in the presence of gas. Hydrogen or inert gases (helium, argon) are used as a carrier gas. The basic idea of the MOCVD method can be illustrated in Figure 2.7.

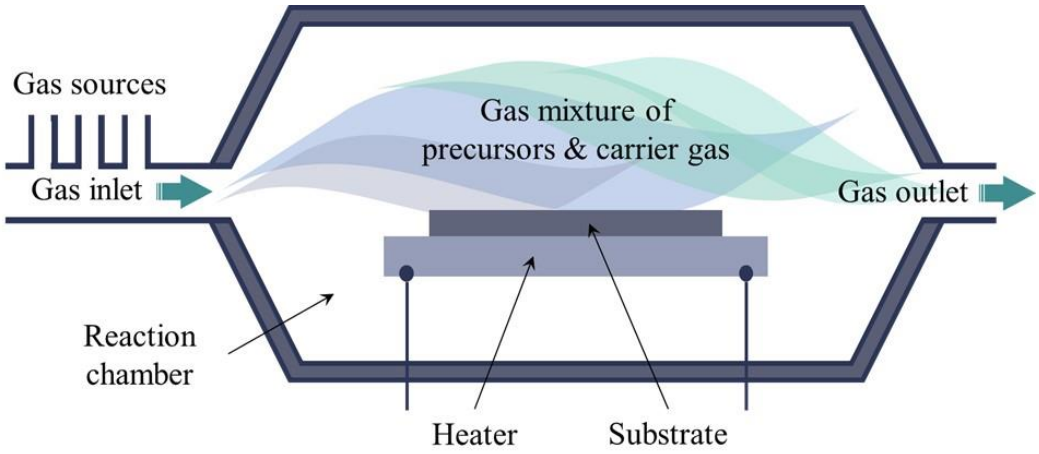

Figure 2.7. Schematic illustration of the chemical vapor deposition horizontal reactor.

A gas mixture of precursors and carrier gas is passed over the heated substrate. As a result, on the hot surface, the gaseous compounds decompose into components, forming a stable solid layer. Using the MOCVD method, multilayer, multicomponent epitaxial structures can be grown sequentially in a single growth cycle: several sources with different precursors (or different precursors concentrations) are connected to the reactor. To change the composition of the gas mixture during the deposition process, the material is supplied sequentially from different sources. If necessary, the chamber is purged with carrier gas to remove excess material and filled with a new gas mixture. Pyrolysis (thermal decomposition of compounds) occurs in a reactor at atmospheric or low pressure. At lower pressures, the deposition is conducted at higher gas flow rates than at atmospheric pressure, which enables the formation of more homogeneous layers. At high flow rates, the change in the gas mixture composition can be performed quite quickly, so that heterojunctions with a clear boundary can be obtained.

Thus, the MOCVD enables to grow structures of sufficiently high quality, whose individual layer thickness is only 5-6 interatomic distances. Another important advantage of this method is the ability to quickly obtain structures of large lateral dimensions with high reproducibility that meet the requirements of mass industrial production.

However, thermally stimulated deposition is not always appropriate. Heating increases the activity of diffusion of elements from the substrate into the film. In

addition, some samples, such as polymers or biological materials, degrade at high temperatures. In such cases, other methods of initiating reactions in the CVD process are used.

Plasma-enhanced chemical vapor deposition (PECVD). PECVD is used to deposit thin films of various materials at lower substrate temperature (up to 350°C) than is required by the traditional CVD method (ranges between 600 and 800°C). In PECVD, source *gases are decomposed in plasma* by the collisions between energetic electrons and gas molecules. Plasma is usually created by a current flowing between two electrodes placed in a filled with reacting gases chamber area. To implement this method, the pressure in the chamber must be very low.

The use of vacuum provides the ability to produce thin chemically stable coatings, to reduce the substrate temperature and the deposition time. But at the same time, it increases the cost of production compared to the standard CVD.

Physical vapor deposition (PVD). PVD is a process in which the source *material is transferred from solid or liquid phase into vapor*, and then deposited onto the substrate where it condenses. The procedure can be performed in a vacuum or a low-pressure gaseous environment. There are two main ways of converting the source substances to the gas phase during the PVD process: *evaporation* under the influence of thermal energy or *sputtering* due to the kinetic energy of particles collision with the surface of source material.

According to the *thermal evaporation* method, the transition of the coating material from solid to vapor phase is performed by heating of an evaporation source. This is usually done by using thermally heated sources (for example, tungsten wire coils) or by a high energy electron beam that heats the source material directly. It is desirable that the source-to-substrate distance is large enough to reduce the radiant heating of the substrate by the evaporation source. Thermal evaporation requires a relatively high vacuum. In addition, the vacuum provides an opportunity to increase the purity of applied layers by reducing the gaseous contamination in the deposition system. A simple thermal evaporation system is shown in Figure 2.8.

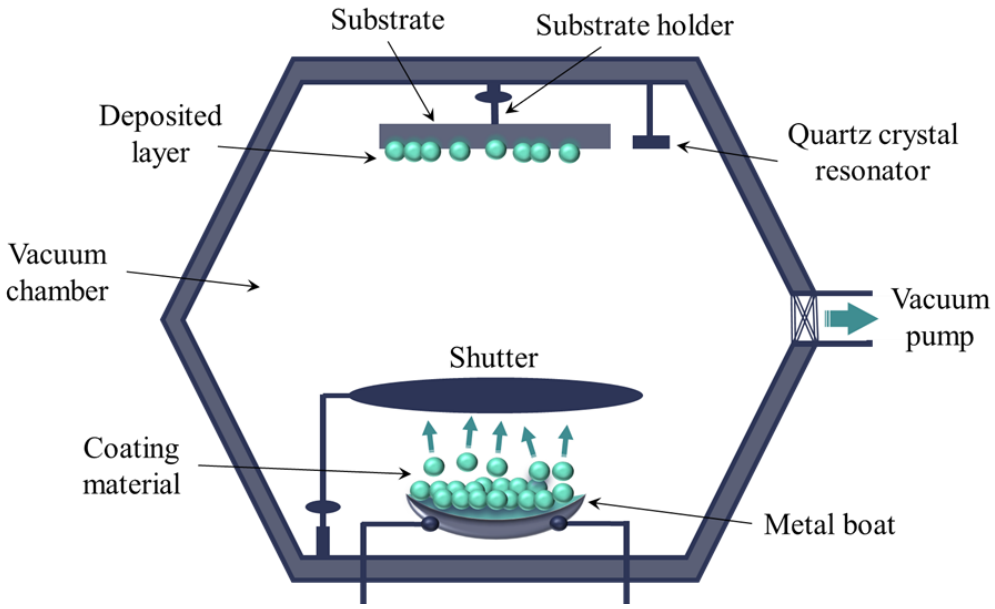

Figure 2.8. Schematic illustration of the operation principle of thermal evaporation.

The sealed chamber is evacuated via the vacuum pump. Electric current heats the metal boat, what leads to the evaporation of contained material. The evaporation process can be controlled by altering the current (i.e., the temperature of the boat) and the shutter position. The shutter is an important element, as it keeps the evaporation source closed during the initial stages of heating, without exposing the substrate to volatile pollutants that evaporate first. It also minimizes radiant heating from the vaporization source. At the initial stages of operation, the shutter is closed. It opens only when the required temperature of the boat is reached, and the coating material has already started to evaporate. As soon as the film grows to the desired thickness, the shutter closes. In some PVD setups, the substrate holder can rotate or tilt relative to the vertical axis, which allows growing more uniform layers. The thickness of an evaporated film is controlled by the thickness monitor based on a quartz crystal. It measures variation of mass on the surface of a quartz crystal resonator.

Sputtering is a non-thermal vaporization process that uses charged particles to bombard a target made of a coating material. The target atoms are knocked out by high-energy particles and deposited onto the substrate surface. Generally, the source-to-substrate distance is short compared to the vacuum deposition. The basic idea of this method can be understood by considering the operation principle of *plasma sputtering* (Figure 2.9).

The sealed chamber is filled with a carrier gas (for example, argon). Due to the high voltage supply, the gas is transferred to the plasma state. The positively charged ions move towards the cathode (the target of the coating material) at high velocity and knock out the target atoms.

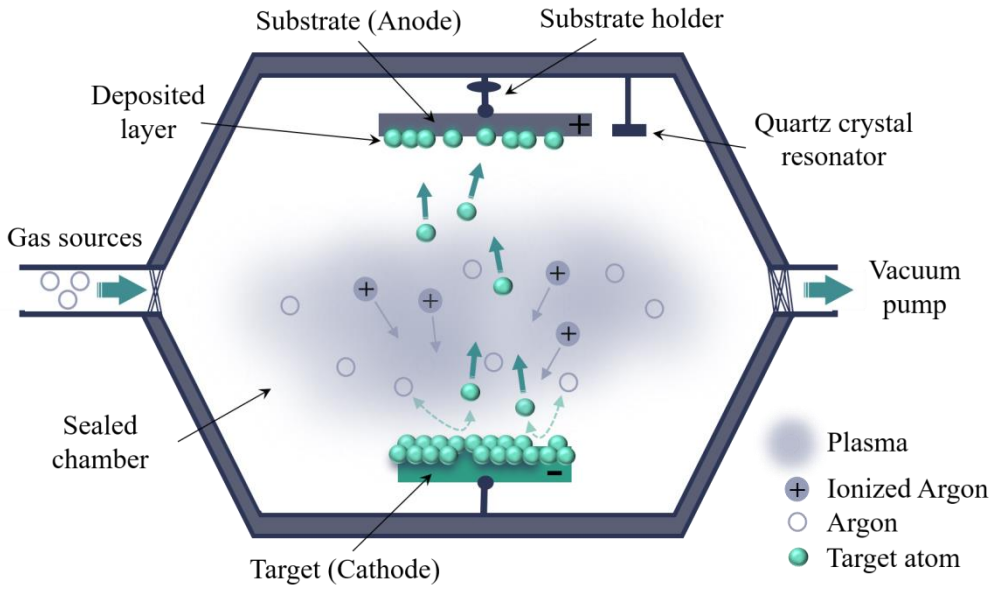

Figure 2.9. Schematic illustration of the operation principle of plasma sputtering.

2.1.4 Molecular-Beam Epitaxy (MBE)

Molecular-beam epitaxy (MBE) is an improved version of *thermal evaporation*. The main feature of the MBE is a very low deposition rate (usually several Å per second), implemented by the sublimation of extremely pure solid elements previously evaporated from the separate effusion cells. To reduce the number of impurities, the epitaxial growth is performed in ultrahigh vacuum (UHV) conditions. The idea of the method can be understood by considering the schematic illustration of the MBE system shown in Figure 2.10.

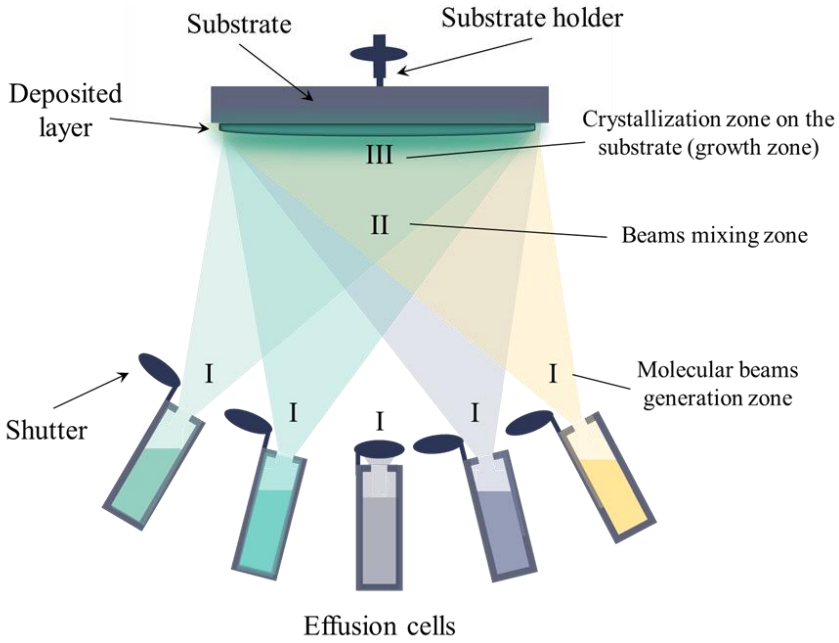

Figure 2.10. Schematic illustration of the MBE system.

The *high purity materials* (purity ~99.9999%) are placed in the effusion cells (crucibles with a hole, acting as sources of deposited material). Due to the heating of the effusion cells, the materials placed there evaporate and enter the generation zone (I) in the gas phase. From there, the streams of atoms (molecules) fall into the mixing zone (II). Further, the resulting gas mixture rushes to the growth zone (III), where it is deposited onto the substrate. The number of effusion cells used in the MBE depends on the number of unique components needed to create the desired coating. For example, to grow pure elementary semiconductors of silicon (Si) or germanium (Ge), only one cell is required. If a doped semiconductor is needed, then at least one more cell must be added for the alloying impurities. It is obvious that to obtain films of complex semiconductors, a separate cell is required for each component. In front of the outlet openings of the effusion cells, there are movable shutters that block certain streams of particles, thereby enabling control of the composition of the grown film.

The temperature of the effusion cell affects the stream of particles directed to the substrate, and therefore it is carefully controlled. If the structure growth requires a sharp change in the concentration of the same impurity, then several effusion cells with an alloying substance are used, heated to different temperatures. In some MBE setups, the substrate holder can rotate, which allows growing more uniform layers.

It is worth noting that *the quality of the epitaxially grown layers* depends on the chemical purity and smoothness of the substrate surface. Thus, before the deposition process, the substrate is thoroughly cleaned. Cleaning can be performed in several stages, which may include, for instance, mechanical polishing, chemical etching, and boiling in organic solvents.

The temperature and surface properties of the substrate, coating materials, deposition rate, and other parameters determine the processes involved into the epitaxial growth, and therefore strongly influence the morphology of the resulting nanostructure. Figure 2.11 illustrates schematically possible types of atomic (molecular) packing of the grown system. For example, if the temperature of the substrate is low, the atoms tend to remain at their landing point and *form amorphous layers* (Figure 2.11, left). Another situation, shown in Figure 2.11, middle, is an example of «layer-by-layer» growth. The temperature of the substrate is low enough for the *two-dimensional layers* to grow, but not so low as to prevent the possibility of single atoms to move along the surface or re-evaporate. With other settings, the film initially forms *a three-dimensional* cluster on the substrate (Figure 2.11, right), which subsequently enables the formation of structures where the electrons can be confined in space, giving quantum wells or even quantum dots.

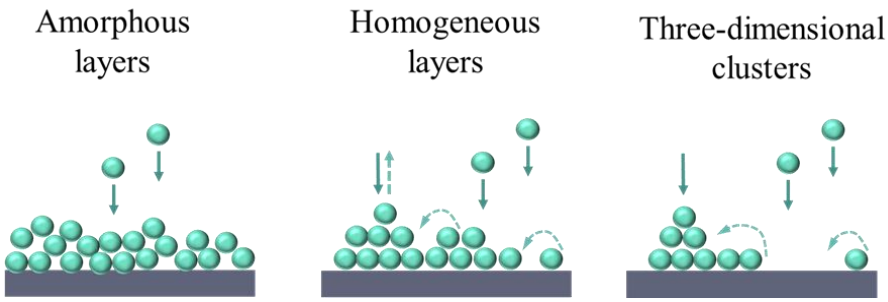

Figure 2.11. Schematic illustration of surface processes that occur during the MBE growth.

The main advantage of the MBE is the ability to produce nanostructures with very high purity, uniformity, sharp interfaces, and a small number of defects. The obvious disadvantages of the method are the high cost of equipment and materials, extremely low growth rate, and the need to maintain ultrahigh vacuum throughout the entire process. As a result, it is a very resource- and time-consuming method of nanofabrication.

2.1.5 Synthesis of Colloidal Quantum Dots

Colloidal quantum dots (QDs) are not tightly bound to any matrix or substrate, and therefore they are extremely attractive nanoobjects from the application point of view. They can be embedded in a variety of matrices, planted on various surfaces, connected to other nanoparticles or molecules, and used as "building blocks" in the development of devices.

Their properties are markedly different from those of epitaxially grown QDs. The clear advantages of colloidal QDs are the high fluorescence quantum yield, narrow emission spectrum, and strong optical absorption. Besides, the synthesis process of colloidal QDs provides better control over the shape and composition of semiconductor nanocrystals compared to epitaxial growth.

The most successful method for producing colloidal nanocrystals with high quantum yield and low size dispersion is organometallic synthesis. This method utilizes organic solvents with a high boiling point and is used to obtain bright and stable hydrophobic nanoparticles. Nevertheless, the majority of practical applications require water-soluble samples. Therefore, in addition to a brief review of the synthesis, we will also discuss the difficulties associated with the transfer of quantum dots into polar solvents.

Organometallic synthesis involves combining an organometallic precursor with a corresponding chalcogen precursor in a boiling solvent at high temperatures. Figure 2.12 shows a schematic illustration of the main synthesis steps of CdSe/ZnS quantum dots.

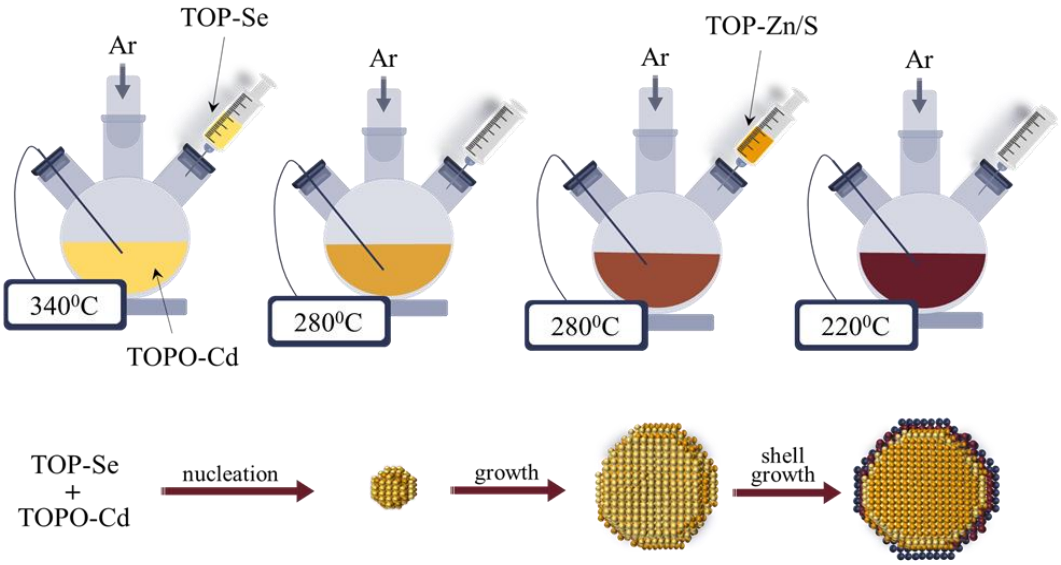

Figure 2.12. Schematic illustration of the main steps of the organometallic synthesis of CdSe/ZnS core-shell quantum dots.

The basic setup for producing colloidal nanocrystals includes a three-necked flask, an electromagnetic stirrer with a heating plate, a thermometer or thermocouple to control the solution temperature, and argon gas supply systems to avoid oxidation of organometallic salts. In a standard procedure, the CdSe/ZnS QD synthesis begins with the rapid injection of selenium (Se) and cadmium (Cd) precursors into a boiling solvent at a high temperature (~340 °C). Typically, the solvents are trioctylphosphine oxide (TOPO), trioctylphosphine (TOP), and octadecene which have high boiling points. Then the growth phase begins. CdSe nanocrystals with a diameter of approximately 2 nm are formed within a few minutes. Next, the temperature is reduced to ~280 °C and kept stable until the QDs reach the required size. The QD size can be monitored during the growth period by measuring the luminescence wavelength of aliquots (a small portion of the QDs solution taken from the flask) collected at various intervals. When the desired nanocrystals size is reached, the solution is cooled down to the room temperature and the resulting product is removed from the flask.

To improve the fluorescence quantum yield, the QD surface can be passivated with an inorganic capping layer—the so-called shell. In a typical procedure for the ZnS shell growth, TOP-dissolved zinc (Zn) and sulfur (S) precursors are injected into the QD solution at a temperature of ~220 °C. Different shell materials can be used for different types of colloidal nanocrystals to alter the nanocrystal optical properties. For instance, passivation of the QD surface with the wide-bandgap material enables better localization of the charge carriers within the QD core, which increases the probability of their radiative recombination.

The colloidal nanocrystals synthesized in a way as discussed above have a CdSe core with a diameter of 2 to 6 nm and a ZnS shell with a thickness of 1–2 monolayers.

Typically, they have a narrow size dispersion (<5%) and a high luminescence quantum yield in hexane (>50%). Even though the synthesis must be performed in an inert atmosphere to avoid oxidation of organometallic salts, prepared QDs are stable in air. Unfortunately, the QDs obtained by the discussed chemical synthesis are insoluble in water, which significantly limits the range of their potential applications. To obtain water-soluble quantum dots, the surface of nanocrystals is modified by attaching special molecular groups.

Various ligand exchange schemes have been developed to make hydrophobic quantum dots soluble in polar solvents (after synthesis, the quantum dots can be suspended in water rather than dissolved). However, it is important to keep in mind that during the transfer, the quantum dots are vulnerable to oxidation and formation of the surface trap states, which dramatically reduces their quantum yield. For example, CdSe/ZnS QDs exhibit a reduction in luminescence quantum yield, from 50% to 20±10%, when TOPO ligands are replaced by hydrophilic ligands.

2.1.6 Self-Organization of Quantum Dots

The *self-assembly* provides an opportunity to create aggregates with extremely diverse geometries from disparate components. Systems with different chemical compositions and shapes (e.g., molecules, quantum dots, nanoparticles, etc.) can act as building blocks for self-assembly. Using the method, these components can be gathered into homogeneous layers, as well as more complex structures (various linear, branching planar structures, three-dimensional particle clusters of different shapes and internal organization). Self-organization of fluorophores or quantum dots into layers enables the creation of stable luminescent coatings that can be used as elements of imaging systems or sensors. The packaging of nanoparticles into three-dimensional structures that resemble soap foam gives the opportunity to produce porous materials with exceptional thermal insulation properties. The variety of possible applications of self-assembly is unlimited.

Since the elements are assembled into ordered structures by themselves, this technology should not require expensive installations, highly skilled specialists, and should be relatively fast. All of this explains the extreme attractiveness of the use of self-organization in mass production.

Among the different nanocomponents, *colloidal quantum dots (QDs)* are especially appealing in the creation of ordered assemblies. It is caused by several factors. The clear advantages of colloidal QDs over organic fluorophores are their high fluorescence quantum yield (may approximate 70–85%), high photostability, and strong optical absorption. By changing the size, shape, and surface molecules of nanocrystals, it is possible to control the self-organization process more precisely and fabricate a variety of ordered structures (which is not available in the case of

molecules). In addition, in the self-assembly of nanoscale components, interactions can include such mechanisms as gravitational attraction, external electric and magnetic fields, or capillary interactions, which are not relevant in the case of molecules. These interaction mechanisms provide new ways to control the structure growth. Finally, the size dependence of the optical, electrical, and magnetic properties of individual nanocrystals allows us to control the corresponding parameters of the created ensembles. All these features make the quantum dots attractive as building blocks for self-assembly.

It is worth noting that the growing popularity of research on the nanocrystals self-organization has been significantly stimulated by breakthroughs made in the development of the QD synthesis. An example of a modern well-developed method for the fabrication of QDs is the high-temperature organometallic synthesis described in the previous section.

In *self-assembly experiments*, colloidal solutions of nanocrystals in organic solvents (ethanol, acetone) are usually used. In this case, self-organization is determined by the combined action of Van der Waals, dipole-dipole, gravitational, capillary forces, as well as surface tension. The experiments demonstrated the principal possibility of nanocrystal self-assembly at the liquid/air, liquid/liquid, and liquid/solid interfaces. Using these approaches, nanowires, dendrite-like structures, two-dimensional hexagonal lattices, and dense spherical clusters (0.2–2.0 microns) were formed. The images of these structures are shown in Figure 2.13.

Early studies of the QD-based self-assembly systems have revealed the field of their potential application, that is, conversion of the *solar energy*. The amount of solar energy available for consumption exceeds all alternative renewable energy sources (wind, geothermal, wave energy and hydropower). Unfortunately, currently available solar cells (for example, the ones based on single-crystal or amorphous silicon cells) are extremely expensive to produce and have relatively low efficiency (~20%). Therefore, the development of more efficient materials for solar energy is still an urgent challenge.

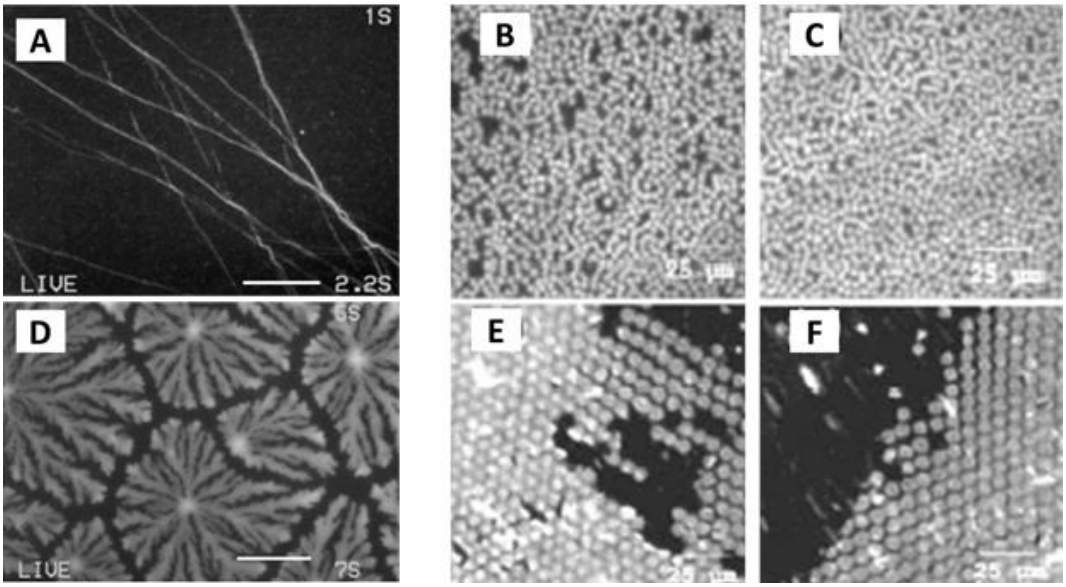

Figure 2.13. Fluorescent images of A) nanowires and D) dendrites formed by water-solubilized CdSe/ZnS quantum dots and quantum rods, respectively [2.1]. Fluorescent images of B), C) dense spherical clusters of CdSe/ZnS quantum dots, and E), F) regular hexagonal lattices of quantum rods formed under different self-assembly conditions [2.2].

A *solar cell* must be capable of absorbing, accumulating, and transferring the light energy. It is well known that quantum dots effectively absorb energy in the visible and UV range, which accounts for a significant part of the solar radiation reaching the Earth's surface. The solar radiation spectrum is shown in Figure 2.14.

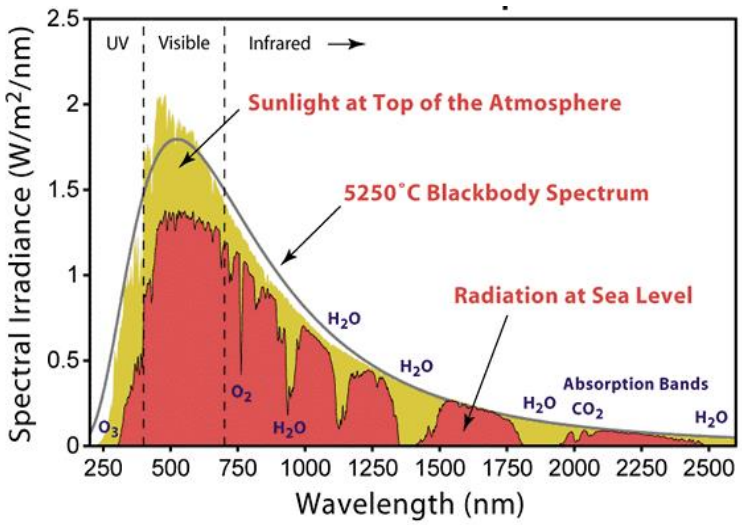

Figure 2.14. Solar radiation spectrum [2.3].

However, despite effective absorption, colloidal QDs cannot perform the other two functions of solar cells. To implement the accumulation and transfer of light energy, dendrite-like structures were formed from CdSe/ZnS nanocrystals by self-assembly. Experiments demonstrate that for closely spaced nanocrystals of various sizes, there is an effective nonradiative energy transfer from smaller particles to larger

ones. Subsequent studies have confirmed that interstructural energy transfer is a characteristic property of self-organized structures of densely packed non-monodisperse nanocrystals. Moreover, by controlling the self-organization of nanocrystals, it is possible to create hierarchical structures whose morphology provides a cascade energy transfer along the structure or from the peripheral regions of the structure to the center (in the dendrites). Such dendrites formed as a result of the evaporation of a colloidal aqueous solution on the modified slide surface are shown in Figure 2.13D.

It is worth noting that the self-organization of nanostructures can be performed not only at the flat phase boundaries. There is a huge variety of approaches that involve the employment of different elements and lead to the formation of various structures. For example, in recent years, methods of QD self-assembly based on the use of a liquid crystal solvent have been developed. The corresponding approach was presented in 2019 [2.4]. The two main elements used in this research were nematic liquid crystal and ligand-modified CdSe/ZnS (core/shell) quantum dots.

According to the method, the liquid crystal solvent undergoes a nucleation process on cooling through the isotropic–nematic phase transition, in which the dissolved in liquid crystal QDs act as impurities. During nucleation, QDs spontaneously segregate to the surface of the isotropic domains, thus forming hollow 3D microstructures: spheres, foams, and tubular networks (Figure 2.15).

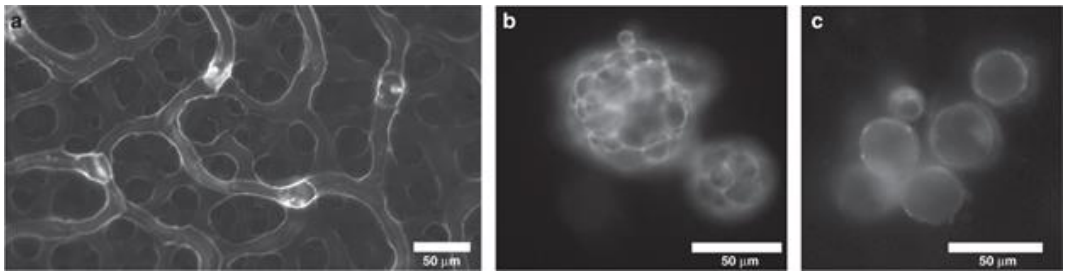

Figure 2.15. Fluorescence microscopy images of distinct quantum dot structures formed under different conditions: a) branching network of tube-like structures; b) multi-compartment droplets of foam; c) single compartment hollow capsules [2.4].

Observations revealed that the final structure type and size could be controlled by varying either the particle concentration or the cooling rate. However, there are great difficulties in controlling the mechanisms that provide self-organization of colloidal nanocrystals. In addition, there are still no proper models that explain the relationship between the morphology of structures and their optical properties. Therefore, the development of a simple method that enables the creation of ordered structures with reproducible properties is still an important challenge of nanotechnology.

§ 2.2 Top-Down Approach

According to this approach, a certain volume of material is processed to obtain a nanoscale structure with the desired parameters. Some top-down methods resemble carving a sculpture out of marble, others represent sequential grinding processes similar to milling of flour. But the basic idea is the same: nanofabrication is carried out in a *downward* direction, from a large piece of material to nanoscale objects.

2.2.1 Photolithography

Photolithography is a delicate surface microfabrication method that allows selective removal of material from the upper layers of an object. There are several different photolithography techniques. Schematic illustration of the photolithography process is shown in figure 2.16.

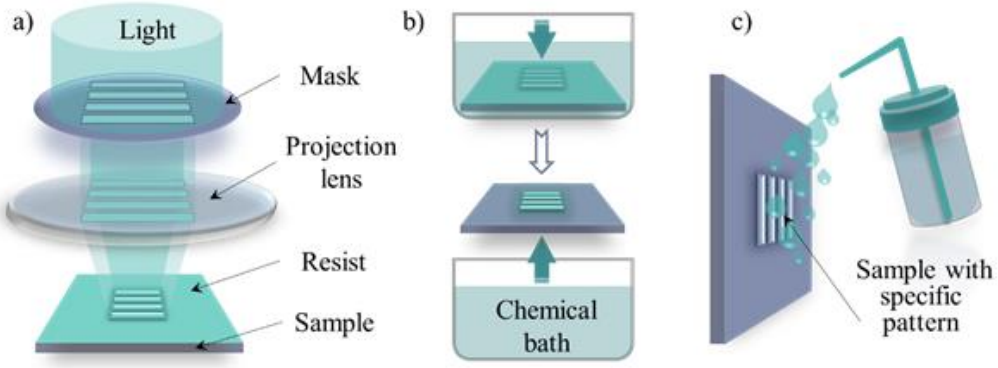

Figure 2.16. Main technological stages of photolithography. Schematic illustration of (a) exposure of the resist through the mask, (b) etching of the resist and sample surface in a chemical bath, (c) washing the sample from the resist and chemical residues.

At the first stage, the sample is prepared. Its surface is thoroughly cleaned and covered with a resist. Resists are usually polymer compositions that are sensitive to radiation (optical, X-ray, ion, or electron).

Further, the prepared sample is combined with a mask. The mask is a stencil with transparent and nontransparent areas for radiation, the pattern of which will be transferred to the surface of the sample. There are two ways of mutual positioning of the mask and the resistor, in which the image is transferred without changing its size: 1) *contact*—the mask is put in contact with the resistor, 2) *with a gap*—the mask is located at a small distance from the surface of the resistor. In practice, the third configuration is more often implemented: 3) *projection*—the focusing lenses are placed between the mask and the resistor to reduce the size of the projected image. The corresponding scheme is shown in figure 2.16.

The next step is the *exposure* of the photosensitive material through the mask. The light illuminates the mask and projects the "pattern" of the mask onto the surface of the resist. Irradiation leads to formation or rupture of chemical bonds between the

resist molecules, and, as a result, the properties of the resist (solubility, chemical resistance) change. Depending on the nature of the corresponding reactions, resists are divided into positive and negative. In *negative resists*, the structure polymerizes due to the radiation, and the solubility of the resist in the irradiated areas decreases. In *positive resists*, on the contrary, the bonds between the polymer molecules are broken in the irradiated areas, and the solubility of the resist increases.

After exposure, the treated sample is placed in a chemical bath (usually an acid bath). The *negative resist* remains on the surface of the substrate after the manifestation, and areas of material that have not been exposed to light are etched (Figure 2.17, right). In the case of *positive resist*, the irradiated areas are removed, and the non-irradiated areas remain on the substrate (Figure 2.17, left).

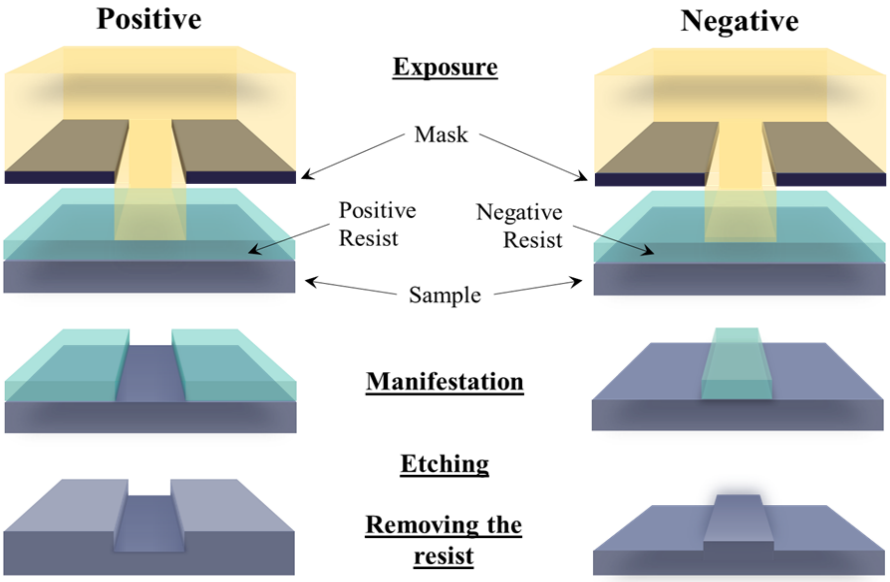

Figure 2.17. Operation principle of the positive and negative resists.

Finally, the resist is removed, and the sample is washed from chemical residues and dried. On the surface of the sample there is a profile repeating the pattern of the mask. Photolithography is actively used in the semiconductor industry for mass production of devices, as it allows to create elements with linear dimensions of several tens of nanometers.

The resolution in lithography is determined by the wavelength of the incident radiation, the aperture of the lenses used, as well as the processes occurring in the resist and on the substrate. The minimum size of the object that the projection system can transfer to the resistor can be approximately determined by the Rayleigh criterion:

$$CD = k \cdot \frac{\lambda}{NA}, \qquad (2.1)$$

where *CD* is the critical dimension (minimum feature size), λ is the wavelength of the radiation used, and *NA* is the numerical aperture of the lens, *k* is the coefficient that includes corrections related to the specifics of a particular experiment and varies from 0 to 1.

According to this equation, the minimum feature size can be decreased by decreasing the wavelength. Depending on the radiation used, the following types of lithography are distinguished:

- Photolithography (light, λ ~200–450 nm);
- X-ray lithography (X-rays, λ ~0.01–1 nm);
- Electron beam lithography (focused beam of electrons, λ ~1–0.001 nm);
- Ion beam lithography (focused beam of ions, λ ~0.05–0.1 nm).

Depending on the particles that are used to bombard the sample, the technological solution of the lithographic installation elements changes. For example, electron or ion beams cannot be controlled with conventional optical lenses. Electromagnetic lens systems are used to control the flow of such particles. The choice of a particular installation for lithography is carried out depending on the sample properties and the requirements for the final product, however, the general idea of the method remains the same.

§ 2.3 Synthesis of Fullerenes, Carbon Nanotubes, and Graphene

Carbon can be found in nature in its elemental form as graphite, diamond, and coal. The first one is opaque, soft, and conductive, while the second is transparent, hard, and insulating. By simply comparing only these two forms, we can conclude that carbon exhibits fundamentally different properties depending on its structure.

The property of chemical elements to exist in two or more different forms is called *allotropy (or allotropism)*, and the various structural modifications of a given element are called *allotropes*. The diversity of the crystal lattices arises due to the existence of several available hybridizations. In the case of carbon, sp, sp2, sp3, and even intermediate hybridization are possible (Figure 2.18).

The allotropes of carbon are not restricted to graphite, diamond, and coal. In this section, the most prominent nanoscale carbon allotropes will be briefly considered. The synthesis techniques and properties of fullerenes, nanotubes, and graphene will be discussed, as well as a historical overview of their discovery.

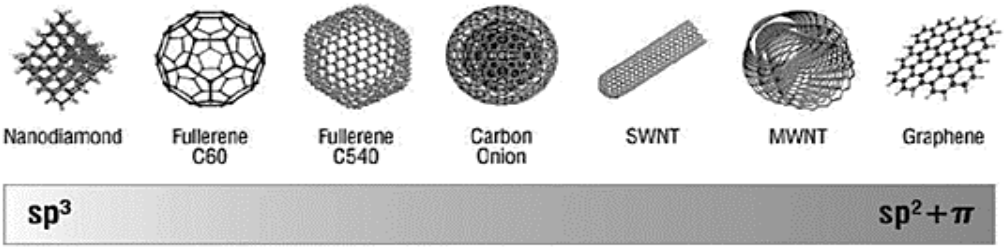

Figure 2.18. Hybridization states of carbon-based nanomaterials: single-walled carbon nanotubes (SWNTs) and multi-walled carbon nanotubes (MWNTs) [2.5].

2.3.1 Fullerenes

These carbon allotropes were independently predicted and theoretically studied by Japanese (Osawa E.) and Russian (Bochvar D.A. and Halpern E.G.) researchers in the 1970s. However, they were physically obtained only in 1885 by Kroto H., Smalley R., and Curl R. The *first fullerenes* were an unexpected product of laser evaporation of carbon from a graphite target, accidentally discovered during laser spectroscopy experiments. The mass spectrometry detected lines from C_{60} (as the dominant reaction product) and several lines from C_{70}. The nuclear magnetic resonance showed that C_{60} was a spherical structure (~ 10 Å diameter) composed of 60 carbon atoms. As presented in Figure 2.19, the C_{60} fullerene crystal lattice is organized similarly to a soccer ball and consists of 12 pentagons and 20 hexagons.

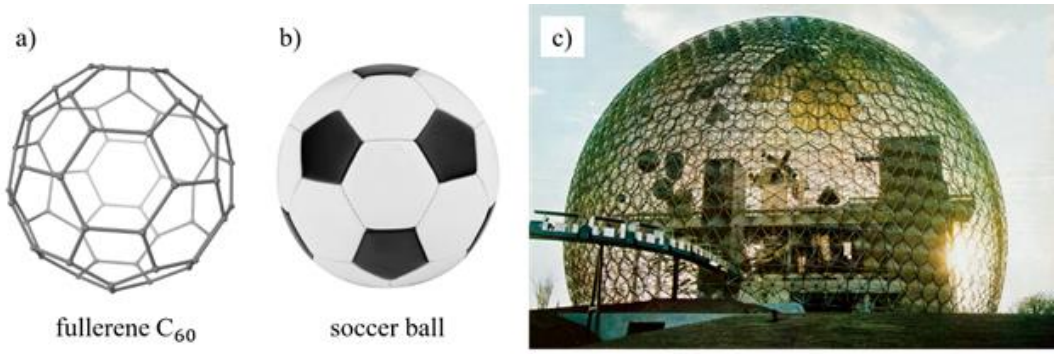

Figure 2.19. Comparison of the structure of a) fullerene 60, b) a soccer ball, and c) an architectural structure designed by Buckminster Fuller.

This visual similarity explains why in literature this structure is sometimes called a *Bucky ball*. The "Bucky part" and the name fullerene (C_{60}) were inspired by the resemblance of the molecule to the architectural structures, designed by Buckminster Fuller (Figure 2.19.). It had exceptional load-bearing qualities and brought the author international recognition. In 1996, the Nobel Prize in chemistry was awarded jointly to Kroto H., Smalley R., and Curl R. *"for the discovery of fullerenes*", which firmly attached the name fullerene to this structure.

The first method to synthesize fullerenes involved laser evaporation of carbon in an inert atmosphere. This technique provides the ability to produce very small amounts of fullerenes and is more suitable for research purposes.

An upscaled *method for the fullerene synthesis* (several grams per day) was developed by Kratschmer et al. This technology involves passing an arc discharge between high-purity graphite rods in an inert atmosphere. For the fullerene formation, a temperature of about 2000 °C is required. At this temperature, the carbon evaporates and forms the fullerene-containing soot that condenses onto the reactor's cool walls. Usually, the concentration of fullerenes in the soot is about 15% (~13% C_{60} and ~2% C_{70}). The mixture of fullerenes obtained as a result of the synthesis is called fullerite. The composition of fullerite includes various crystal formations: not only C_{60} and C_{70} but also a small amount of higher fullerenes (up to 3%). C_{76}, C_{78}, C_{84}, and even larger clusters, such as C_{240} and C_{330}, can be produced during the synthesis.

Since the processes in the region of arc combustion are thermodynamically unstable, the mechanism of fullerene formation in the arc is still unclear. At least, it was proven that a fullerene is assembled from individual carbon atoms (or C_2 fragments). In the corresponding experiment, graphite of a high degree of purification (13C) was used as the anode electrode, the other electrode was made of ordinary graphite (12C). Nuclear magnetic resonance spectroscopy showed that the 12C and 13C atoms in the synthesized fullerenes are located randomly. This indicates that graphite initially decays to individual atoms and only then forms into fullerene molecules.

Unfortunately, despite active attempts to optimize the method, it is extremely difficult to exceed the fullerene yield in 20% of the total mass of burned graphite. This result seems especially unattractive, considering the high cost of the initial product (pure graphite). It should be noted that the high cost of fullerenes is determined not only by their low yield but also by the complexity of fullerene purification from the soot and separation of fullerenes with different masses from each other. Therefore, the efforts of many research groups are aimed at finding alternative methods for the fullerene production.

2.3.2 Carbon Nanotubes (CNTs)

Carbon nanotubes are graphite sheets rolled up into tubular structures. Typically, they have a nanometer diameter and a length of up to several centimeters. CNTs are divided into two types: *single-walled carbon nanotubes (*SWNTs*)* and *multi-walled carbon nanotubes (*MWNTs*)*. SWNTs consist of single layers of graphene and their diameter ranges from 0.4 to 3 nm. MWNTs are made of several concentric cylinders of graphene layers, with a distance between adjacent shells of about 0.34 nm.

The way the graphene sheet is rolled up determines the transport properties, especially the electronic properties of a CNT. It is described by the so-called chiral vector, whose components are denoted as a pair of indices (n,m). The integers n and m represent the number of unit vectors along the two directions in the honeycomb crystal lattice of graphene, as shown in Figure 2.20.

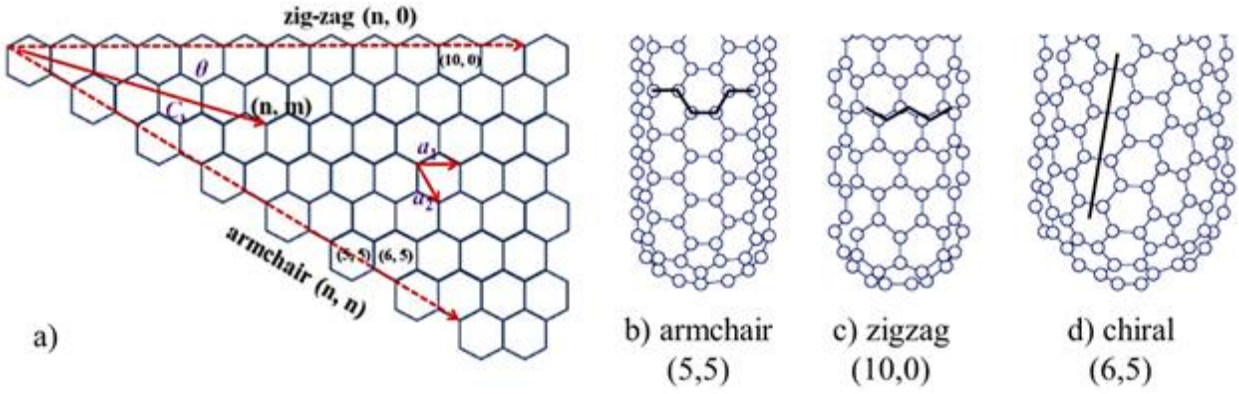

Figure 2.20. a) Schematic illustration of a graphene sheet and its corresponding chiral vector (n,m) [2.6]. Schematic illustrations of three nanotube types: b) armchair, c) zig-zag, and d) chiral [2.5].

If n = m, the SWNT configuration is called armchair; if m = 0, it is zig-zag, otherwise, the nanotubes are chiral. For a given SWNT, if (2n+m) is a multiple of 3, then the SWNT is metallic; otherwise, it possesses semiconductor properties. In the case of MWNTs, where each layer can have its own chirality, the prediction of electronic properties is much more difficult.

The first evidence of the CNT existence was reported back in 1952 by Radushkevich and Lukyanovich in the Soviet Journal of Physical Chemistry. The hollow graphite carbon fibers with 50 nm in diameter were described there. However, due to the Cold War and the fact that the journal was published in Russian, this important discovery remained unknown to the world scientific community.

Worldwide interest in carbon nanotubes was aroused by Iijima's work. The structures that he obtained consisted of several coaxial tubes (from two to seven concentric graphene cylinders) with an external diameter from 5.5 nm (two graphene cylinders) to 6.5 nm (seven graphene cylinders). The ends of these tubular structures were formed by the fullerene halves. Partly, Iijima's work attracted so much attention because it appeared soon after the discovery of fullerenes.

Currently, the most common technology for carbon nanotubes manufacturing is the thermal sputtering of graphite electrodes in an arc-discharge plasma. In the *arc-discharge method*, a high current passes through an opposing carbon anode and cathode located in a chamber with helium. As a result, the helium goes into the plasma state and evaporates the carbon from the anode. Then the vaporized substance is deposited on the cathode surface, where the formation of carbon nanotubes takes place. During

the synthesis, about 90% of the anode mass is deposited on the cathode. The resulting nanotubes have a length of about 40 microns. They grow on the cathode perpendicular to its surface and, due to the strong Van der Waals interaction, assemble into cylindrical bundles with a diameter of about 50 microns. Nanotube bundles cover the surface of the cathode regularly, forming a honeycomb structure. It can be detected with the naked eye by examining the layer deposited on the cathode. The space between the nanotube bundles is filled with a disordered mixture of nanoparticles and single nanotubes. The content of nanotubes in the carbon deposit can reach 60%. Ultrasonic dispersion is used to separate the components of the resulting deposit. As a result of long-term processing, a light, porous material is obtained, consisting of MWNTs with an average diameter of 20 nm and a length of about 10 microns. The technologies for producing nanotubes are quite complicated and inefficient (several grams per day), so nanotubes are currently a very expensive material.

2.3.3 Graphene

Graphene is a carbon allotrope that consists of a single atomic layer of carbon atoms bonded together in a honeycomb (hexagonal) lattice. Three extremely strong in-plane σ-bonds provide the mechanical stability of the carbon sheet. The π-orbitals, perpendicular to the plane of interaction of graphene with the substrate or between the graphene layers, are responsible for the electronic conductivity. The thickness of the graphene layer is 0.34 nm and a carbon–carbon distance is 0.142 nm (Figure 2.21).

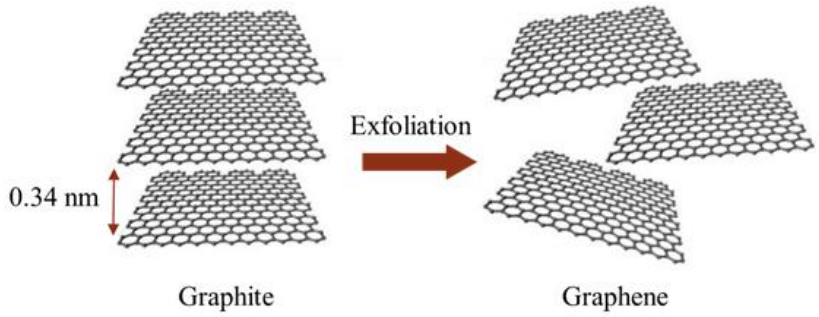

Figure 2.21. Schematic illustration of graphene production.

The idea of creating a strong monolayer formed by carbon atoms was often discussed in scientific papers, however, for a long time, graphene remained only a theoretical model. In 2004 a physicists group led by Andre Geim and Konstantin Novoselov used a mechanical exfoliation approach to obtain graphene. Soon, in 2010, they won the Nobel Prize in Physics *"for their groundbreaking experiments on the graphene material"*. The successful experience of producing isolated graphene monolayer has attracted wide attention to this carbon nanomaterial.

As already mentioned, graphene flakes were first produced by mechanical exfoliation of graphite sheets from a bulk graphite crystal. The graphite was cleaved using ordinary adhesive tape (scotch tape), after which the thinned graphite was transferred to a purified oxidized silicon substrate. The process began with three-dimensional graphite and ended with a single sheet (a monolayer of atoms). Until now, mechanical exfoliation of graphite is the best method to provide a small amount of high-quality samples for scientific purposes. However, it is necessary to develop new, more productive methods to ensure a high yield of graphene for industrial production.

Check Questions

1. Which stages can be seen on the compression isotherm of the Langmuir-Blodgett technique?
2. Describe the principle of photolithography.
3. What is the key difference between physical and chemical vapor deposition methods?
4. Describe the stages of organometallic synthesis.
5. What is the purpose of molecular beam epitaxy? How does it work?
6. What forces determine the self-assembly of quantum dots?
7. What are the methods for obtaining graphene?

CHAPTER 3. DETERMINATION OF MORPHOLOGY

By *morphological properties* of nanostructures, we usually mean their shape, size, crystal lattice parameters, and, in case of composite structures, mutual arrangement of single particles. In other words, when studying morphology, we aim to determine (ideally) the position of all atoms that make up the nanostructure of interest—that would give us all we want to know at once. In practice, however, we are limited by the capabilities of the devices and instruments that we use.

All the experimental approaches for studying the morphology of nanostructures can be roughly divided into several categories by the underlying physical or engineering principle.

Optical microscopy, for instance, utilizes visible light for the image formation. It is a nondestructive approach that allows for determination of the sample geometry, although its resolution (the power to resolve two closely spaced point objects) is limited by the diffraction of light. The family of microscopic techniques includes, but not limited to, *bright-field*, *dark-field*, *fluorescence*, and *super-resolution* techniques. The latter are especially interesting in nanoscience.

Electron microscopy is different from the optical microscopy in a way that the electron beam rather than the light ray is used to probe the material. As the wavelength of an accelerated electron is much shorter than of the visible light, the resolution of an electron microscope can be as high as 0.05 nm. Such resolution allows for the determination of crystal lattice parameters, i.e., symmetry and lattice constants.

The family of *scanning probe microscopy* implies direct analysis of the material surface. It includes, for instance, *scanning tunneling microscopy* and *atomic force microscopy*. These methods allow for characterization of the surface profile; hence they are widely used to study thin films and nanoparticles deposited on substrates.

Scattering is another physical phenomenon that is also effectively implemented to study the morphology of various nanostructures. The *X-ray scattering techniques*, including *wide-angle X-ray scattering* (WAXS) and *small-angle X-ray scattering* (SAXS), as well as *dynamic light scattering* (DLS), are highly relevant experimental methods in nanoscience. In WAXS, high-energy photons undergo diffraction on the crystal lattice, and the resulting pattern allows for the determination of the lattice parameters. SAXS, on the other hand, as well as DLS, enables the study of structural features on the nanometer scale.

In the present chapter, we are going to discuss all the mentioned techniques and their modifications shortly. In the later chapters, the selected methods will be considered in detail.

§ 3.1 Optical Microscopy of Nanoscale Systems

Optical microscopy is a broad family of techniques that aims to obtain highly enlarged images of objects as well as details of their structure by using visible light and a set of lenses (Figure 3.1).

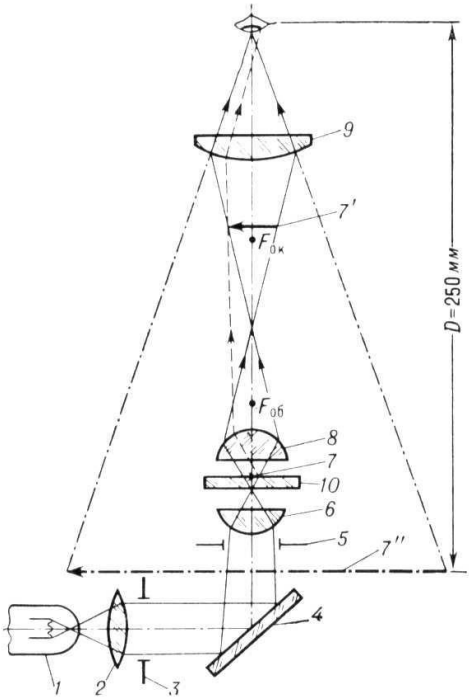

Figure 3.1. Optical microscope scheme in the transmission mode. 1—light source; 2—collector; 3—field diaphragm; 4—rotary mirror; 5—aperture diaphragm; 6—condenser lens; 7—object (7'—inverted and enlarged real image of the object, 7''—virtual image of the object); 8—objective lens; 9—eyepiece; 10—slide.

With the help of microscopes, the shape, size, structure, and other properties of micro-objects can be determined. The most important characteristic of a microscope is its spatial resolution, i.e., the shortest possible distance at which two-point objects can be visibly discriminated. The microscope resolution is always limited due to the wave properties of light. When a point source of monochromatic light passes through an optical system of the microscope, it forms an image that resembles a round spot (the so-called Airy disc) of a finite diameter:

$$d = \frac{1.22\lambda}{A}, \tag{3.1}$$

where λ is the wavelength of light, and A is the numerical aperture of the objective, equal to $A = n \cdot sin(u_m)$. Here, n is the refractive index of the medium between the luminous point and the lens, and u_m is the half of the opening angle of the light beam outgoing from the point and entering the lens. Formula 3.1 is correct for self-luminous

objects, when the sample is a source itself. For non-self-luminous objects, the limiting resolution formula is slightly different:

$$d = \frac{1.22\lambda}{A + A''}, \tag{3.1}$$

where A and A'' are the numerical apertures of the objective and the condenser lens, respectively (the values of the apertures are usually engraved on the lens frames).

As follows, it is impossible to observe separately the elements of an object with dimensions smaller than the limiting resolution of the microscope. Hence, at first sight, optical microscopy can be considered quite useless for nanoscience. Nevertheless, there are several ways to enhance the microscopic resolution even up to a nanometer scale. One of the "traditional" ways is to increase the refractive index n. This is done in immersion systems, where the value of A can be increased to 1.4 by placing a liquid with n > 1 between the object and the lens. As a result, the optical microscope makes it possible to distinguish structural elements with a distance between them up to 0.20 μm. Although this value is significantly larger than the characteristic sizes of individual nanostructures, optical microscopes of various types are widely used to study the structure of microscale objects as well as one-, two-, and three-dimensional ordered structures formed during the self-organization of nanoparticles on surfaces of various types.

The technique of fluorescence microscopy has become an essential tool in biology and medicine, as well as in materials science due to the capabilities that are not available in other modes of traditional optical microscopy. The principal advantages of fluorescence approach are very high contrast, sensitivity, specificity, and selectivity. The use of fluorophores requires several critical modifications in the illumination and imaging systems. Fluorescence excitation requires specific light sources, and their emission is often recorded with advanced light detectors. As will be mentioned in a later chapter, fluorescence microscopy is often combined with laser scanning and confocal regime. The latter provides greater spatial resolution and the possibility to build three-dimensional images of samples by collecting light only from a tiny, focused spot within the studied object.

§ 3.2 Electron Microscopy

Electron microscopy is undoubtedly the most common method for determining morphological parameters of nanostructures. It is widely used to study the structure and geometry of single particles, as well as the mutual arrangement of nanoparticles deposited on substrates. The electron microscopy devices can be found in two main variants: *transmission electron microscopy (*TEM*)* and s*canning electron microscopy (*SEM*)*.

The electron microscopy technique utilizes accelerated electrons to probe the material of interest. Since moving electrons possess the wave-like properties, they can be used to form images that are not fundamentally different from those formed by an optical microscope. As in optics, the spatial resolution of an electron microscope is determined by the diffraction limit, hence, the radiation wavelength. The wavelength of moving electrons, determined by their mass and velocity, is 3–4 orders of magnitude shorter than the wavelength of optical radiation. Therefore, the spatial resolution of an electron microscope can reach tens of picometers, enabling high-precision analysis of the nanostructure topology.

In an electron microscope, electrons, typically emitted by thermionic emission, are accelerated by an electrical potential, and focused by electromagnetic lenses on the sample. The transmitted or reflected beam contains information about the electron density of the sample areas, which is used to construct a topological image of the object.

TEM (Figure 3.2, left) uses a beam of high-energy electrons that passes through a thin sample, interacting with its elements as it passes through. The image formed by passing electrons is amplified and focused on the receiving region of the detector. Several types of detectors are usually used: fluorescent screens, photographic films, and array image sensors, like CCD cameras. Thus, the device allows us to study the structure of thin samples with a spatial resolution up to 0.04 nm with a magnification up to 5×10^7 times.

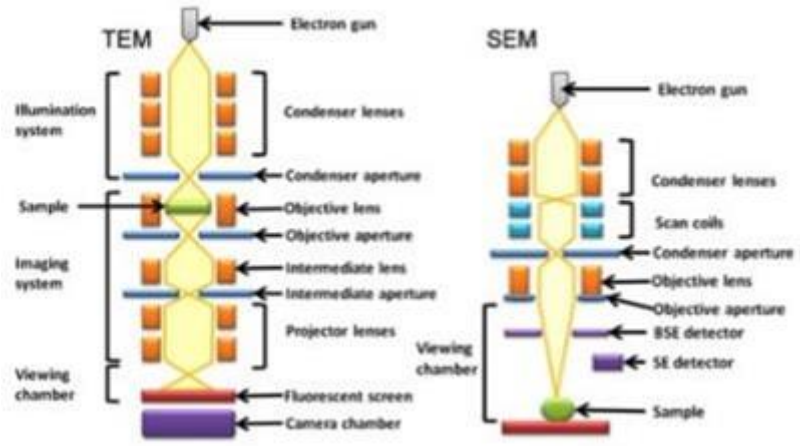

Figure 3.2. The principal scheme of TEM (left) and SEM (right) [3.1].

SEM (Figure 3.2, right) works on a slightly different principle. SEM image is formed by detecting low-energy secondary electrons or back-scattered electrons emitted by the sample under the influence of primary electrons. The electron beam scans the surface of the sample (hence the name), and the detector registers the parameters of secondary electrons at each point on the surface. The spatial resolution of SEM is limited not by diffraction, as in TEM, but by the focusing area of the primary electron beam. As a rule, SEM resolution is an order of magnitude less than that of

TEM and reaches, at best, 0.5 nm. Nevertheless, due to the deep depth of field, SEM enables the three-dimensional analysis of the object's topology.

When the surface is irradiated with a fast electron beam, in addition to low-energy secondary electrons, the selective reflection of fast electrons occurs, together with characteristic X-rays and cathodoluminescence. Analysis of the images formed by the last two processes allows one to study not only the topology, but also the chemical composition of surface and subsurface layers.

Undoubtedly, the electron microscopy technique has a few disadvantages. In the case of TEM, the sample preparation procedure may be rather complex and expensive, as samples must be transparent for the electron beam (typical thickness of less than 1 micron). Furthermore, both TEM and SEM require a high vacuum and a high voltage power supply. Finally, it is a "single-use" destructive measurement technique, as the electron beam easily destroys the sample.

§ 3.3 Scanning Probe Microscopy

*Scanning probe microscopy (*SPM*)* is a huge branch of microscopic techniques. The interest towards SPM in nanoscience originates from the possibility to create images of sample surfaces with atomic precision. In SPM, an image is created by scanning a sample (line by line) with a probe and recording the probe/surface interaction as a function of the probe coordinate. Different types of interactions can be recorded in SPM, and different types of probes are used. The most common examples of SPM are scanning tunneling microscopy (STM), atomic force microscopy (AFM), near-field scanning microscopy (NSOM).

The quantum tunneling of electrons between conducting surfaces of a sample and an extremely sharp conducting tip is used in STM (Figure 3.3). As the probe approaches the surface at a distance of several nanometers between them, the tunneling current appears. During the scanning process, the probe moves along the sample surface, registering the tunnel current. The feedback loop, which tracks changes in the tunnel current, adjusts the position of the system so that the current value remains constant. Usually, changes in the tunnel current value are processed by the feedback system that controls the position of the sample or probe (depending on which part is mobile and which is stationary) along the vertical coordinate. Such position changes of the probe are recorded, and the 3D surface is reconstructed from the acquired data.

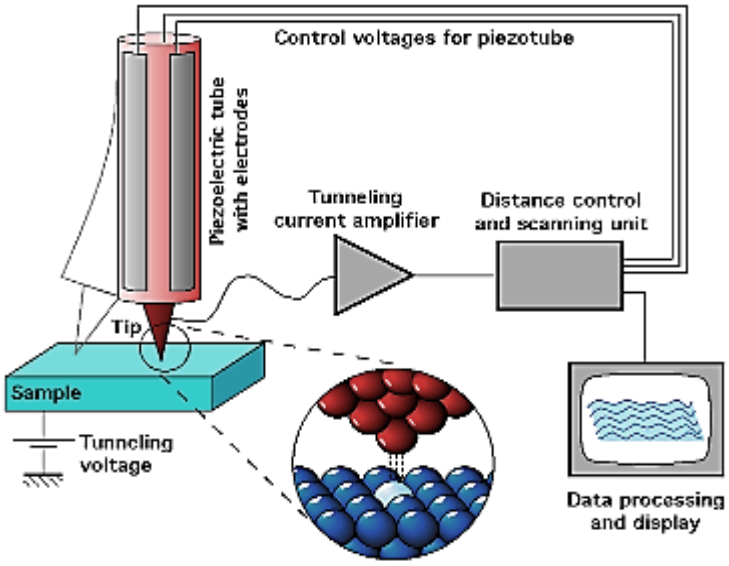

Figure 3.3 Operation principle of an STM [3.2].

To achieve the best spatial resolution, STM requires ultra-clean flat surfaces and the sharpest tip. It is possible to achieve a resolution of 0.1 nm in lateral direction (along the surface) and 0.01 nm in vertical direction. The STM technique can be used not only in high vacuum conditions, but also in the air, inert gases, and several liquids, which makes it possible to study biological objects. Operating temperature range is zero to several hundred degrees Kelvin.

The *atomic force microscopy (*AFM*)* is another method for studying the surface topology, based on mechanical probe-sample interaction (Figure 3.4). In AFM, the tip is attached to a flexible cantilever. The top side of the cantilever is reflective (sometimes metallized to amplify the reflected laser signal), which makes it possible to use a laser system to monitor the cantilever bending. The cantilever bends when the tip at its end is "touching" the sample surface during the scanning procedure. The reflected laser light is used to measure the bending; therefore the interaction and the sample surface structure can be analyzed.

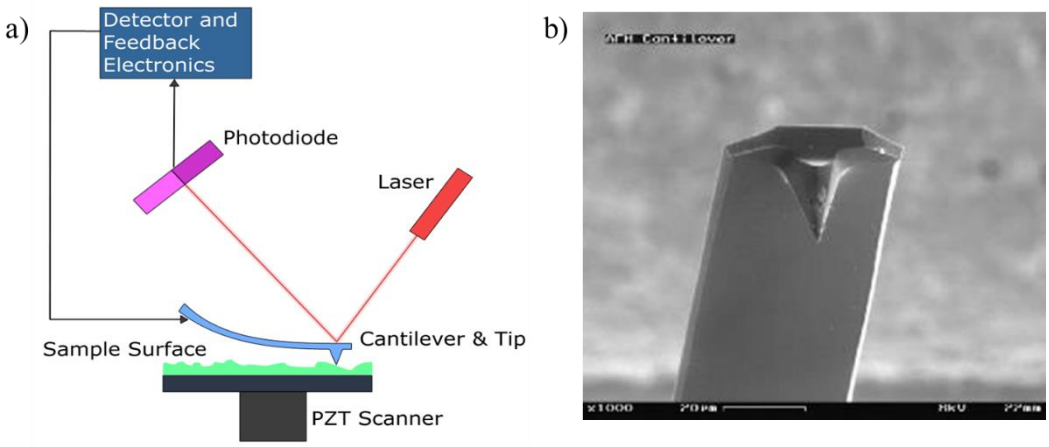

Figure 3.4. a) The scheme of an atomic force microscope [3.3]. b) The image of a cantilever obtained using a scanning electron microscope with the ×1000 magnification [3.4].

AFM is an advantageous method for studying nanostructured surfaces. Firstly, unlike scanning electron microscopes that create a pseudo-3D image of the sample, AFM constructs a real 3D surface visualization. In addition, AFM does not require the conductive metallic or carbon coating for non-conductive surfaces, which often leads to a noticeable deformation of the surface. AFM does not require a vacuum, and most AFM modes can be implemented in the air or even in liquid, which opens the possibility of studying biomacromolecules and living cells. Nevertheless, the best working conditions are still the low temperature and the vacuum. Thus, it was shown that AFM can provide real atomic resolution under ultrahigh vacuum conditions. The ultrahigh vacuum AFM resolution is comparable with a scanning tunneling microscope and a transmission electron microscope. The disadvantages of an atomic force microscope are a small sample scanning area and long sample scanning time, namely, from several minutes to several hours.

Near-field scanning optical microscopy is another technique that allows probing surfaces directly at the point of interaction. While STM and AFM study surface geometry, NSOM opens the possibility of optical characterization with sub-diffraction spatial resolution. This method uses the effect of spatial localization of electromagnetic fields in the distance of 10–50 nm (the so-called "near-field" regime) near the exit aperture of a metallized fiber-optic probe (aperture SNOM) or near the tip of a metal probe (apertureless SNOM). This field can be used to excite luminescence or Raman scattering in the local area of the sample. Scanning over the whole surface allows obtaining a two-dimensional luminescence (or Raman) image with a nanometer spatial resolution. The apertureless NSOM technique is of high interest in nanoscience. It uses the effect of a sharp increase in the intensity of optical fields near the metal surfaces during the resonant excitation of plasmons at the top of the tip. This method is optimal for recording and subsequent analysis of Raman spectra and allows us to obtain information on the local chemical composition and mechanical stresses in single nanostructures. It has been called *tip-enhanced Raman spectroscopy* (TERS).

§ 3.4 X-Ray Scattering Techniques

The family of X-ray scattering methods is a diverse set of analytical techniques that utilizes scattering of X-rays on a material of interest. Crystalline solids, polymers, nanoparticles, thin films, and other samples can be analyzed in terms of their geometrical features, internal structure, symmetry, mechanical stresses, and chemical composition. The general principle of all X-ray scattering methods is that the X-ray beam incident on an object is scattered due to the elastic or inelastic interaction with the atoms and molecules of the object. During the measurement, the scattered signal

intensity is recorded as a function of incident and scattered angle, polarization, and photon energy.

The most important X-ray scattering techniques are *small-angle X-ray scattering (*SAXS*)* and *wide-angle X-ray scattering (*WAXS*)*. The latter is often referred to as *X-ray diffraction* or *X-ray powder diffraction (*XRD*)*. The term WAXS is often used in polymer science, whereas XRD is more popular in solid state physics. The main difference between the small- and the wide-angle techniques is the spatial scale on which the scattering features are observed. Larger objects scatter at smaller angles. As a result, SAXS is an efficient tool for characterizing nanometer-sized inhomogeneities, whereas WAXS (XRD) allows for the determination of the crystal lattice parameters.

SAXS is used both in scientific research of materials and in the routine characterization of materials during the production (production metrology). In SAXS, X-rays (wavelengths from 0.1 to 0.2 nm) are elastically scattered from a sample with nanoscale inhomogeneities, and then recorded at small angles (typically 0.1–10°) to the direction of the incident beam. This angular range contains information about the shape and size of the heterogeneities, the characteristic dimensions of the partially ordered materials, the pore sizes, and other data. SAXS can provide structural information about inhomogeneities (for example, quantum dots) with sizes from 5 to 25 nm and areas of ordered systems up to 150 nm.

In a SAXS device, an incident monochromatic X-ray beam is partially scattered on a sample, while most of the radiation passes without interacting with it. Scattered X-rays form a pattern (a scatter plot), which is recorded by a detector. The latter is usually a two-dimensional flat X-ray receiver, positioned behind the sample perpendicular to the direction of the beam (Figure 3.5, left). The scatter plot contains information about the structure of the sample. The main problem of SAXS instruments is the separation of a weak scattering signal from a strong signal of incident radiation. The smaller the scattering angle, the more difficult the problem is.

WAXS (XRD) is based on the same principle, although the implementation is somewhat different. As wide angles need to be registered, the X-ray diffractometer is equipped with a wide-angle X-ray goniometer (Figure 3.5, right). During the measurement, the scattering intensity is plotted as a function of the 2θ angle, where the peaks indicate the diffraction maxima and enable direct identification of the crystal structure.

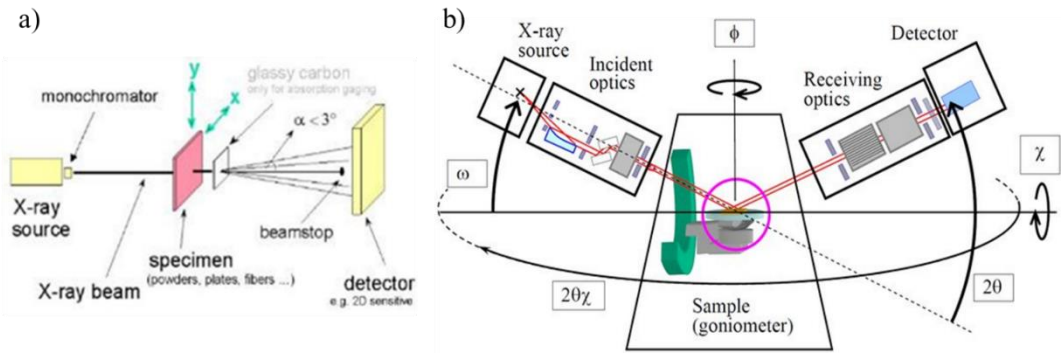

Figure 3.5. Operation principle of X-ray scattering techniques [3.5].

§ 3.5 Dynamic Light Scattering (DLS)

*Dynamic light scattering (*DLS*)* is a technique in physical chemistry that can be used to determine the size distribution profile of colloidal particles or polymers in solution. Typically, the sizes from nanometers to several microns can be determined by DLS, which explains its popularity as a method for characterizing nano-and microparticles in solution.

In DLS, a monochromatic light source, usually a laser, is shot into a sample. The scattered light is then collected by a detector. The scattering intensity fluctuates over time due to the *Brownian motion* of the particles in suspension. This fluctuation is constantly changing with time, resulting in either constructive or destructive interference of the beams scattered by the surrounding particles. Within this intensity fluctuation, information about the time scale of movement of the scatterers is contained. Large particles move slower; hence the intensity pattern also changes at a slower pace (Figure 3.6). The diffusion coefficient is then derived from the scattering intensity autocorrelation function, which is used to calculate sizes via the Stokes–Einstein equation.

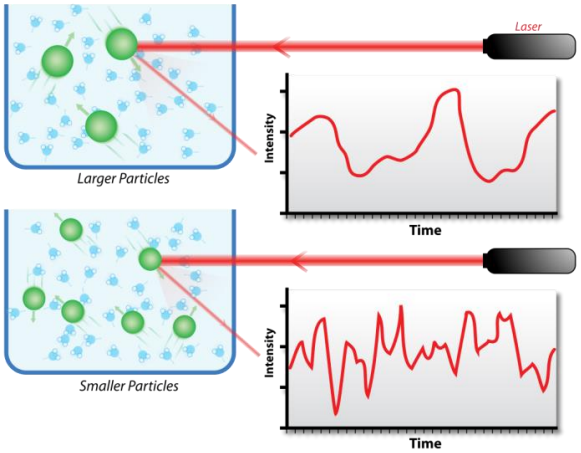

Figure 3.6. Schematic representation of dynamic light scattering principal technique [3.6].

It is worth noting that the value derived from the DLS measurement is not the particle size itself, but the so-called *hydrodynamic diameter*—the size of a sphere that moves in the same manner as the scatterer. It is determined by a number of parameters, including the particle shape and the surface morphology.

Apart from size, so-called zeta-potential can also be measured using the DLS technique. *Zeta-potential* is determined by the charge that is acquired by a particle in polar media. Since particles of similar charge will repel each other, those with high charges will resist flocculation and aggregation for longer periods making such samples more stable. Hence, measuring zeta-potential can provide important insights into the colloidal stability of nanoparticles.

The charge or zeta potential of particles and molecules is determined by measuring their velocity while they are moving due to electrophoresis. Particles and molecules that have a zeta potential migrate towards an electrode when a field is applied. Their speed is proportional to the field strength and their zeta potential. If we know the field strength, we can simply measure the speed of movement, using laser Doppler electrophoresis, and then apply established theories to calculate the zeta potential.

§ 3.6 Low-Frequency Raman Scattering (LFRS)

Low-frequency Raman scattering (LFRS) is a variant of Raman scattering spectroscopy, used to determine the size of nanoparticles, as well as structural and chemical nanoscale inhomogeneities in bulk material. In LFRS, the Raman spectra of acoustic phonons with frequencies less than 100 cm^{-1} are registered in nanoparticles. The frequency of acoustic phonons in finite-size objects is directly proportional to the speed of sound in the material and inversely proportional to the size of the object. Therefore, the analysis of the spectra makes it possible to determine the size and, in some cases, the shape and composition of nanoparticles. LFRS is capable of measuring nanoparticles with the size from 1 nm to 50–70 nm, which, depending on the material, corresponds to the spectral bands with Stokes shifts from several dozens to units of cm^{-1}. Since the phonon frequencies are low and the corresponding bands in the LFRS spectra differ slightly from the frequency of the exciting radiation (Stokes shift), the implementation of the method requires taking special measures to suppress the exciting radiation. This is usually achieved by using double or even triple monochromators for spectral selection of the scattered radiation.

Check Questions

1. What is the physical basis of electron microscopy?
2. What is low-frequency Raman scattering used for?
3. How is the particle size determined using dynamic light scattering?
4. What is the conceptual difference between small-angle and wide-angle X-ray scattering? What are their capabilities?
5. What is the spatial resolution of optical microscopes? How can we improve it?
6. What microscopes can investigate surface profiles with atomic resolution?

CHAPTER 4. FLUORESCENCE MICROSCOPY

Fluorescence microscopy is widely used in microbiology, microchemical analysis, defect identification, and to study the morphology of structures formed by luminescent semiconductor or metal nanocrystals. A variety of applications are associated with a high contrast image of a luminescent object against a dark background. Furthermore, spectral properties of luminescent samples can be elucidated, that allows a researcher to quickly identify them and analyze their structure and composition.

§ 4.1 Operation Principles of Fluorescence Microscopy

Fluorescence microscopy is based on irradiation of specimens with external excitation light and detection of emitted luminescence. In this case, two optical filters are introduced into the optical scheme. The first is placed in front of the condenser lens; it only transmits the excitation light that is directed onto the studied sample. The second filter is used to prevent the excitation light from falling directly onto the photodetector or the observer's eye. It is typically installed after the objective lens and allows only the low-energy fluorescence photons to pass through it (the so-called long-pass filter). For a sample to be studied in a fluorescence microscope, it must either be luminescent itself (intrinsic luminescence) or be stained with the special molecular dyes or fluorescent nanoparticles (secondary luminescence).

The excitation filter ensures that only wavelengths within the required range are transmitted. For this purpose, bandpass filters are used that effectively block all radiation beyond the region of the filter transmission. However, in fluorescence microscopy, it is crucial to obtain enough light to create a useful image; passing light through filters always results in a loss of intensity.

In fluorescence microscopy, samples can be illuminated from above through the lens, which in this case serves as a condenser, and from below, through a conventional condenser. Observation with above illumination is sometimes called *reflected fluorescence microscopy*. Reflected fluorescence microscopy is often combined with contrasting techniques such as phase contrast and/or differential interference contrast.

Fluorescent microscopes are usually equipped with a set of interchangeable optical filters that select which part of the spectrum will be used as the excitation light. An additional optical filter is chosen to pass only the sample fluorescence. Typical fluorophores, such as molecular dyes and semiconductor quantum dots, strongly absorb (hence, can be easily excited) in the UV and the blue region of the visible spectrum. Therefore, the excitation source in fluorescent microscopes must be chosen accordingly. Typically, the radiation from ultrahigh pressure lamps (gas-discharge

light sources) is used. In some cases, sets of LEDs or laser diodes emitting are implemented, which can produce nearly monochromatic radiation. For narrow-band excitation sources, optical filters in the excitation channel are not required.

The principal optical scheme of a fluorescent microscope with the reflection setup is presented in Figure 4.1. Here, to separate the excitation beam from the sample fluorescence, an interference beam splitting plate is used. This scheme is used in a majority of industrially manufactured fluorescent microscopes.

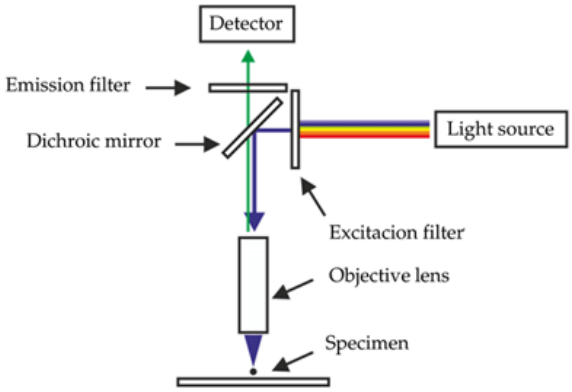

Figure 4.1. Optical scheme of a fluorescence microscope.

It is important to note that in case of excitation in the UV or the blue region of the spectrum, all optical components, including lenses, glasses, and slides, as well as immersion media, should not have their own luminescence.

Polarized fluorescence microscopy is also worth mentioning. In this method, a polarization analysis of the sample fluorescence is performed by its excitation with linearly polarized light. Polarization-dependent measurements make it possible to determine the orientation and ordering of nanocrystals in nanostructured objects, as well as their anisotropy. Figure 4.2 shows polarized fluorescent images of patterns formed from quantum dots and quantum rods. The examples demonstrate birefringence at crossed polarizers. Polarization-dependent fluorescence imaging experiments can be useful for studying anisotropic objects. For instance, fluorescent one-dimensional quantum rods and nanowires emit light with a priority polarization direction, which indicates that the band edge emission is distinctly linearly polarized along their axis. Fluorescence polarization anisotropy can also be used for measuring and mapping the temperature growth near the nano-sized heat sources.

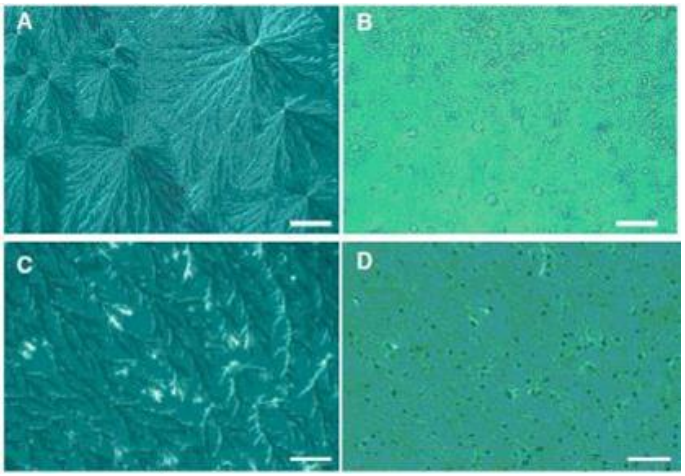

Figure 4.2. Polarized images of patterns formed by quantum dots (A, B) and quantum rods (C, D). The patterns show clear birefringence when recorded under crossed polarizers (A, C) as compared to the images recorded under parallel polarizers (B, D). Scale bars are 20 μm [4.1].

§ 4.2 Laser Confocal Scanning Microscopy (LCSM)

The development of fluorescence microscopy has led to the creation of *fluorescence laser scanning microscopes*. Here, a set of lasers emitting collimated monochromatic radiation at different wavelengths is used as an excitation source. The excitation light is then focused by the lens into a spot of minimum size. The sample is therefore locally excited, and the luminescence is collected by the same lens from the local region. To construct a luminescent image, step-by-step XY scan is performed. Two scanning schemes can be implemented: either the object moves relative to the focal spot, or the special optics are used that enable the focal spot migration over the surface of the object. At each point, emission intensity is recorded, thereby creating the luminescent image of the sample. The scanning step (up to 10 nm), the signal accumulation time, the number of points, and other parameters of the image acquisition can be programmed. The latter represents the emergence of digital computer microscopy, which can simultaneously analyze large amounts of data.

Microscopy technique that is described above allows one to obtain two-dimensional (XY) fluorescence images of objects. Further improvement of this technique has led to the development of *laser confocal scanning microscopy* (LCSM) that can obtain three-dimensional images of microscopic objects. The concept of a confocal microscope is based on the use of a spatial pinhole (aperture) in the optical path that selects the luminescence coming exclusively from the focus of excitation. Confocal microscopy provides an improvement in the optical resolution both along the optical Z axis and in the XY plane of the object as compared to the traditional wide-field fluorescence microscopy. In Figure 4.3, one can see a comparison of two image

series obtained in a traditional (a-c) and confocal (d-f) fluorescence microscopes. Images obtained on a confocal microscope reveal more structural details.

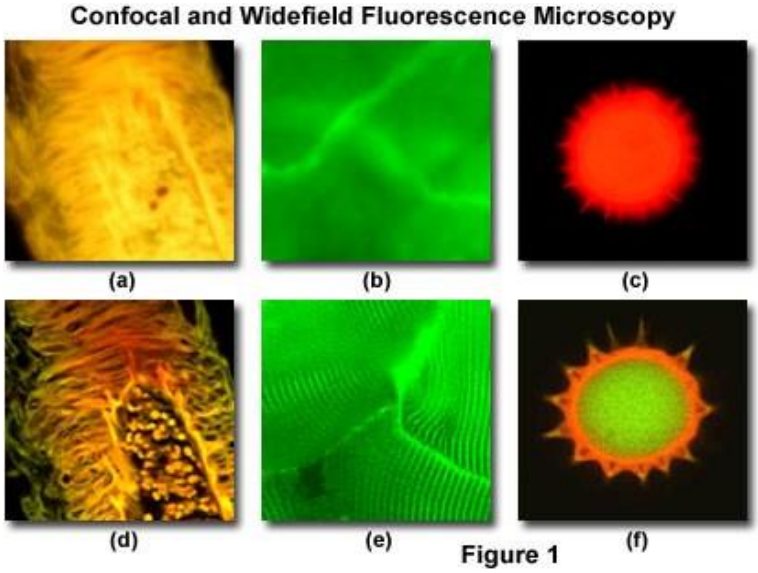

Figure 4.3. Fluorescent images of biological structures obtained by a traditional fluorescence microscope (a-c) and a laser confocal scanning microscope (d-f) [4.2].

The simplest scheme illustrating the principle of LCSM operation is shown in Figure 4.4.

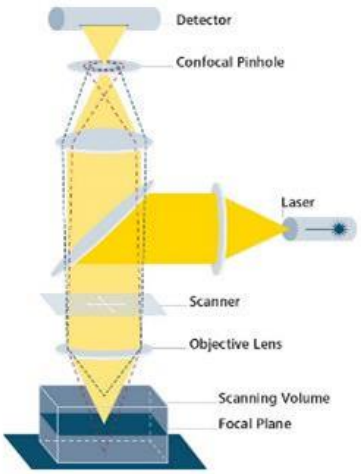

Figure 4.4. The principle of a laser scanning confocal microscope.

In a typical confocal microscope, the luminescence excited by a laser is projected by the lens onto a micron-sized pinhole (~50–150 μm) in front of the detector. The pinhole plays the role of a spatial filter and blocks the out-of-focus emission. The dichroic filter is used to separate the excitation and the emission light. At every moment of time, the luminescence of a single point is recorded, with the horizontal coordinates (x_k, y_k) and the vertical coordinate (z_n). The latter corresponds to the focal plane and

defines the “slice” of the object that is going to be imaged. Next, by scanning the sample over the XY plane, a two-dimensional luminescent image on the height z_n is plotted. Images in other focal planes are acquired by changing the objective lens focus or the vertical position of the sample. Together, the two-dimensional slices make up a “z-stack”, which is processed to create a 3D image (Figure 4.5) or analyzed using an image processing software.

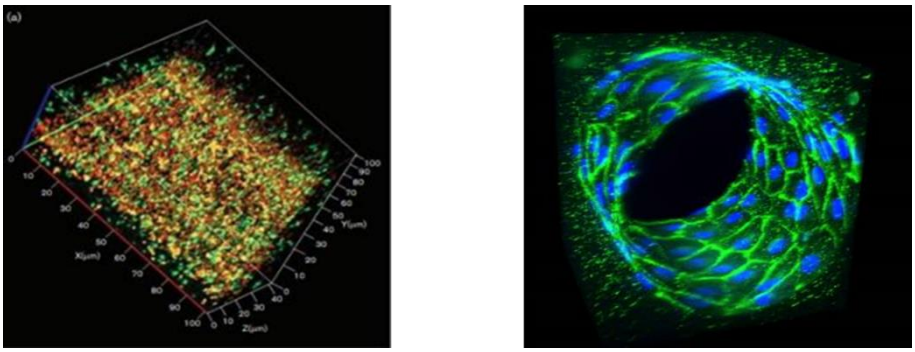

Figure 4.5. Left: fluorescent staining of bacterial cells followed by reconstruction of 3D confocal images on LCSM [4.3]. Right: human umbilical-vein endothelial cells forming a functional blood vessel stained with molecular dyes [4.4].

The slices can also be assembled and shown in transverse XZ and YZ planes. Once a fully segmented, surface-rendered reconstruction has been made, it is possible to extract quantitative information from the sample. This includes counting objects, measuring length, volume, and depth, or quantifying the spatial arrangement of parts (such as measuring distances or angles between features). Certain image parameters, such as opacity, can be interactively modified to demonstrate the internal structure of an object.

The main advantage of laser confocal scanning microscopy is the possibility of obtaining consecutive fluorescent images of thin (from 0.4 to 1.5 μm) slices of objects with a thickness of 50 μm or more with diffraction-limited spatial resolution. Confocal microscopy provides an increase in image contrast, which leads to the possibility of resolving the elements whose intensity is 200 times different. Additional advantages of laser scanning confocal microscopy are the ability to use electronic magnification when changing the scanning area without changing the lens.

The disadvantages of confocal microscopy are a long time for obtaining a three-dimensional image—from tens of minutes to several hours, and a limited number of excitation wavelengths. Finally, confocal microscopes are typically much more expensive compared to traditional fluorescence microscopes, so they are only affordable to highly financed laboratories and production facilities.

The modern fluorescence microscopy combines the power of high-performance optical components with computerized control of the instrument and digital image

acquisition. Together, these features help to achieve a level of complexity that far exceeds that of simple observation by the human eye. Computerized control of focus, stage position, optical components, shutters, filters, and detectors is in widespread use and enables experimental manipulations that are not possible with mechanical microscopes. The introduction of electro-optics in fluorescence microscopy has led to the development of optical tweezers capable of manipulating sub-cellular structures or particles, imaging of single molecules, and a wide range of other interesting applications.

Check Questions

1. In what cases polarization-dependent measurements are important?
2. What type of polarization is typically used for excitation in polarized fluorescence microscopy?
3. How does the laser confocal scanning microscope select the luminescence exclusively from the focus of excitation?
4. What excitation sources are used in fluorescence laser scanning microscopes?
5. How does the laser confocal scanning microscope create a 3D image?

CHAPTER 5. ELECTRON MICROSCOPY

The history of electron microscopy dates back to 1927, when Hans Bush discovered the geometric optics (or ray optics) of charged particles. He showed that magnetic and electrostatic fields with axial symmetry act as lenses for charged particles. By that time Louis de Broglie had already discovered the wave optics of electrons and electron diffraction experiments had been performed. Another contributor was Denis Gabor, who constructed the first magnetic lens but could not understand how it worked. Later, in 1932, the German physicist Ernst Ruska built the first transmission electron microscope (Nobel Prize in Physics in 1986), and in 1939 the first commercial model was introduced on the market by Siemens.

Today, electron microscopy is one of the most common and widely spread methods for determining the geometric parameters and the mutual arrangement of nanoparticles on various types of substrates. Electron microscopy techniques can be classified into two types: *transmission electron microscopy* (TEM) and *scanning electron microscopy* (SEM).

The electron microscopy technique is based on the fact that moving electrons possess properties similar to those of an electromagnetic wave (light) due to the wave–particle duality. Hence, accelerated electrons can also be emitted, focused, diffracted and collected by a detector in a similar way as it happens in an optical microscope. As in optics, the spatial resolution is determined by the diffraction limit, i.e., by the radiation wavelength. Since the wavelength of moving electrons, determined by their mass and velocity, is 3–4 orders of magnitude less than the wavelength of optical radiation, the spatial resolution of electron microscopy can reach hundredths of a nanometer. Therefore, it is widely used to analyze the topology of nanostructures with the required spatial resolution.

§ 5.1 Transmission Electron Microscopy (TEM)

A transmission electron microscope (TEM) is a microscope that uses electron beams to visualize specimens and generate high-resolution, two-dimensional images. TEM uses electrons accelerated up to 50–1000 keV under high vacuum conditions (10^{-5}–10^{-10} mm Hg). TEM can obtain morphological, compositional, and crystallographic information of the object. The samples can be thin objects (up to 1 micron thick), island films, nanocrystals, crystal lattice defects or, using the replica method (discussed later), the surface of microscale samples. The highest achievement of modern electron microscopy is the visualization of individual atoms, heavy elements, direct observation of the crystal lattice and even the protein's tertiary structure. Electronic microscopes are widespread in different fields such as life

sciences, nanotechnology, medical, biological and materials science, forensic analysis, gemology, and metallurgy as well as industry and education. For example, cell elements, protein structure, nucleic acids, viruses are investigated using an electron microscope in biology. In materials science, an electron microscope allows researchers to study the processes of growth and crystallization of thin films, structural transformations during heat or another physical treatment. In industry TEM can also be used in semiconductor analysis and silicon chips manufacturing.

5.1.1 Operation Principles of Transmission Electron Microscope

An electron microscope consists of an electron gun and a system of magnetic lenses. Some of them are used to create an illuminating beam with a small divergence, while others create an enlarged image. Figure 5.1 shows a general view of the electron-optical column of a TEM device.

There are two types of electron guns. The *electron thermionic gun* is a thin tungsten filament heated up to 2700 °C (or lanthanum hexaboride, that is about ten times "brighter" than tungsten cathodes and has ten times longer lifetime). The *"cold" field emission gun* emits electrons from a sharp tip that are expelled by applying the negative potential of several kilovolts. When the electron beam is formed in the gun, it is focused by condenser lenses that create an electron spot with a diameter of 1–100 microns on the object. After passing through an object the electrons are collected by an objective lens. Strongly scattered electrons are not used for the image formation and are stopped by the objective aperture. Unscattered electrons pass through the aperture and are focused on the object plane by the first projector lens. There, the first intermediate image is formed. Besides the objective lens, intermediate lenses further magnify the electron image to form the second, third and subsequent images. The last projector lens forms an image on a cathodoluminescent screen, which is detected by the digital camera and may be transferred to a computer. The image is focused by adjusting the current of an objective lens, changing its focal length. The currents of other electronic lenses adjust the magnification of TEM.

The degree of electron absorption and scattering depends on thickness, density, structure, and chemical composition of the studied object. The number of electrons passing through the aperture diaphragm and, consequently, the current density on the screen, changes accordingly. As a result, an amplitude contrast is created, which is then converted into the light contrast on the screen. Under the screen, in modern devices, there is a digital imaging sensor instead of previously used photographic plates and films.

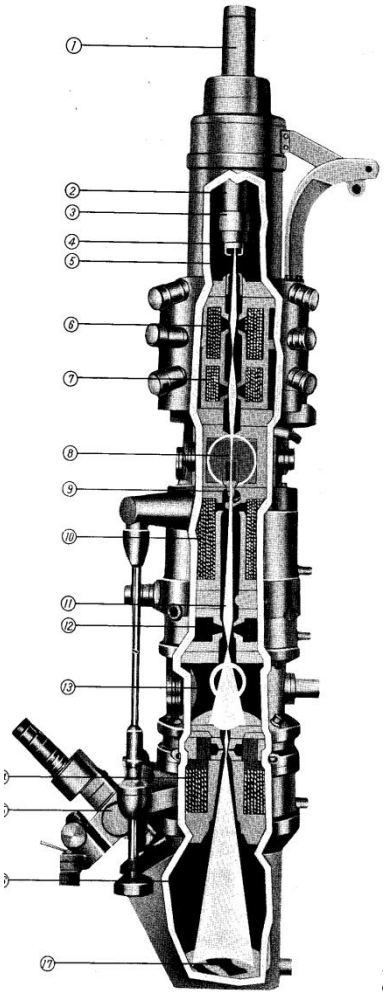

Figure 5.1. General view of the TEM column: 1—high-voltage cable, 2—electron gun, 3—cathode unit, 4—control electrode, 5—anode, 6—first condenser lens, 7—second condenser lens, 8—deflection alignment system of the illuminator, 9—sample chamber, 10—objective aperture diaphragm, 11—objective lens, 12—field diaphragm, 13—intermediate lens, 14—diffraction chamber, 15—projection lens, 16—microscope, 17—observation camera, 18—cathodoluminescent screen.

As discussed in the previous chapter, the resolution limit of an optical microscope is approximately half the used wavelength and is about 250 nm for the visible range. The wavelength of an electron with the energy of 100 keV is equal to 0.0037 nm, which is orders of magnitude lower than the wavelength of a visible photon. Nevertheless, such resolution cannot be obtained in practice due to uncorrectable aberrations of the electron optics. Despite that, the guaranteed resolution of a serial TEM device is still high: accelerating voltage of 100–300 keV provides the spatial resolution of 0.1–0.2 nm. The champion resolution obtained so far is 0.04 nm, which is up to 10^4 times higher than the resolution of an average optical microscope.

§ 5.2 Direct Methods of Object Research

The object investigated in TEM must be prepared either as a thin film or as finely dispersed particles. The object must be stable and resistant to charging under the electron beam. The maximum thickness of the object is 100–200 nm for inorganic objects and up to 1000 nm for organic objects at 100 keV electron energy. Typically, samples with the thickness of about 50 nm are studied using TEM as it is difficult to get a focused image for samples with the thickness of 80 nm and greater. Objects of greater thickness cause a decrease in the electron energy and lead to chromatic aberration that reduces the resolution of the microscope. In cryo-TEM though, the typical sample thickness is around 0.5–1.0 μm.

Usually, the specimen is placed on a thin formvar or carbon support film, which is placed in a TEM grid—a flat disc with a mesh with a hole size of about 80 μm. The grid is mounted in the object holder and installed inside TEM.

The support film, like a microscope slide in an optical microscope, should be transparent for electrons and have no structure that could affect the image quality. Also, it should be resistant to mechanical manipulations, pressure changes, as well as heating and charging under the electron beam. The most suitable films are produced by vacuum thermal evaporation of carbon. Carbon films are amorphous, chemically inert, hydrophobic, durable, and well tolerated by the electron bombardment. The formvar film allows the use of TEM grids with larger holes.

5.2.1 The Study of Powders

One of the important applications of TEM is the study of various powdered materials, since many of their physical and even chemical properties depend on the size, shape and crystalline structure of the particles. Two methods of preparing powdered materials are most often used: dry preparation and deposition from suspensions. With dry preparation, the powder is put onto the support film and then brushed off, or nanoparticles are trapped from smoke or gas streams. The second way implies using liquid particle suspension. The solvent should be chosen so as to prevent aggregation of particles as well as be harmless to the grid material. Furthermore, the solution should have very low concentration to allow the observation of individual particles in the electron microscope. The suspension is sonicated to break any aggregates, and a drop is then applied to the support film. After drying the liquid, the powder is examined in the TEM. This method is widely used to prepare samples of colloidal nanoparticles for electron microscopy analysis.

5.2.2 The Study of Nucleation and Growth of Thin Films

Electron microscopy in combination with electron diffraction is the most effective way to study the growth of thin layers. TEM enables the study of material deposition process by vacuum evaporation, even at the early stages of layer formation.

In the first case, to study the growth of thin layers, the test substance is sprayed onto a support film or substrate in a special vacuum chamber, and then the sample is transferred to an electron microscope. To trace the kinetics of the process, the spraying process is repeated several times. In the second case, the study is carried out directly during the sputtering process. The object holder with the support film is installed into the vacuum column and the sample substrate is applied to it from a nearby evaporator. In this case, it is possible to trace all the stages of layer formation. Figure 5.2 shows the change in the structure of the deposited layer with increasing the amount of deposited metal.

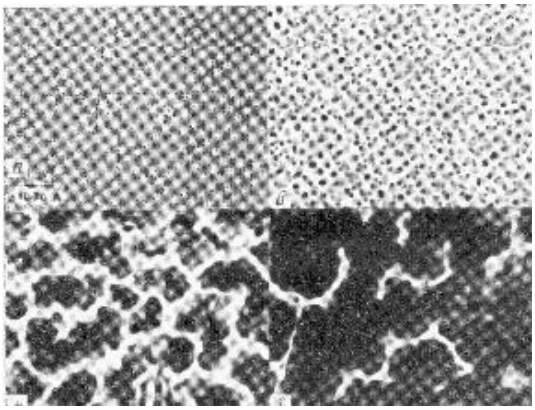

Fig. 5.2. TEM images of the gold film formation on the surface of sodium chloride crystal. Different pictures correspond to a film thickness of 0.5, 3, 30, and 50 nm.

5.2.3 The Study of single Atoms and Crystal Planes

An impressive achievement of TEM research is the possibility to acquire images of isolated single heavy metal atoms. The most convincing evidence of this is comparison of images of the same area of the substrate before and after deposition of the atoms. The most important practical task here is the preparation of an “invisible” substrate to deposit the atoms. In this case, thin monocrystalline layers of mica, flakes of graphite, or other monocrystals about 2 nm thick are used as the support film. Figure 5.3 shows the image of a graphite flake before and after deposition of tungsten atoms inside a microscope. It is seen that the atoms stick to the surface steps. After a five-minute electron beam exposition (Figure 5.3, bottom), atoms migrate to each other, forming metallic tungsten particles.

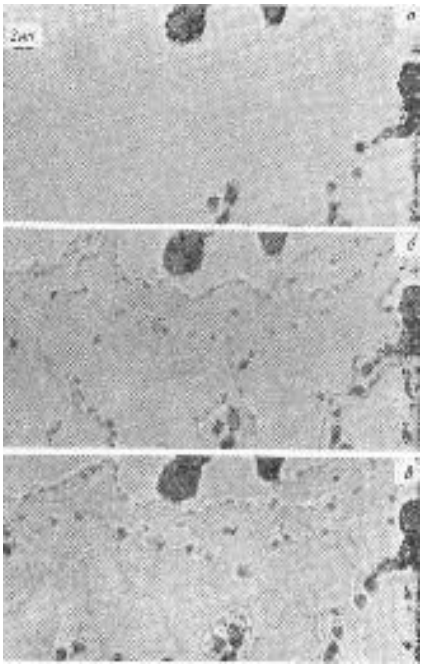

Figure 5.3. TEM image of graphite flakes before (top) and after (middle, bottom) deposition of tungsten atoms inside a microscope.

TEM is often used to obtain high-resolution images of the crystal lattice (Figure 5.4). The main goal of such studies is to determine the symmetry, characterize the lattice parameters, and visualize the structure for the presence of defects in it. To date, there are no other methods capable of providing such information at the atomic resolution level. TEM makes it possible to study very small crystals of various materials, which is not possible in case of X-ray diffraction methods or scanning tunneling microscopy.

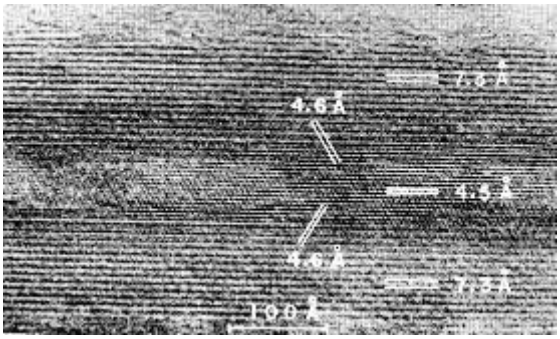

Figure 5.4. Micrograph of atomic planes in a chrysotile asbestos crystal, obtained in an electron microscope.

5.2.4 The Study of Nanoscale Profile Using Replication

Currently, scanning probe microscopy has become a widely used method for studying the surface of solid materials. However, TEM can provide even higher

resolution by implementing the so-called replication technique. A replica is a thin film of a material, transparent to electrons, that precisely resembles the surface topography of the sample. The most suitable replicas, both in terms of their properties and simplicity of manufacturing, are obtained by thermal evaporation of carbon in a vacuum. Figure 5.5 schematically represents the replica formation process.

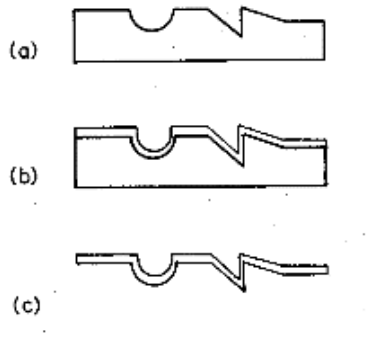

Figure 5.5. The replica production: (a) sample, (b) carbon coating, (c) final replica.

A thin film is first applied to the surface of the bulk sample, so that it precisely resembles the surface profile. It is then detached by using an acid bath, enzymes, or by mechanical separation. The separated replica is finally examined by TEM. Carbon is typically used to form replicas, although the resulting contrast is very low. To enhance the contrast, the "shadowing" method can be used. This method implies oblique vacuum deposition of a thin electron-opaque layer on the surface of a sample or replica. When the deposition is performed under a certain angle, "shadows" appear behind protrusions on the sample surface. These "shadows" do not contain heavy atoms and are hence transparent to the electron beam. Knowing the length of the shadow and the evaporation angle, it is possible to calculate the height of the specimen/particle. The simplest way to produce a "shadow" on a replica, known as self-shadowing, is to vaporize carbon and platinum at the same time. To do this, a thin channel is drilled along the axis of the sharpened carbon rod, where a piece of platinum wire is placed. When the tip of the rod is heated with an electric current, carbon and platinum evaporate simultaneously. The separation of the carbon-platinum replica from the surface of the bulk sample is carried out by the same methods as in the production of free films or substrates.

5.2.5 Analysis of the Crystal Structure by Electron Diffraction

Each time an image is formed on the TEM screen, a diffraction pattern appears in the back focal plane of the objective lens. This occurs regardless of whether the sample is amorphous or crystalline. For the crystalline objects, the scattering is in accordance with the Bragg's law. Changing of focal length of the intermediate lens can display any plane below the objective into the object plane of the projector lens. Thus,

a magnified image of the object and a diffraction pattern from the selected area can be observed on the screen (the area can be decreased by a selective diaphragm in front of the intermediate lens).

The difference between the normal and the diffraction modes arise from the strength of the intermediate lens (Figure 5.6). In the normal mode, the focus of the 1st intermediate lens is adjusted to the image plane of the objective lens where a selected area aperture is located. However, in the diffraction mode, the focus of the 1st intermediate lens is adjusted at the back focal plane of the objective lens. If there is no intermediate lens, then switching to diffraction mode can be done by adjusting the focus of the projection lenses.

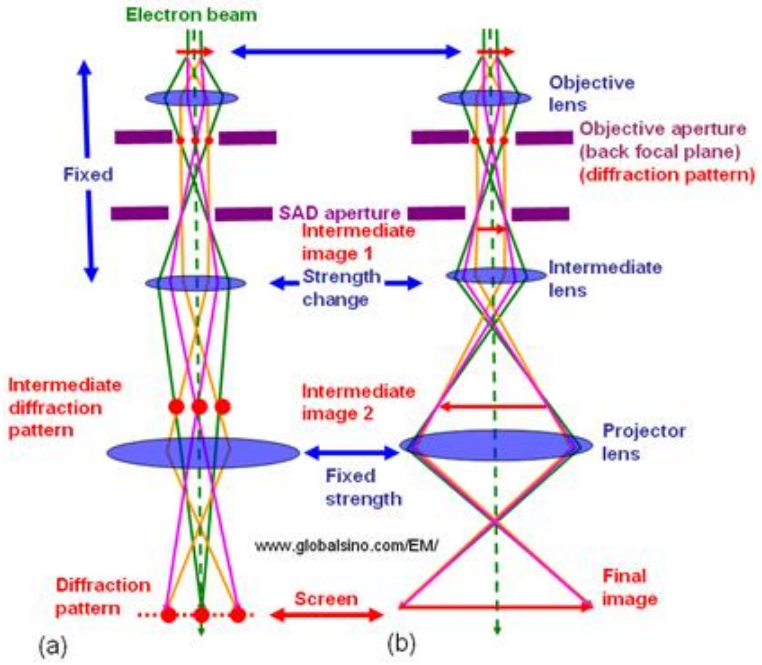

Figure 5.6. Comparison of the lens conditions between TEM diffraction (a) and TEM imaging (b) modes [5.1].

The selected area diffraction (SAD) aperture is used to exclude unnecessary parts of the area so that we can make sure the diffraction pattern originates from a small, specific area. Depending on the microscope, the smallest diameter of the area from which the diffraction pattern can be recorded is 20–200 nm. Figure 5.7 shows an image of a MoO single crystal and a diffraction pattern superimposed on it from a selected area. Diffraction analysis performed on small areas of a sample is commonly referred to as microdiffraction.

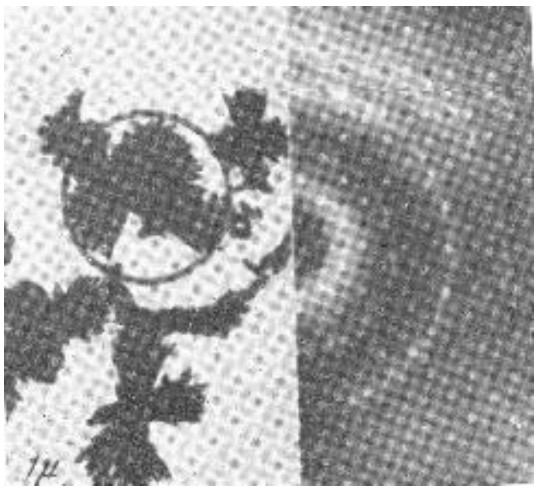

Figure 5.7. TEM image of the MoO crystal and a diffraction pattern from a selected area.

§ 5.3 Scanning Electron Microscopy (SEM)

The primary difference of *scanning electron microscopy* (SEM) in comparison to TEM is a different way of collecting information about an object of study. In the case of TEM, the classical microscopy scheme is applied: the incident beam undergoes diffraction on a sample, and the transmitted electrons are collected by the objective lens and passed over to the detector. In a scanning electron microscope, on the contrary, the image is acquired by collecting the so-called secondary electrons that are emitted from the sample upon interaction with the primary electrons coming from the gun.

The "scanning" part in "scanning electron microscopy" means that the device works on the principle of sequential movement of a thin electron beam over the surface of an object from point to point throughout the frame. Hence, the resolution of the SEM is largely determined by the diameter of the electron probe, which significantly depends on the "brightness" of the electron gun. The resolution of a microscope with a thermionic gun is 5–10 nm, and with a field emission gun it is 1–3 nm. The accelerating voltage is usually adjustable from 0.5 kV to 50 kV.

The main advantages of SEM over TEM are its high information content due to the ability to observe images using signals from various detectors as well as the possibility to analyze a more diverse set of samples. The investigated object can be massive or in the form of a thin film. SEM can be used to study, for instance, the nanoscale profile, local distribution of chemical elements over the surface of an object, p–n junctions, and cathodoluminescence.

5.3.1 Operation Principles of Scanning Electron Microscope

Figure 5.8b shows a schematic diagram of an SEM with a tungsten hot cathode. With the help of two or three electromagnetic lenses, the beam entering from the electron gun is focused on the surface of the object into a form of an electron probe

with an extremely small diameter. Magnetic deflection coils deploy the probe on the object in a frame of a given size. The interaction of the probe electrons with the object gives rise to multiple effects (Figure 5.8b). Among them—elastically reflected and secondary electrons, X-ray bremsstrahlung and characteristic X-ray radiation, visible light, Auger electrons, local changes in conductivity and temperature. Any electron radiation that is transmitted, absorbed, and reflected, as well as the voltage induced on the object, can be recorded by appropriate detectors, which convert these emissions, currents and voltages into electrical signals.

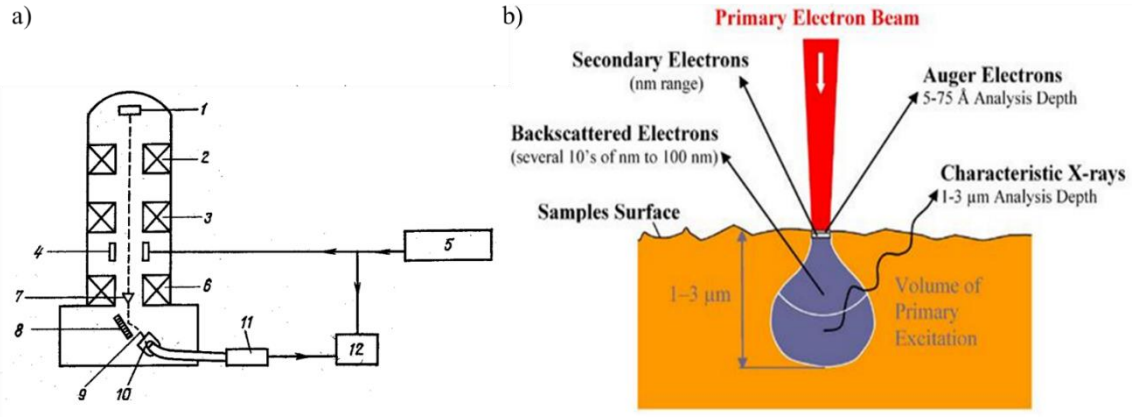

Figure 5.8. a) Schematic of a scanning electron microscope with a hot cathode: 1—electron gun, 2—first condenser lens, 3—second condenser lens, 4—deflecting coils of the scanning system, 5—scan generator, 6—objective lens, 7—primary electron beam, 8—investigated object, 9—secondary electrons, 10—scintillator, 11—photomultiplier, 2—display. b) Electron-matter interactions [5.2].

Secondary electron emission is typically used for sample imaging. The secondary electron detector consists of a scintillator and a photomultiplier tube. The number of scintillator flashes is proportional to the number of secondary electrons emitted from a given point of the object. The magnitude of the signal at each point of the raster depends on the topography of the sample, the elemental and chemical composition, and the presence of local electric and magnetic fields. Apart from the secondary, the reflected electrons can also be detected in SEM. The reflected electrons are captured by a semiconductor detector. In this case, the image contrast is determined by the dependence of the number of electrons on the angle of incidence of the illuminating beam at a given point of the object and by the atomic number of the substance.

5.3.2 Chemical Analysis by Electron Microscopy

To analyze the local elemental composition of the sample, characteristic X-ray emission is detected either by *wavelength dispersive spectrometer* (WDS, WDXS) or by *semiconductor energy dispersive spectrometer* (EDS, EDX, EDXS).

WDS sorts the X-rays based on their wavelengths. It consists of an analyzing single crystal and a detector (a gas-filled proportional counting tube). The crystal diffracts photons which are collected by the detector. The angle depends on the wavelength, orientation of the crystal and the crystal lattice spacing, therefore only X-rays of a given wavelength are detected at any single time. Spectral resolution is about 10 eV. Crystals with different spacing (0.2–20 nm) are used to work with various elements. Development of the layered synthetic crystals has enabled the analysis of the elements with lower atomic mass, from Be to O.

EDS sorts the X-rays based on their energy and consists of a semiconductor detector. The detector absorbs the incident X-ray photons by a series of ionizations within the semiconductor crystal. As a result, several electron-hole pairs appear. When the electrodes are applied, the current is generated that is proportional to the X-ray energy. For example, in a Si detector, each electron ejected from a silicon electron shell consumes 3.8 eV of X-ray energy. With EDS, it is possible to quickly analyze a full characteristic X-ray spectrum for the elements from B to U. EDS has lower spectral resolution (~150 eV), but its sensitivity is higher than that of WDS.

Check Questions

1. Why is carbon used as a material for the electron microscopy substrates?
2. How is focusing performed in an electron microscope?
3. Why do the TEM samples need to be very thin?
4. What kind of image is observed in the back focal plane of the TEM objective lens?
5. What is the purpose of the replica method? How does it work?
6. What techniques are often used for elemental analysis in SEM?

CHAPTER 6. SCANNING PROBE MICROSCOPY

The history of high-resolution microscopes began with the invention of an electron microscope in the 1930s. The resolution of an electron microscope is orders of magnitude higher than one available for optical microscopy and can reach the atomic level. However, it has obvious drawbacks. The research should be performed under high vacuum, that significantly restricts the range of samples that can be studied in it. The test specimen must be thoroughly dried, that prevents the examination of living organisms and any systems requiring fluids using this method. The electron microscope provides a high-quality image of the bulk sample surface only for conducting minerals. To study dielectric ones, they must be covered with a conductive coating, that complicates the process and leads to a smoothing of the surface topography. In addition, in an electron microscope, the sample is bombarded with high-energy electrons, which leads to its destruction and the inability to conduct multiple or long-term studies. Some of these drawbacks were overcome when *scanning probe microscopy (*SPM*)* was invented.

SPM includes a large group of instruments used to study morphology and local properties of a solid surface with high spatial resolution. Prominent examples of SPM are scanning tunneling microscopy (STM), *atomic force microscopy (*AFM*)*, and *near-field scanning optical microscopy (*NSOM*)*. In general, their operation principle is to scan the sample surface with a sharp probe, whose interaction with the surface is short-range. The probe moves along the sample, with a slight step, sequentially collecting information about an ever-new small area of the surface. Usually, the probe initially captures information about one line, and then, making a small indent begins to record a new line, moving in the opposite direction. This method of recording images is called raster scan (Figure 6.1).

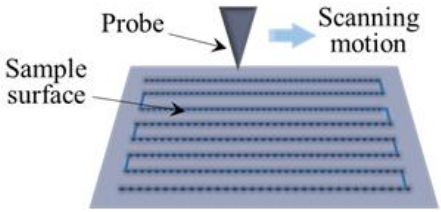

Figure 6.1. Schematic representation of a raster scan of the sample surface by a probe.

In this chapter, the three scanning probe microscopy techniques will be discussed, as well as the fundamental physical principles underlying these methods. In addition, examples of practical implementation and the advantages and limitations of all three techniques will be presented.

§ 6.1 Scanning Tunneling Microscopy (STM)

The *scanning tunneling microscope* was the first among the probe microscopes mentioned. The principle of operation of the STM is based on the *tunneling of electrons* through a narrow potential barrier between a metal probe and a conducting sample. In STM, the probe is brought to the sample surface at the distance of several angstroms. In this case, a potential barrier is formed, and electrons can tunnel through it from the sample to the probe (or vice versa), resulting in a tunneling current. The exponential dependence of the tunnel current on the distance provides high accuracy in determining the distance between the probe and the sample surface.

6.1.1 Main Operating Modes of Scanning Tunneling Microscope

The image of the surface topography in the STM can be formed by two methods, the *constant current method (I = const)*, and the *constant height method (Z = const)* (Figure 6.2).

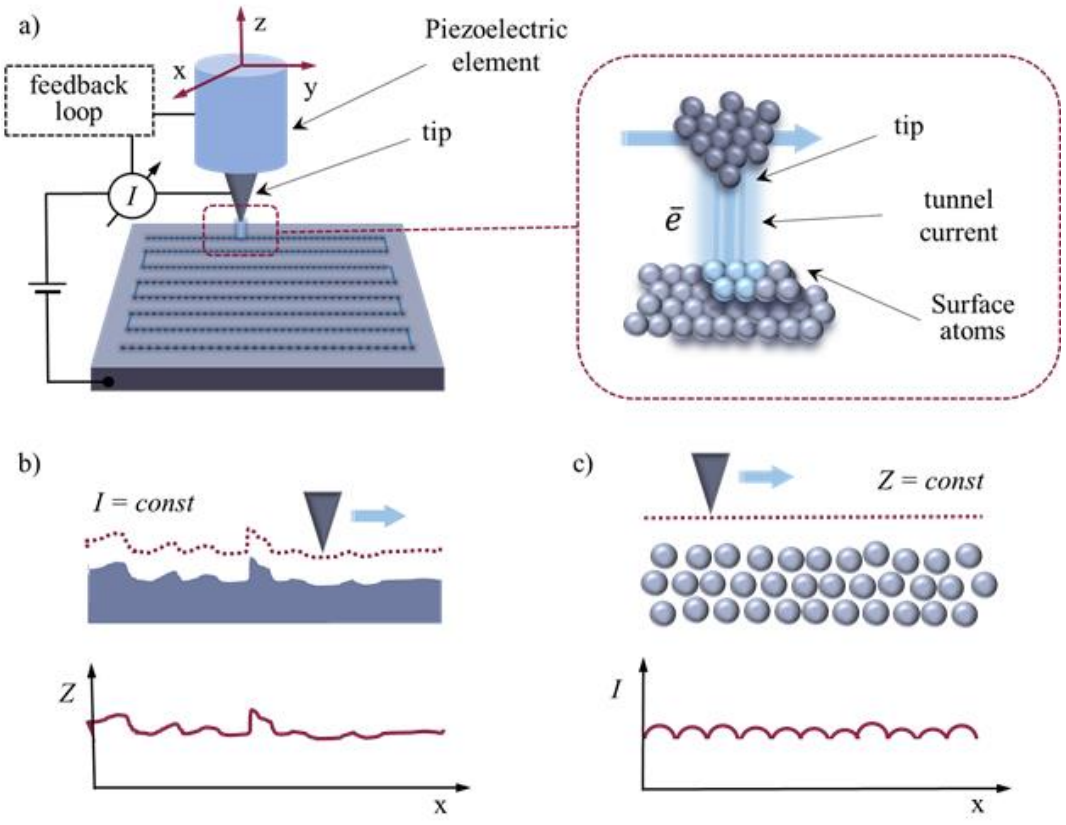

Figure 6.2. a) Simplified scheme of the STM principle. Simplified illustration of the formation of surface images on the STM by the method of b) constant tunnel current and c) constant average distance.

According to the *constant current method (I = const)* (Figure 6.2b), the probe moves along the surface, determining the value of current over each new point and, based on the received signal, adjusts the position of the installation using a feedback

system. The task of the feedback system is to maintain constant the value of tunnel current between the probe and the sample, at the level specified by the operator (I_0). The tunnel current value (and, consequently, the probe-surface distance) is kept at the same level by moving the probe along the Z-axis using a piezoelectric element. The state of the piezoelectric element changes due to the voltage applied to it through the feedback circuit. The change in the voltage at the Z-electrode repeats the surface topography with high accuracy and is written as a function Z = f (x,y).

Often, in the case of atomically smooth surfaces, it is not necessary to constantly adjust the position of the probe along the Z-axis ***(Z = const)***. In this case, the feedback system can be disabled. The probe moves above the surface of the sample at the same height (at several angstroms) (Figure 6.2c), using changes in the tunnel current to build an image. This method makes it possible to significantly increase the speed of scanning and almost in real time to monitor the processes occurring on the sample surface.

6.1.2 Scanning Tunneling Microscope Resolution

The *STM* gives the highest spatial resolution along the Z axis. It is determined by the exponential dependence of the tunnel current on the surface-probe distance and can reach fractions of an Angstrom (the tunnel current changes approximately by an order of magnitude when the distance changes by 1 Å). Also, due to the strong dependence of the tunneling current on the distance, the electrons tunnel primarily between the sample surface and the protruding atom at the probe tip. Because of this, the lateral resolution depends on the quality of the probe and is mainly determined by the tip geometry. If the probe is properly prepared, either a single protruding atom or a small cluster of atoms should be located at the tip. As a result, the lateral resolution of STM can reach the atomic level.

The currently most popular technology for manufacturing STM probes is quite simple. The thin wire is cut at an angle of about 45 degrees with simultaneous stretching. As a result of wire breaking, a spike with a ragged edge with numerous protrusions is formed. One of these protrusions becomes the working tip of the STM probe (Figure 6.2a). The probe created according to this technique guarantees atomic resolution of the STM in most cases.

6.1.3 Tunneling Spectroscopy

Using a scanning tunneling microscope, it is possible to obtain the *current-voltage characteristics (*CVC*)* of the probe-surface tunnel contact at any point of the sample and to study its local electrical properties. The nature of the tunnel CVC significantly depends on the position of the energy levels in the sample and is primarily

determined by the electrons located near the Fermi level. Figure 6.3 shows the energy diagram of the probe-surface tunnel contact of the sample.

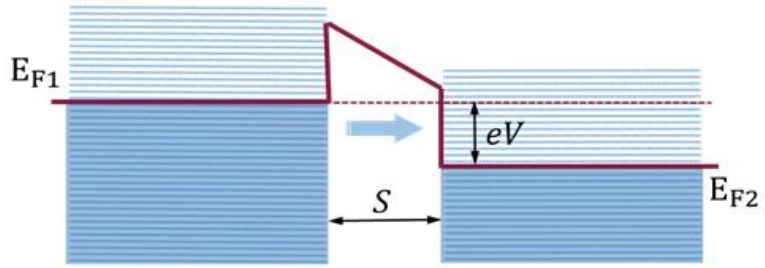

Figure 6.3. Energy diagram of a tunnel transition between two metals. S is the barrier thickness.

Thus, the study of the CVC of the probe-surface tunnel contact provides an opportunity to receive information about the electronic spectra of the sample at a certain point. In the study of semiconductors, tunnel spectra make it possible to determine not only the positions of the edges of the valence and conduction bands relative to the Fermi level, but also to identify spectral peaks associated with impurity states inside the bandgap.

It is worth noting that since the tunneling current strongly depends on the state of the sample surface, the analysis of local tunneling spectra is preferably conducted under a high vacuum. Also, the quality of the obtained data is significantly affected by thermal excitations, which strongly blur the features in the electronic spectra. For this reason, the relevant studies are often performed at low temperatures.

6.1.4 STM Capabilities and Examples of Application

During the analysis of the surface, the tip of the probe can be moved controllably in increments of less than 0.1 A. The maximum available area of the scanning field is ~150×150 mm^2, and the maximum height difference should not exceed a few microns. For STM, a good resolution is 0.1 nm for lateral resolution (along the x and y axes) and 0.01 nm for vertical resolution (along the Z axis).

Unlike an electron microscope, the working medium of an STM can be not only high vacuum but also various gas or liquid media (air, water, nitrogen). Depending on the setup type and the tasks formulated, studies in the STM can be conducted in the temperature range from absolute zero to several hundred degrees Celsius.

The main field of STM application is the physics of the surface of solids, in particular, the visualization of the atomic and molecular structure of surfaces. Even in the first studies on STM, scientists were able to obtain a device resolution of the order of several angstroms. Figure 6.4 illustrates STM images of the silicon sample surface with atomic spatial resolution. Historically, this is the very first STM-image of the

Si(111) surface with atomic resolution [6.1], obtained by the method inventors Binnig and Rohrer in 1982.

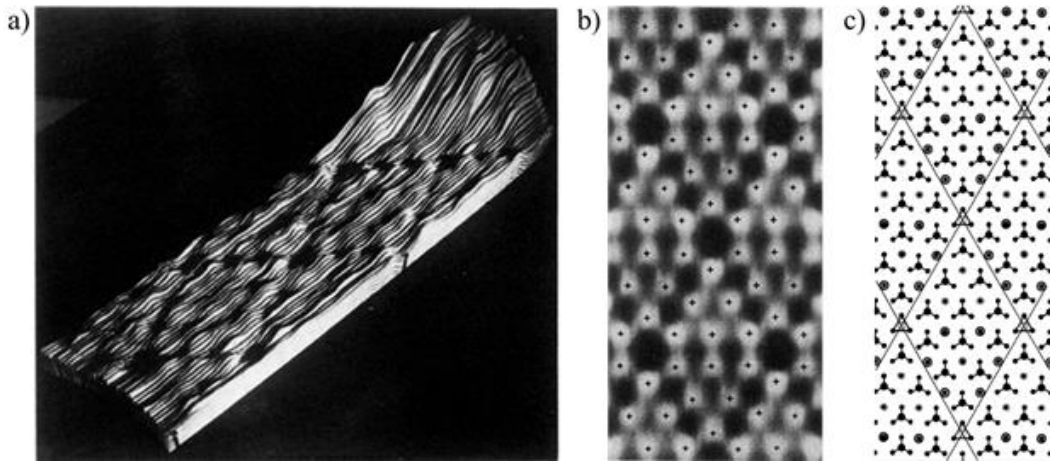

Figure 6.4. STM image of the Si(111) surface: a) scan profile of two complete 7x7 unit cells, b) top view of the scan profile. c) Modified atom model [6.1].

STM methods give the best results when studying conductive surfaces, but the examination of low-conducting samples is also possible. The ability of the microscope to register extremely low values of the tunnel current (up to 0.03 nA) provides the opportunity to study poorly conducting surfaces, e.g., biological objects. Figure 6.5 shows the STM image of a ring configuration of a DNA molecule obtained in 1987, in the pioneering work on the study of biological samples using STM [6.2].

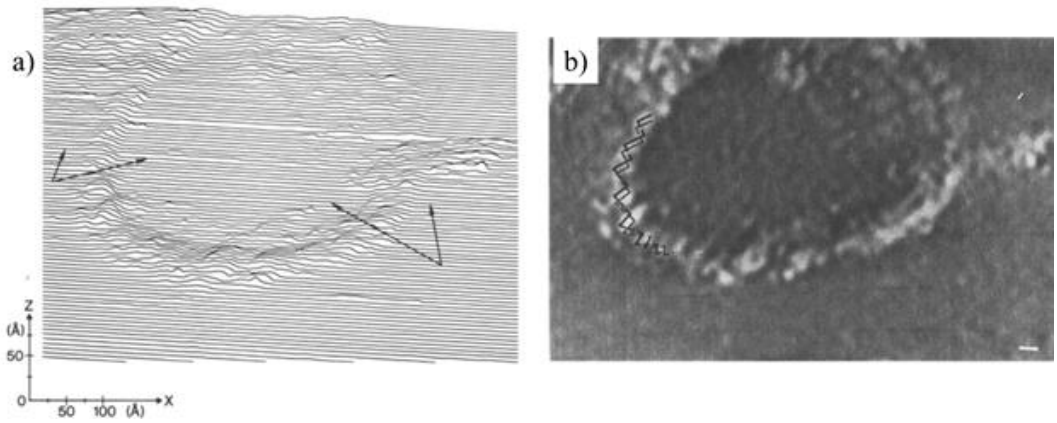

Figure 6.5. a) STM image, and b) its top view of a ring configuration of a DNA molecule. The two strands of the DNA are indicated by the thick and thin lines in the top view [6.2].

In Figures 6.4a and 6.5a, the individual lines forming the image are clearly distinguishable, which demonstrates the essence of the raster method of surface scanning.

Eight years after the creation of STM, physicists have shown that it can be used not only to obtain an image with atomic resolution, but also to *move atoms on the surface*. In 1989, Don Eigler and his colleagues at the IBM research center used a scanning tunneling microscope to lay out the word «IBM» from 35 xenon atoms (Figure 6.6). The technique requires vacuum conditions and ultra-cold temperatures.

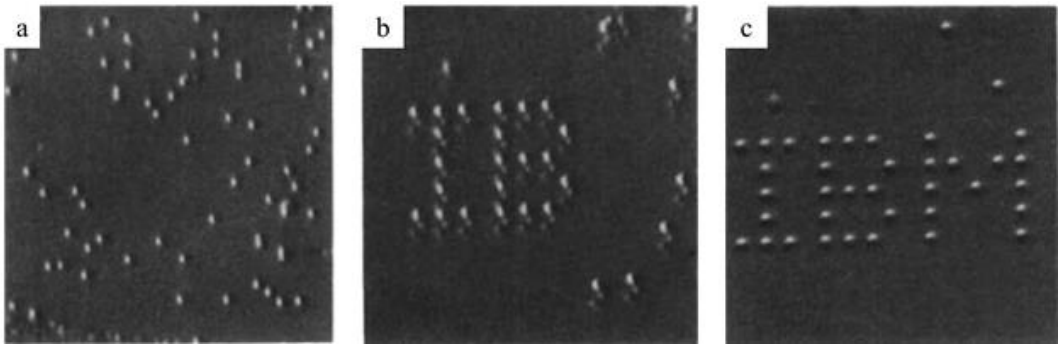

Figure 6.6. A sequence of STM images taken during the construction of a patterned array of xenon atoms on a nickel (110) surface [6.3].

This achievement showed that the STM can be used not only for studying the sample surface, but also for the fine control of its profile.

§ 6.2 Atomic Force Microscopy (AFM)

The *atomic force microscope (*AFM*)* was invented in 1986 by Gerd Binnig, Calvin Quait, and Christopher Gerber. AFM is a high-resolution scanning probe microscope based on the force interaction between the tip and the sample surface. The tip is located at the end of an elastic console (*cantilever*), while the sample is positioned in close proximity to it. The force interaction between the probe and the surface causes the cantilever to bend. By registering the magnitude of the bending, it is possible to determine and control the force of the probe-surface interaction, and therefore the distance between them.

The interactions between the cantilever tip and the sample surface are caused by various types of forces, such as Van der Waals forces, capillary, and adhesive forces. Among these, *Van der Waals force* makes the greatest contribution to the processes involved in the AFM. Most often, the energy of the Van der Waals interaction is approximated by the *Lennard-Jones potential*:

$$V(r) = 4\varepsilon\left[\left(\frac{\sigma}{r}\right)^{12} - \left(\frac{\sigma}{r}\right)^{6}\right], \qquad (6.1)$$

where ε is the depth of the potential well, r is the distance between the tip and the surface, and σ is a constant that determines the distance r corresponding to the

equilibrium of the repulsive and attractive forces, at which the potential energy is zero. σ has the order of magnitude of the diameter of the interacting atoms and is often referred to as «size of the particle». The dependence of the potential (expression 6.1) on the distance is shown in Figure 6.7.

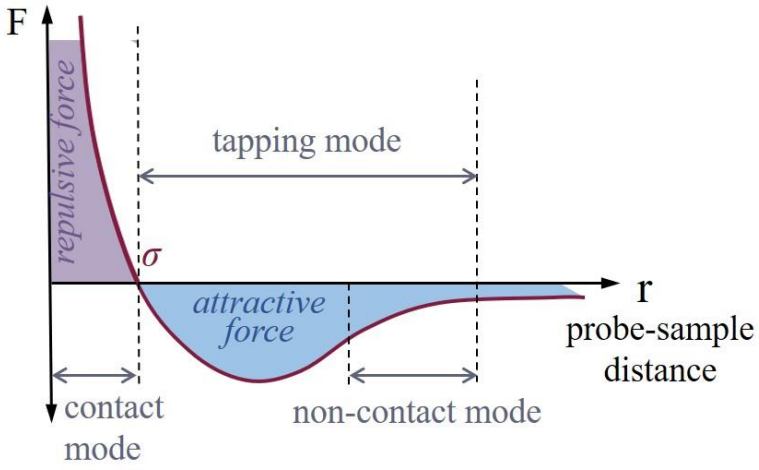

Figure 6.7. Dependence of the interaction forces of tip atoms with the sample surface.

It can be seen that at large distances, the attractive Van der Waals interaction dominates, while at small distances, due to the overlap of the electron shells of the interacting atoms, the repulsive force prevails. The principle of operation of an atomic force microscope is based on the measurement of these forces.

Depending on the distance between the tip and the sample surface, the operating mode is different. In the region where the distance between the tip and the sample is less than a few angstroms and the probe experiences a Van der Waals repulsive force, the microscope operates in *contact mode*. The *non-contact mode* is implemented when the distance between the tip and the surface is from several tens to hundreds of angstroms, and they are attracted to each other. There is also an *intermittent (tapping)* mode that lies in the intermediate region. These modes of AFM operation will be discussed in more detail in section 6.2.3.

6.2.1 Registration of the AFM Probe Interaction with the Sample

AFM images of the surface profile are obtained by registering small bends of the cantilever, at the end of which the probe interacting with the sample is located. In atomic force microscopy, optical methods are often used for this purpose. A simplified scheme of this method is shown in Figure 6.8.

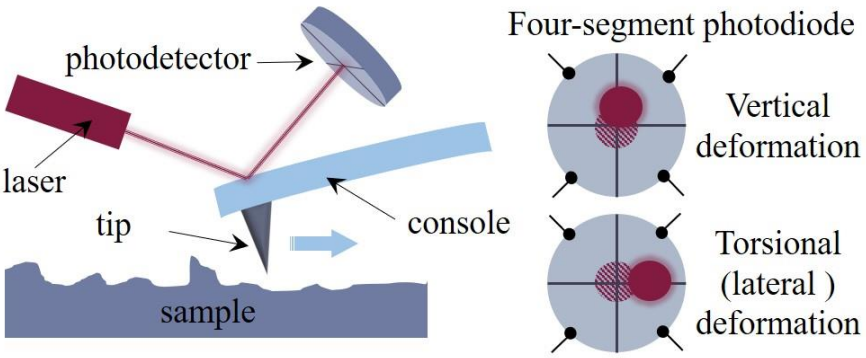

Figure 6.8. Schematic illustration of the optical registration of the AFM console bend.

The idea of the *AFM optical system* is quite simple: a laser beam falls on the upper surface of the console, reflects on it and hits the center of the photodetector. Four-section photodiodes are usually used as photodetectors. The signal recorded by the optical system provides information about the vertical deformation and the torsional deformation of the cantilever. The former arises from the Z-component, while the latter corresponds to the X,Y-components of the probe-surface interaction. The change in the photocurrents in the photodiode segments characterizes the magnitude and direction of the AFM cantilever bending. The change in the photocurrent that characterizes the bending in the Z direction is used as an input signal in the feedback circuit. The *feedback system* changes the distance between the table and the probe to keep the photocurrent constant (using a piezoelectric element), and hence maintains the cantilever bending at the initial level set by the operator.

6.2.2 Atomic Force Microscope Probes

The cantilever is an important element of an AFM, and its characteristics directly affect the properties of the microscope. The cantilever is a flexible bar (average sizes 175×40×4 mm^3) with a tip at its end (Figure 6.9).

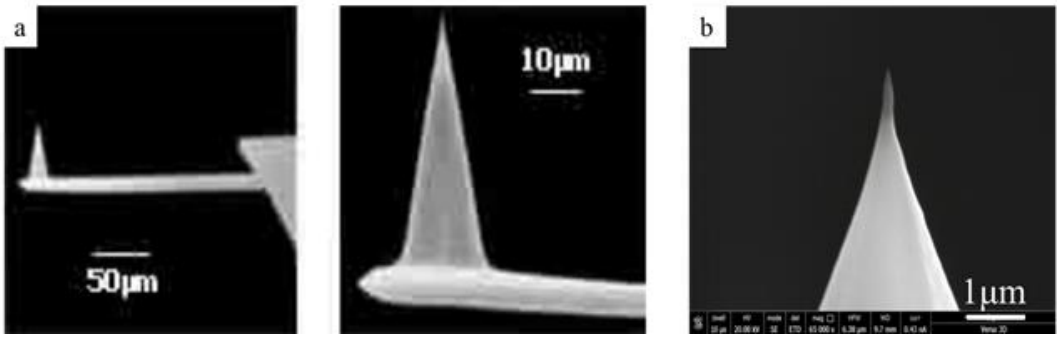

Figure 6.9. Electron microscopy image of a) the AFM probe located on a rectangular console [6.4], b) the probe tip obtained by chemical etching [6.5].

As AFM progressed, the radius of tip curvature varied from 100 to 5 nm. Obviously, reducing the radius of the AFM tip provides an opportunity to obtain images with a higher spatial resolution. The angle at the tip of the probe is also an important characteristic of the probe, on which the image quality depends. Its value can vary from 20 to 70 degrees. The smaller the angle at the tip of the probe, the higher the quality of the resulting image.

The quality and reliability of the images depend on the physical and chemical properties of the probe. As a rule, AFM probes are made of Si, SiO_2 or Si_3N_4, and probes with various chemical coatings are also used to perform specific tasks. For example, to detect individual molecules, a sensor molecule, such as an antibody, is attached to the tip of the probe. To obtain the magnetic profile of a sample, probes with a special coating of thin films of ferromagnetic materials (Fe, Ni, Co, CoPtCr) are used. To study the electrical properties of the surface, low-resistance silicon probes are utilized, or a metal layer (Pt, Au, Ag, Ti) with a thickness of about 10 nm is applied to the probe. Working with such probes is fraught with some difficulties since after several scanning sessions the coating layer can collapse. Besides, additional coating significantly increases the radius of the probe tip.

Apart from the cantilever, the other microscope elements (vibration isolation, electronics, data processing) are not so different from those used in other methods of scanning probe microscopy.

6.2.3 Operating Modes of Atomic Force Microscopes

***Contact mode*.** The most intuitive method is the contact mode, where the AFM probe is brought to the sample surface at *distances comparable to the atomic size*. In this approach, the change in the surface profile is proportional to the displacement of the laser beam on the segmented photodetector, which occurs due to the bending of the cantilever. In the contact operating mode, it is possible to achieve the maximum resolution of the surface image, however, this mode is also associated with disadvantages. The most significant ones are the wear of the probe, which leads to a decrease in resolution and the possibility of damaging soft samples. These problems can be partially solved by using the tapping mode of AFM operation.

Tapping Mode. Tapping mode or the intermittent contact AFM is the most preferred operating mode for high-resolution topographic imaging of soft and delicate samples. In this operating mode, a small piezoelectric crystal makes the cantilever oscillate up and down at its resonance frequency of elastic vibrations. The tip oscillates vertically, alternately contacts the surface and lifts off it. The amplitude of this oscillation typically ranges from 20 nm to 100 nm. As the tip approaches the surface of the sample, the force interaction between them begins to influence the vibrations of the cantilever. Thus, in the absence of the probe-surface interaction, the spatial pattern

of the oscillation phase distribution will be described by a harmonic law with a given period and amplitude. However, when interacting with the surface, the phase of the oscillating cantilever will change. These changes will carry information about the topography of the studied surface.

Non-Contact Mode. As the name suggests, in a non-contact AFM (or NC-AFM), the probe is held at a considerable distance from the sample surface, and they do not directly contact each other. The cantilever oscillates over the sample surface with a small amplitude at a frequency higher than its resonant frequency. This provides a better AFM sensitivity compared to that of the tapping mode, but at the same time, the device becomes particularly sensitive to contamination and various fluctuations. To achieve a high spatial resolution of the AFM, the operation of the microscope must be performed in a high vacuum. Due to its delicacy and sensitivity, the non-contact mode is widely used in biological research.

6.2.4 AFM Capabilities and Examples of Application

AFM can provide images with a resolution close to atomic, and under vacuum conditions even exceeding it. As mentioned earlier, the lateral resolution directly depends on the radius of the probe tip and can reach 1 angstrom. Vertical resolution can be sub-angstrom, but such values are achievable only under a high vacuum. This spatial resolution provides images of atoms in the crystal lattice of solids. Figure 6.10a shows an AFM image with atomic resolution of a copper crystal lattice coated with an oxide film obtained in the contact mode [6.6].

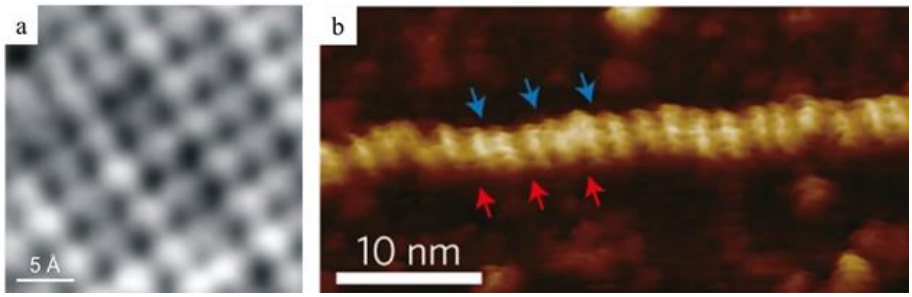

Figure 6.10. a) AFM image with atomic resolution of a copper crystal lattice coated with an oxide film obtained in the contact mode [6.6]. b) Circular plasmid DNA imaged in buffer solution by frequency modulation AFM. Red and blue arrows indicate major and minor grooves of the DNA, respectively [6.7].

It is worth remembering that the vacuum environment is not a mandatory condition for AFM. Instead, imaging can be performed in a liquid medium, which permits the samples to be analyzed in close to natural conditions. This is especially important for the study of biological objects. When studying properly prepared biological samples, a resolution of 2–3 nm can be achieved. Figure 6.10b shows DNA

imaged in buffer solution by frequency modulation AFM [6.7]. In addition, AFM is widely used in the composition of *near-field microscopes* as a node that provides a topographic image of nanostructured objects.

§ 6.3 Near-Field Scanning Optical Microscopy (NSOM)

As mentioned at the beginning of the chapter, traditional methods of obtaining object optical images have significant limitations associated with light diffraction. There is a so-called *diffraction limit* that restricts the minimum size of an object that can be imaged by an optical system using light. For the visible range, the minimum size is about 200–350 nm, which provides an opportunity to obtain only averaged information over the nanostructure or the ensemble of nanoparticles. In near-field optical microscopy, the construction of an object image is performed in a different way, which overcomes the limitations associated with light diffraction and achieves a resolution of tens of nanometers.

The *near-field scanning optical microscope* (NSOM) was invented by Dieter Pohl in 1982, soon after the invention of the scanning tunneling microscope. This microscope is based on the effects of spatial localization of the electromagnetic field, or rather, the optical field in the region smaller than the wavelength of light. The idea of such localization can be simply illustrated by considering the electromagnetic fields generated by an oscillating electric dipole. As shown in Figure 6.11, the dipole field can be roughly divided into two parts.

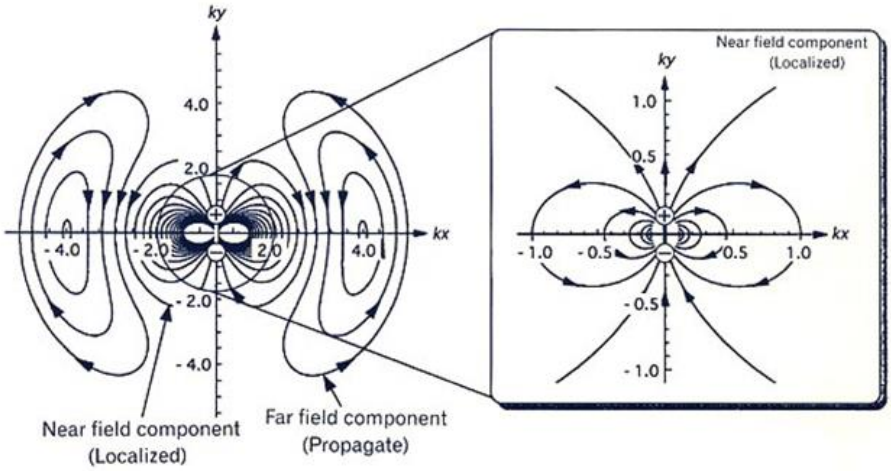

Figure 6.11. Electromagnetic fields generated by an oscillating electric dipole. On the right, an enlarged image of the near-field region of the dipole.

The first field, whose force lines are shown as curved looped lines, is a wave propagating into the *far zone*. These waves are registered by the observer. The second field is concentrated around the electric dipole in a volume of order R^3, where R is the arm of the dipole. The corresponding waves do not propagate over long distances,

forming a so-called evanescent or near field. The strength of this field is high, and although its energy is much greater than the energy of the propagating wave, all of it is concentrated in the near zone of the dipole and is unavailable to the observer.

The analysis of the *near-field* spatial distribution can be performed using a test (second) dipole. If the test dipole is placed in the near-field region of the primary dipole, the test dipole will be excited and generate a field in the far zone that can be registered by an observer. Thus, by moving the test dipole in the near field, it is possible to study the field structure of the dipole of interest. Similarly, if the localized near field is brought to the structure under study, then the elements of the structure that fall into the near-field region can be selectively excited. This is the main idea of achieving high spatial resolution in near-field optical microscopy. Methods of near-field microscopy are usually separated into two groups depending on the type of probe used: with or without aperture.

The first method is based on the formation of an evanescent field that originates when light passes through subwavelength diaphragms, such as holes with a diameter much smaller than the wavelength of the incident radiation. The resulting field is localized in the region of the aperture and rapidly attenuates at distances comparable to the hole diameter ($10\ \text{nm} \sim d \ll \lambda$). This is the so-called *aperture method*.

The second method is to use a real electric dipole with a size much smaller than the wavelength, oscillating in the visible part of the spectrum. This is an *apertureless method*. Good candidates for the role of such dipoles are semiconductor quantum dots and metal nanoparticles immobilized on the tip of a dielectric probe. Also, for these purposes, sharp metal probes with a nanoscale radius of the tip curvature can be used. The latter behave as dipoles with a large optical transition oscillator strength.

To sum up, in NSOM, the sample is scanned in the immediate vicinity of the aperture or dipole. The resolution of NSOM is primarily determined by the aperture diameter at the end of the waveguide, the quantum dot size, or the radius of tip curvature of the metal probe. In commercial NSOM devices, the resolution can reach 5–30 nm.

6.3.1 Aperture Near-Field Scanning Optical Microscopy

There are several schemes for building a near-field optical microscope. Currently, aperture NSOMs are the most common, where s*harpened optical fibers ended by a nanoscale hole* (10–50 nm) are used as probes. Figure 6.12 represents the main configurations used in the aperture NSOM to illuminate the sample and collect the secondary radiation. In these schemes, a nano-aperture is utilized either as a nano-collector, or as a local source, or both.

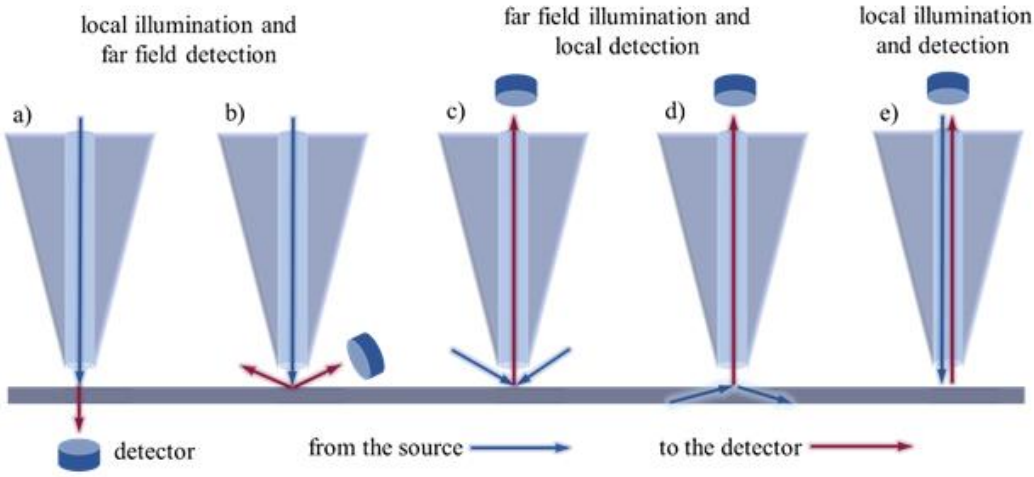

Figure 6.12. Schematic images of sample illumination and secondary radiation collection in the aperture NSOM. Local illumination and far-field detection for: a) reflection and b) transmission. Local detection with c) far-field illumination and d) illumination by total internal reflection, e) local illumination and detection.

The most commonly implemented scheme is the one in which the near *field is used to illuminate the sample* (Figure 2a, b). According to the scheme, the laser radiation is spatially localized using a fiber probe, resulting in a near field at its output. This field is placed in close proximity to the sample surface and excites it. The resulting secondary radiation is collected in the far zone by classical optics. This scheme enables the study of samples for both reflection (Figure 6.12a) and transmission (Figure 6.12b) and provides a minimum level of background illumination and maximum sensitivity.

According to another approach, the probe aperture is placed close to the surface to *collect the object emission in the near field*. In this case, the sample can be illuminated by various methods (Figure 6.12c, d, e). The most obvious one is the illumination of the object from the far-field using standard optics (laser beam), represented in Figure 2c. The simplest configuration from the implementation point of view is the one where the sample is illuminated by total internal reflection (Figure 6.12d). In this case, an uncoated probe can be used to collect the light. The scheme shown in Figure 2e is also interesting, in which illumination and collection are both locally performed in the near field of an object. This mode usually provides the highest spatial resolution but at the same time the lowest signal intensity.

***The main disadvantages of the aperture method are*:**

1. Extremely low probe throughput. The transmission of nanoscale apertures is proportional to the sixth power of the aperture diameter to the wavelength ratio. As a result, the transmittance of such probes is lower than 10^{-4}, which limits the signal intensity.

2. Low probe strength. When the intensity of the laser increases, the metal coating begins to disintegrate under the influence of light. Therefore, acceptable laser radiation power is limited to 1–2 mW.

These factors lead to the low *sensitivity* of the measurements. An attempt to improve it by increasing the aperture leads to a deterioration in the spatial resolution of the method. Therefore, the aperture NSOM is primarily used for the luminescent analysis of nanostructures and is not suitable for acquiring Raman spectra of most materials. Exceptions are materials with extremely large Raman scattering cross-sections, such as diamond and silicon.

The very nature of *evanescent waves* requires the probe to be close to the surface, usually at a distance of a few nanometers. Unlike other scanning probe methods based on the measurement of tunnel current or mechanical interaction, the quantity observed in optical microscopy (electromagnetic intensity) cannot be used to control the vertical separation between the probe and the object. The difficulty is that there is no direct correlation between the intensity of the detected electromagnetic radiation and the probe–sample distance. Therefore, as mentioned in Section 6.1.4, in the near-field microscope setups, the AFM is often used as a node for topographic scanning of nanostructures. In addition, AFM can also be used for the sequential or parallel recording of the structure profile, which provides an opportunity to compare AFM and luminescent (Raman) images of the object obtained by NSOM.

As an example, Figure 6.13 shows the images obtained from the AFM and transmission NSOM channels for single golden dots arranged in an orderly manner on the surface [6.8]. The sample scan was performed with an aperture of 120 nm and transmitted light was collected in the far field. On the AFM image (Figure 6.13b), the position of the dots corresponds to the high intensity on the scale bar, while the NSOM channel (Figure 6.13c) shows dot positions as the low-intensity spots.

As can be seen from Figure 6.13, the single golden dots create a distinct shadow on the transmission NSOM image. When the NSOM probe is not blocked by the dot structure, the NSOM intensity is very high, but when the probe position matches the dot position, the NSOM intensity becomes very low.

There is usually a clear correlation between the sample characteristics discovered in the AFM and NSOM. The ability to obtain nanometer-resolution topographic data and optical data simultaneously from the same area of the surface provides a more accurate determination of the particle size, shape, and optical properties. The data becomes particularly informative if multiple excitation wavelengths can be used in the NSOM.

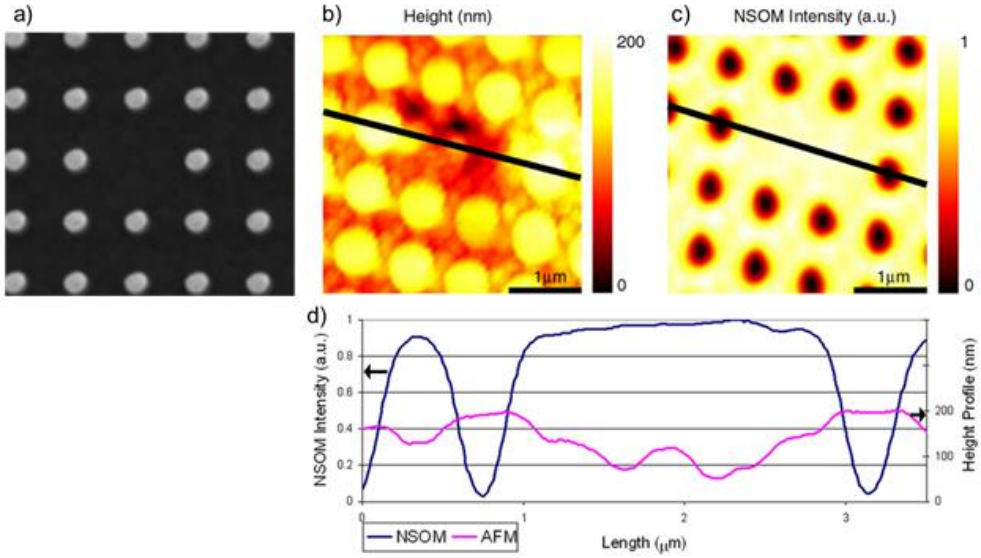

Figure 6.13. Scan results for ordered golden dots: a) SEM topography of dots; b) AFM channel, in nm; c) NSOM channel, in arbitrary units; d) a representative cross-section of the AFM and NSOM channels. The line drawn through b) and c) shows for which points of the images the signals are compared [6.8].

It is important to note that it is often difficult to separate the effects of topography from the response of a different nature (for example, optical), that does not allow us to unambiguously interpret the surface data obtained by only one of the methods.

6.3.2 Apertureless Near-Field Scanning Optical Microscopy

Apertureless technique implies the use of a strong near field of an *isolated dipole* with large oscillator strength. The main challenge in this method is the creation of such a dipole. The most suitable candidates are plasmons, i. e. collective oscillations of electrons localized in metal nanoparticles or near the tip of a sharpened metal probe, resonantly excited by light. In the literature, this phenomenon is called *tip enhanced Raman scattering (*TERS*)*. The idea is that a local plasmon is resonantly excited near the tip of a metal probe. This plasmon forms a near field localized in a small volume around the tip, whose strength is significantly higher than that of the original electromagnetic excitation field. The characteristic size of the localization area of the enhanced field is approximately equal to the radius of tip curvature. This value determines the spatial resolution of the method and is significantly lower than the diffraction limit (Figure 6.14).

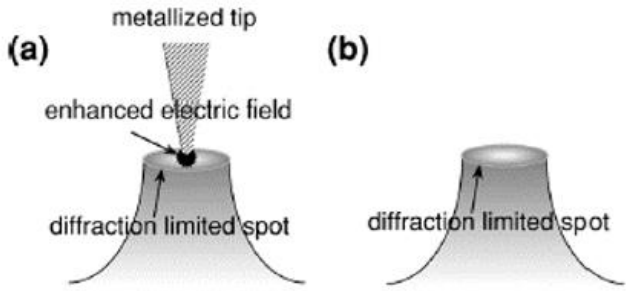

Figure 6.14. a) The scheme of using a metal probe in an apertureless NSOM for the formation of an enhanced local electric field in a region much smaller than the diffraction limit. b) The minimum excitation region in conventional micro-Raman spectroscopy.

The *enhancement factor* and *spatial distribution of the enhanced field* depend on the material and shape of the tip, as well as on the exciting radiation (its wavelength and polarization direction relative to the probe axis). Figure 6.15a shows the calculation results of the electric field strength near the golden tip illuminated by linearly polarized laser light. Figure 6.15b represents a similar calculation for the silver probe illuminated by linearly polarized light incident at an angle of 45 degrees relative to the probe axis. In both cases, it is assumed that the optimal conditions for resonant excitation of the local plasmon have been achieved.

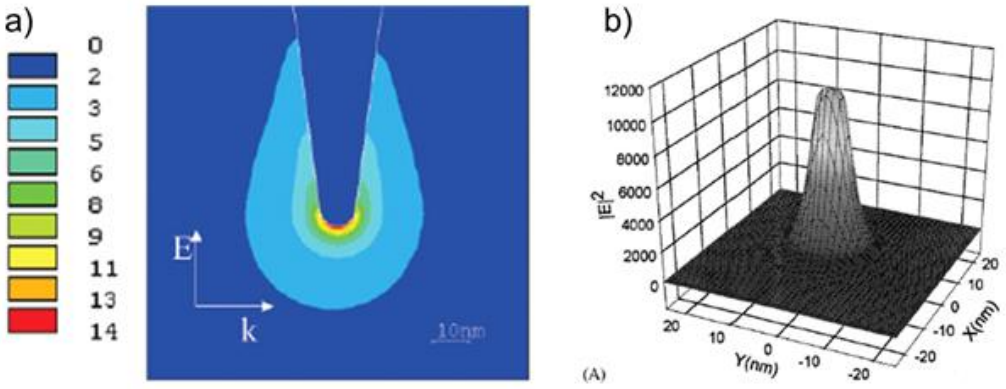

Figure 6.15. The calculation results of the electric field strength near the: a) golden tip illuminated by linearly polarized laser light; b) silver probe illuminated by linearly polarized light incident at an angle of 45 degrees relative to the probe axis.

According to the calculation, at the tip of the probe, the strength can increase by ~20 and ~100 times, in turn, the intensity of the excitation field increases by $|K(w_{ex},R)|^2$ times. Here $K(w_{ex},R)$ is the enhancement factor that depends on the excitation frequency w_{ex} and the tip–probe distance R. This naturally leads to a corresponding increase in the efficiency of optical dipoles excitation responsible for luminescence or scattering on nanostructures located at a distance R from the tip of the probe.

It is worth considering that this secondary radiation may have a frequency w_{sc} that is different from the frequency of the laser field w_{ex}. Its intensity will be $|K(w_{ex},R)|^2$

times higher than the intensity of the signals in the absence of the probe, so that it can be detected in the far zone. In addition, the induced dipoles within the sample also create an intense near field in their vicinity, which, in turn, can effectively excite local plasmons at the tip. As a result, estimating the real enhancement is quite a challenge. However, regardless of the details, it is common that the highest enhancement is characteristic of secondary radiation, whose frequencies are not too different from the frequency of the excitation light.

6.3.3 Comparison of Aperture and Apertureless NSOM

The apertureless NSOM has several advantages compared to near-field microscopy utilizing metallized fiber-optic probes. The theoretical limit of sensitivity and spatial resolution of this method is much better, which makes it possible to register Raman spectra of nanostructures of 5-10 nm, which are significantly less intense than the luminescence spectra. The use of metal or metal-coated probes, which are almost identical to the probes in atomic force and scanning tunneling microscopy, provides an opportunity to simultaneously obtain AFM (STM) and optical (Raman) images of the sample. Figure 6.16 shows a schematic illustration of the microscope probe that provides both AFM and Raman images with high spatial resolution.

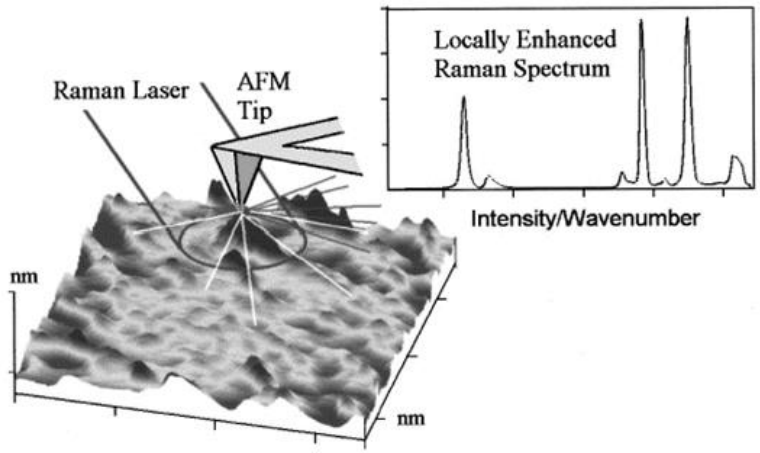

Figure 6.16. Illustration of the AFM/Raman microscope operation providing both AFM and Raman images with high spatial resolution. The local area of nanometer size can be analyzed in terms of chemical composition, structure, and stresses.

Despite the given advantages, the implementation of apertureless NSOM is more complicated due to the difficulties in the probe design optimization. Indeed, the best parameters of the TERS method, both sensitivity and resolution, are achieved only if the frequency of the exciting radiation precisely matches the one of the local plasmon resonance of the probe tip. Besides, the production of metal probes with geometric parameters that provide reproducible values of the field localization and enhancement

factor is a complicated technological task. Additional complexity stems from the fact that the laser light focused on the probe tip also excites secondary radiation from the area of the object located inside the diffraction spot. During the measurement, this radiation acts as a background noise that masks the useful signal.

In the case of massive samples, it is more appropriate to use the same micro-lens both to illuminate the metal probe and to collect light in the far zone. Figure 6.17 shows the Raman spectra on nanocrystals of adenine biomolecules obtained using the TERS and micro-Raman methods, which demonstrate the capabilities of an apertureless NSOM with combined channels of excitation and collection of scattered radiation [6.9].

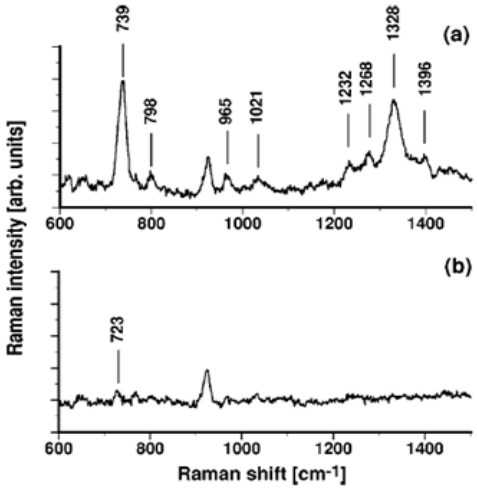

Figure 6.17. The Raman spectra of nanocrystals of adenine molecules obtained using the a) TERS and b) micro-Raman techniques demonstrate the effect of Raman intensity enhancement by the objects near the tip of the metal probe [6.9].

In Figure 6.18, the effect of enhanced Raman intensity in the presence of the metal probe is demonstrated by comparing the Raman spectra obtained under the conditions of the probe-sample proximity and in the absence of the probe [6.10].

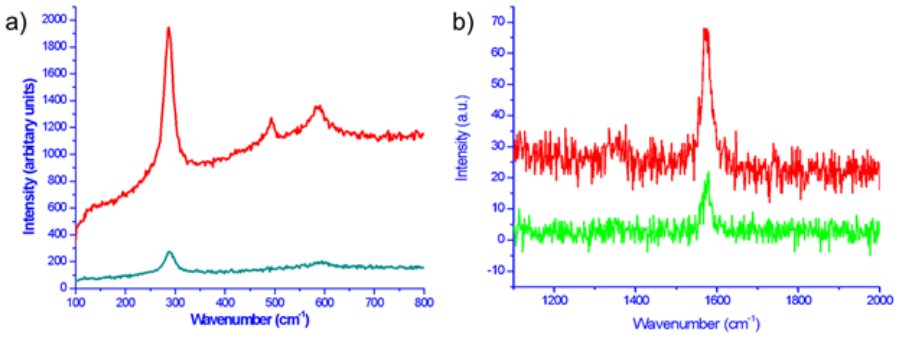

Figure 6.18. Comparison of the Raman spectra intensity of a) CdS crystals and b) a layer of carbon nanotubes on an opaque surface obtained in the presence of a probe (upper spectra) and without a probe (lower curves) [6.10].

These results clearly demonstrate the attractiveness of utilizing locally enhanced optical fields near the tips of metal probes in spectroscopy.

Check Questions

1. How do you think the capillary forces of an aqueous film act on the operation of atomic force microscopes? Do they attract or repel the tip and the sample?
2. What is electron tunneling?
3. How does the tunneling current change when the distance increases?
4. What are the major requirements for reaching the highest possible resolution in AFM and STM?
5. What is the near field?
6. What are the ways of creating the near field in NSOM?
7. Why is it advantageous to combine NSOM and AFM regimes?
8. What is TERS? What do we need it for?

CHAPTER 7. X-RAY SCATTERING TECHNIQUES

It is well known that size, chemical composition, and structure of nanoparticles, as well as local stresses and inhomogeneities in them directly affect their physical properties. Various methods based on a phenomenon of X-ray scattering can be used to study all these characteristics. In this case, the source of information is the spatial distribution of the intensity of the scattered X-ray radiation on the analyzed object. Depending on the type of the sample, as well as the nature of the required information, different X-ray scattering techniques can be employed. Among all these methods, we will focus on *small-angle X-ray scattering* (SAXS) and *wide-angle X-ray scattering* (WAXS).

§ 7.1 Wide-Angle X-Ray Scattering (WAXS)

X-ray photons interact with matter in different ways. If the interaction is coherent and elastic, it is called X-ray diffraction (XRD) or Bragg scattering. In the X-ray diffraction approach, X-ray photons are registered after their collision with electron clouds of atoms, which only changes the photons' trajectories while preserving their phases and energies. The scattered photons form an interference-modulated pattern, called a *diffraction pattern* or a *scattering pattern*. If the system has translational symmetry, then the scattered photons destructively interfere with each other in most directions, except for a few specific directions, where they exhibit constructive interference. These specific directions depend on the lattice structure and symmetry and can be calculated using *Bragg's law*. *Bragg's law* relates the X-ray scattering angle (θ) with an interplanar distance of the crystalline structure (d):

$$n\lambda = 2d \cdot sin\theta, \tag{7.1}$$

where λ is the wavelength of the incident radiation, n is an integer number, d is interplanar distance, and θ is X-ray incident angle, as shown in Figure 7.1.

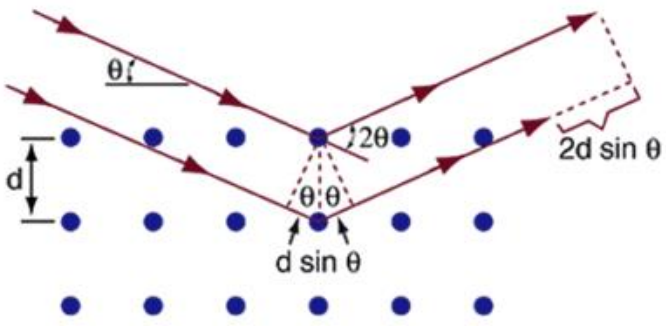

Figure 7.1. Schematic illustration of Bragg's law for the diffraction on a two-dimensional crystal lattice.

The recorded *diffraction peaks* from a sample can be broadened by the finite size of the crystallites. The peak broadening does not correlate with the object size, but with the coherent domain length where the long-range order is preserved. However, in the case of nanostructures (such as quantum dots or quantum rods), often the entire structure is a single ordered crystal. Thus, the size of nanocrystals can be calculated from the position and width of the peaks on the diffractogram using the Scherer equation:

$$D = \frac{k \cdot \lambda}{cos\theta \cdot (\Delta 2\theta)}, \tag{7.2}$$

where λ is the wavelength of the X-ray radiation, $\Delta(2\theta)$ is the width of the reflection at half the height in radians, and k is a constant. This method was used in the experiment below to determine the size of colloidal PBS nanocrystals [7.1].

7.1.1 Application Example. Determination of Nanocrystal Sizes

The linear size of PbS nanocrystals (D) was determined experimentally using the X-ray structural analysis method on the Rigaku diffractometer. A schematic illustration of the 5-circle goniometer system of the diffractometer is shown in Figure 7.2.

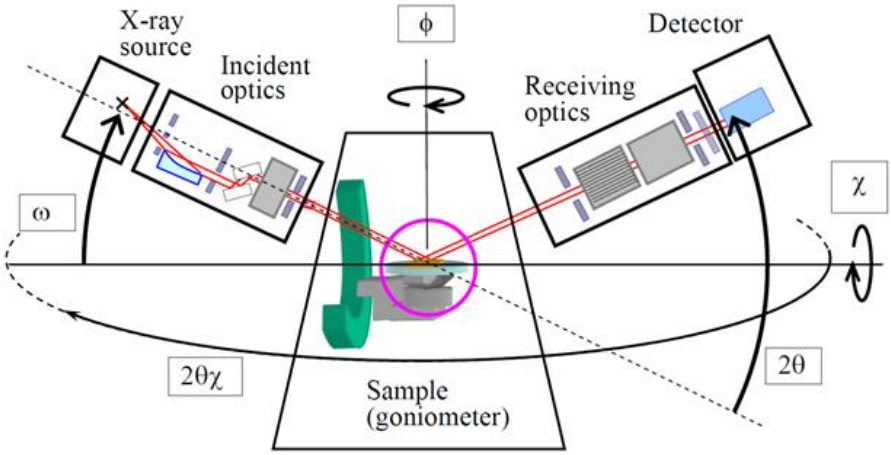

Figure 7.2. A schematic illustration of the 5-circle goniometer system of the Rigaku diffractometer. The sample is manipulated with 3-circles (ω, χ, φ) and the detector is moved with 2-circles (2θ and 2θχ) [7.1].

The obtained diffractograms represent the dependence of the scattered X-ray radiation intensity on the double angle of incidence on a PbS quantum dot ensemble. Examples of the spectra of PbS quantum dots of different size are shown in Figure 7.3.

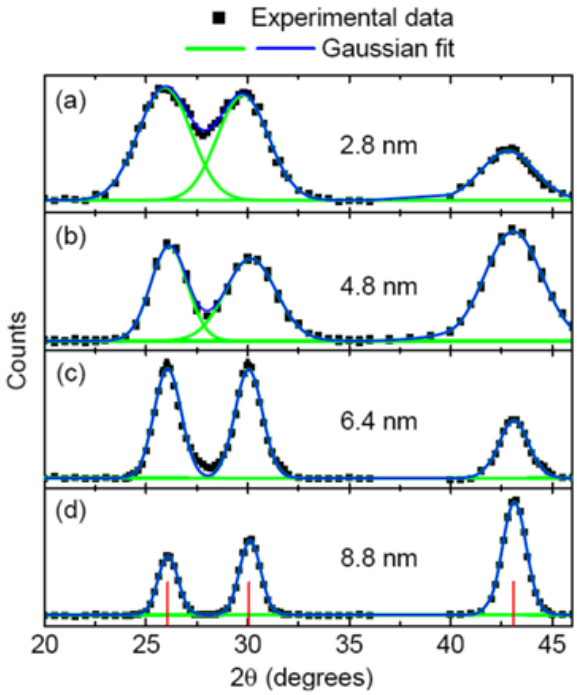

Figure 7.3. Diffractograms of PbS quantum dot samples of different size. The vertical lines show the position of the bulk PbS peaks. The approximation of peaks by Gaussian curves is shown [7.2].

The peak position on the diffractogram of PbS quantum dots almost coincides with the position of the diffraction peaks for the bulk PbS. As the QD size decreases, the diffraction peaks broaden due to the finite nanocrystal sizes and the possible presence of structural defects. The PbS QD diameters were calculated from the position and width of the peaks obtained from the XRD data using the Scherrer equation (expression 7.2). In the calculations, the value of the constant k was assumed to be 1.

It follows from Bragg's law that the smaller the scattering angle at which the radiation is detected, the larger the structural features are investigated. Wide-angle X-ray scattering (WAXS) is based on the analysis of scattered radiation at large angles and examines the sample structure on the smaller length scale than the interatomic distances. In turn, if the sample contains structural features on the nanometer scale, usually in the range of 1–100 nm, then it can also be studied by analyzing the radiation scattered at a very small angle (0.05–5 degrees). This method of X-ray structural analysis is naturally called small-angle X-ray scattering (SAXS). Small angle X-ray scattering and wide-angle X-ray scattering (SAXS and WAXS) are complementary techniques.

7.2 Small-Angle X-Ray Scattering (SAXS)

Small-angle X-ray scattering (SAXS) is a nondestructive method used in determining size, size distribution, shape, orientation, and structure of various nanoparticles. In SAXS, the crystalline or amorphous sample is subjected to an incident

beam of monochromatic X-ray, whose wavelength is about 0.1–0.2 nm. Due to the differences between the electron density inside and on the surface of nanoparticles, the incident radiation is scattered. The intensity of scattered radiation is measured by a detector covering small angles.

Previously, the determination of PbS nanocrystal sizes using X-ray diffraction analysis was considered. To highlight the multifunctionality of this group of methods, the SAXS application for the study of the nanocrystal ordering is further considered.

7.2.1 Application Examples. Determination of Nanocrystal Ordering

In the paper [7.3], the self-assembly of colloidal PbS nanocrystals was studied in real-time during the assembly procedure. A combination of controlled solvent evaporation from the bulk solution and small-angle X-ray scattering (SAXS) in transmission mode was used. To observe the time-resolved assembly of PbS nanocrystals during solvent evaporation, a specially constructed sampling chamber for SAXS measurements in the transmission mode was used (Figure 7.4a).

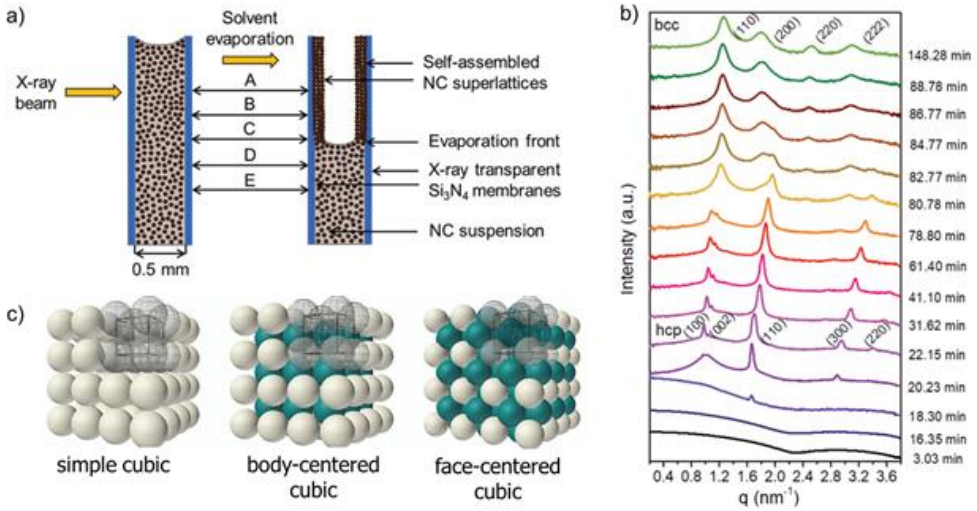

Figure 7.4. a) Illustration of the sample cell used for in situ SAXS measurements, where colloidal PbS nanocrystals self-organize into highly ordered superstructures along the cell windows upon controlled solvent evaporation. Left: schematic representation of the beginning of the experiment (3 min of elapsed time). Right: intermediate stage of the self-assembly process, where part of the solvent has already evaporated. b) 2D representation of selected SAXS curves from. c) Three kinds of cubic unit cell: simple cubic, body-centered cubic, and face-centered cubic [7.3].

Figure 7.4b shows that as the PbS nanocrystals start to form ordered assemblies along the chamber upon the solvent evaporation, Bragg peaks appear in the SAXS patterns. Additionally, the observation of {100}, {002}, and {110} reflections corresponding to different crystallographic directions in the unit cell confirms the formation of a 3D superstructure. During further drying, the Bragg peaks continuously shift to larger q-values indicating lattice contraction, and at 80 minutes of elapsed time, the crystallographic system undergoes a transformation into a body-centered cubic (bcc) superstructure shown in Figure 7.4c.

Check Questions

1. What is the primary difference between SAXS and WAXS? What information do they provide?
2. How do the WAXS peaks depend on the QD size?
3. How can we calculate the interparticle distance using Bragg's law?
4. What are the typical scattering angles studied in SAXS?

SUGGESTED READING

1. John C. H. Spence. High-Resolution Electron Microscopy. Oxford University Press, 2013.

2. А.В. Федоров, А.В. Баранов. *Оптика квантовых точек*. В кн.: Оптика наноструктур. Под ред. А.В. Федорова: – СПб. Недра, 2005. с. 181.

3. Light scattering in solids: Resent results / ed. by M. Cardona, G. Guntherodt. 1982.

4. Г.Е. Скворцов, В.А. Панов, Н.И. Поляков, Л.А. Федин. *Микроскопы*. - Л.: Машиностроение, 1969. –511 с.

5. J. Shah. *Ultrafast Spectroscopy of Semiconductors and Semiconductor Nanostructures*. Springer Series in Solid-State Science,

6. Bangwei Zhang. *Physical Fundamentals of Nanomaterials*. *Chapter 5 - Principles, Methods, Formation Mechanisms, and Structures of Nanomaterials Prepared via Self-Assembly*. Micro and Nano Technologies. 2018, P. 177-210.

7. Shiul Khadka. THESIS. *Colloidal quantum dot based light emitting devices on silicon substrate*. Urbana, Illinois. 2013. P. 42.

8. M.L. Notarianni, V.K Jinzhang, N. Motta. *Synthesis and applications of carbon nanomaterials for energy generation and storage*. Beilstein Journal of Nanotechnology. 2016. 7. P. 149–196.

9. В.Л. Миронов. *Основы сканирующей зондовой микроскопии: учеб. пособие.* Техносфера, 2009. С. 144.

10. Edited by Alicia Esther Ares. *X-ray Scattering. National University of Misiones*. 2017. Open access peer-reviewed Edited Volume: https://www.intechopen.com/books/x-ray-scattering.

11. A.V. Fedorov, A.V. Baranov, A.P. Litvin, S.A. Cherevkov. Special methods for measuring physical quantities. St.-Petersburg, ITMO University. 2014. – P.127.

REFERENCES

CHAPTER 1. NANOSTRUCTURES & NANOTECHNOLOGIES

1.1. C. Murray, C. Kagan, and M. Bawendi. *Synthesis and characterization of monodisperse nanocrystals and close-packed nanocrystal assemblies*. Annual Review of Materials Science. 2000. V. 30. No. 1. P. 545–610.

1.2. Gaponenko S.V. *Introduction to nanophotonics.* Cambridge University Press. 2010.

1.3. Е. Биргер. *Фуллерены в роли полупроводников*. NanoWeek. 8–14 сентября 2008. No. 34.

1.4. F. Zhang, P.X. Hou, C. Liu, H.M. Cheng. *Epitaxial growth of single-wall carbon nanotubes*. Carbon N. Y. 2016. 102, 181–197.

1.5. Zan, X. *Flexible electrochemical biosensors based on interfacially assembled metal nanocrystals and graphene paper.* Doctoral thesis, Nanyang Technological University, Singapore. 2016. P. 141.

CHAPTER 2. NANOFABRICATION

2.1 Sukhanova, Y. Volkov, A.L. Rogach, A.V. Baranov, J.H.M. Cohen, I. Nabiev. et al. *Lab-in-drop: controlled self-assembly of CdSe/ZnS quantum dots and rods into polycrystalline nanostructures with desired optical properties*. Nanotechnology. 2007. V. 18. P. 185602.

2.2 A. Sukhanova, A.V. Baranov, J.H.M. Cohen, I. Nabiev. et al. *Self-assembly of charged microclusters of CdSe/ZnS core/shell nanodots and nanorods into hierarchically ordered colloidal arrays*. Nanotechnology. 2006. V. 17(16). P. 4223–4228.

2.3 Electronic access: https://commons.wikimedia.org/wiki/File:Solar_Spectrum.png

2.4 S.T. Riahinasab, A. Keshavarz, C.N.Melton, A. Elbaradei, H.S. Hirst et al. *Nanoparticle-based hollow microstructures formed by two-stage nematic nucleation and phase separation*. Nature Communications. 2019. 10(1). 894.

2.5 M.L. Notarianni, V.K Jinzhang, N. Motta. *Synthesis and applications of carbon nanomaterials for energy generation and storage*. Beilstein Journal of Nanotechnology. 2016. 7. P. 149–196.

2.6 F. Zhang, P.X. Hou, C. Liu, H.M. Cheng. *Epitaxial growth of single-wall carbon nanotube*s. Carbon N. Y. 2016, 102, 181–197.

CHAPTER 3. DETERMINATION OF MORPHOLOGY

3.1 Electronic access: https://bitesizebio.com/29197/introduction-electron-microscopy-biologists/.

3.2 Electronic access: https://www.slideshare.net/sanashaikh106/scanning-probe-microscopy.

3.3 Electronic access: https://en.wikipedia.org/wiki/File:Atomic_force_microscope_block_diagram.png.

3.4 Electronic access: https://en.wikipedia.org/wiki/File:AFM_(used)_cantilever_in_Scanning_Electron_Microscope,_magnification_1000x.GIF.

3.5 K. Inaba, S. Kobayashi, K. Uehara, A. Okada, S. Reddy & T. Endo. *High Resolution X-Ray Diffraction Analyses of La,Sr)MnO3/ZnO/Sapphire(0001) Double Heteroepitaxial Films*. Adv. Chem. Phys. 2013. V. 3 No. 1A. P. 72–89.

3.6 Electronic access: https://www.pikpng.com/transpng/xmTmbT/.

CHAPTER 4. FLUORESCENCE MICROSCOPY

4.1 A. Sukhanova, Y. Volkov, A.L. Rogach, A.V. Baranov, J.H.M. Cohen, I. Nabiev. *Lab-in-drop: controlled self-assembly of CdSe/ZnS quantum dots and rods into polycrystalline nanostructures with desired optical properties*. Nanotechnology. 2007. V. 18. P. 185602.

4.2 Electronic access: https://micro.magnet.fsu.edu/

4.3 Parastoo Sabaeifard, Ahya Abdi-Ali, Carlos Gamazo, Juan Manuel Irache and Mohammad Reza Soudi. *Improved effect of amikacin-loaded poly(D,L-lactide-coglycolide) nanoparticles against planktonic and biofilm cells of Pseudomonas aeruginosa*. Journal of Medical Microbiology. 2017. V. 66. P. 137–148.

4.4 Electronic access: https://www.nikonsmallworld.com/galleries/photomicrography-competition

CHAPTER 5. ELECTRON MICROSCOPY

5.1 Electronic access: https://www.globalsino.com/EM/page1985.html

5.2 Electronic access: https://joeleriksson.com/auger-electron-spectroscopy-aes-surface-analysis-technique.html

CHAPTER 6. SCANNING PROBE MICROSCOPY

6.1 G. Binnig, H. Rohrer, Ch. Gerber, E. Weibel. 7× 7 reconstruction on Si (111) resolved in real space. Physical review letters. 1983. V. 50. No. 2. P. 120–123.

6.2 G. Travaglini, H. Rohrer, M. Amrein, H. Gross. Scanning tunneling microscopy on biological matter. Surface Science. 1987. V. 181. P. 380–390.

6.3 D.M. Eigler, E.K. Schweizer. Positioning single atoms with a scanning tunnelling microscope. Nature. 1990. V. 344. P. 524–526.

6.4 В.Л. Миронов. Основы сканирующей зондовой микроскопии: учеб. пособие. Техносфера, 2009. С. 144.

6.5 R. N. Jagtap, A. H. Ambre. Overview literature on AFM: Basics and its important applications for polymer characterization. Indian Journal of Eng. & Materials Sciences. 2006. V. 13. P. 368-384.

6.6 Singera, Z. Barakat, S. Mohapatra, S.S. Mohapatra. Drug-Delivery Systems: In Vitro and In Vivo Characterization. Micro and Nano Technologies. 2019. P. 395–419.

6.7 Y.F. Dufrêne, T. Ando, R. Garcia, D. Alsteens et al. Imaging modes of atomic force microscopy for application in molecular and cell biology. Nature. 2017. V. 12. P.295–307.

6.8 R.M. Bakker, V.P. Drachev, H.K. Yuan, & V.M Shalaev. Enhanced transmission in near-field imaging of layered plasmonic structures. Optics Express. 2004. V. 12(16). P. 3701–3706.

6.9 H. Watanabe, Y. Ishida, N. Hayazawa, Y. Inouye, and S. Kawata. Tip-enhanced near-field Raman analysis of tip-pressurized adenine molecule. Phys. Rev. B. 2004. V. 69. P. 155418.

6.10 R.D. Hartschuh. University of Akron (2005)

CHAPTER 7. X-RAY SCATTERING TECHNIQUES

7.1 K. Inaba, S. Kobayashi, K. Uehara, A. Okada, S. Reddy & T. Endo. *High Resolution X-Ray Diffraction Analyses of La,Sr)MnO3/ZnO/Sapphire(0001) Double Heteroepitaxial Films.* Adv. Chem. Phys. 2013. V. 3 No. 1A. P. 72–89.E.V. Ushakova, V.V. Golubkov, A.P. Litvin, P.S. Parfenov, A.V. Baranov et al. *Self-organization of lead sulfide quantum dots of different sizes*. Nanophotonics V. 2014. V. 9126. 912625.Irina Lokteva, Michael Koof, Michael Walther, Gerhard Grübel, Felix Lehmkühler. *Monitoring Nanocrystal Self-Assembly in Real Time Using In Situ Small-Angle X-Ray Scattering*. Small. 2019. 15(20). 1900438.

Baranov Alexander
Miropoltsev Maksim
Parfenov Petr
Tikhodeeva Ekaterina

Methods and Techniques of Physical Experiment

Study Guide

Original version
Editorial-Publishing Department of ITMO University
EP Department Head N. Gusarova
Signed to print
Order No
Printed circulation
Risograph printing

Editorial-Publishing Department of
ITMO University
197101, Saint Petersburg, Kronverkskiy pr., 49